

Automatic estimation of Urban Roughness Parameters for Microclimatic Analysis

Thesis submitted to the Andhra University, Vishakhapatnam in partial fulfillment of the
requirement of the award of
Master of Technology in Remote Sensing and GIS



Submitted By:
Alok Jhaldiyal

Supervised By:

Kshama Gupta
Scientist/Engineer- SE
Urban and Regional Studies Division
Indian Institute of Remote Sensing
Dehradun

Prasun Kumar Gupta
Scientist/Engineer-SD
Geoinformatics Division
Indian Institute of Remote Sensing
Dehradun



**Indian Institute of Remote Sensing, ISRO,
Dept. of Space, Govt. of India Dehradun-248001
Uttarakhand, India**

June, 2015

DISCLAIMER

This work has been carried out in partial fulfilment of masters in technology program in Remote Sensing and Geographic Information System at Indian Institute of Remote Sensing, Dehradun India. The author is solely responsible for the contents of the thesis.

Date: 16 June 2015

Alok Jhaldiyal

CERTIFICATE

This is to certify that the research work entitled "**Automatic estimation of Urban Roughness Parameters for Microclimatic Analysis**" is the original record of work carried out by Mr. Alok Jhaldiyal towards partial fulfilment of the requirements for award of Master of Technology in Remote Sensing and GIS by Andhra University at Urban and Regional Studies Department, Indian Institute of Remote Sensing (IIRS), Dehradun.

The project contains original work carried out by him and he has duly acknowledged the sources of data and resources used. This research project is completed and recommended for evaluation.

.....

.....

(Prasun Kumar Gupta)

Project Co-supervisor

(Kshama Gupta)

Project Supervisor

ACKNOWLEDGEMENTS

I would like to express my most sincere gratitude to Dr. Y. V. N. Krishna Murthy, former Director IIRS and Dr. A. Senthil Kumar current Director IIRS for providing me all the opportunities and environment to successfully complete my project.

I extend my words of thanks to Mr. Pramod Kumar, Head of Department and Scientist, URSD, IIRS, for all the support and motivation he provided during the course of this research. I thank Mrs. Shefali Agarwal Head and Scientist, PRSD, for creating a magnificent curriculum and healthy atmosphere for conducting this study.

I would like to extend my profound gratitude to Mrs. Kshama Gupta for providing her invaluable guidance which enabled me to pursue this mighty task easily. She has been a source of constant support, inspiration and energy during the whole phase of this research. This research would not have been possible without her brilliant ideas and her exceptional knowledge. I would also like to thank my co-guide Mr. Prasun Kumar Gupta, Scientist, GID for his encouragement, ideas and showing trust in me as a programmer. He has been a visionary with all the concepts and solutions he provided while development of Urban Morphology Extractor.

A sincere word of thanks also goes to Dr. Sandeep Maithani, Dr. Sadhna Jain, Mr. B. D. Bharath and Ms. Asfa Siddiqui, all Scientist URSD for their cooperation and support they provided, whenever and wherever needed.

I thank all my colleagues Harjeet, Arshdeep, Amreesh and Pawan for making this research a joyful journey.

I would also acknowledge Ms. Vandana for her constant support and assistance.

My final words of thanks goes to my family for bearing with me all this while, without their support and all the compromises they made, this research would not have not been possible.

- **Alok Jhaldiyal**

ABSTRACT

Constant upsurge in urban population has led to growth of urban area in all the directions. To accommodate this huge population urban areas have seen abrupt increase in the number of high rise structures. This growth in the vertical dimension has influenced flow of wind inside the urban area. Wind flow inside an urban area is a key microclimatic phenomenon as it counters the effect of Urban Heat Island affect and also disperses the accumulated pollution. To model and simulate the behaviour of urban winds inside the urban area knowledge of urban roughness plays a vital role. Urban roughness constitutes of land use and land cover elements that introduce turbulence in the flow of wind. Roughness Length (z_0) and Zero Plane Displacement Height (z_d) are two key parameters that are used to designate urban roughness. Computation of these parameters is complex and is usually done using Micrometeorological methods and Morphometric methods. Micrometeorological methods are expensive and require complex set up to be installed and hence are not feasible to be used in urban areas. The current research has used morphometric approach to compute urban roughness parameters and some other important urban geometric parameters that includes Sky View Factor (SVF). Using a semi-automatic approach a 3D urban database is generated of the study area. To automate the task of computation of required parameters python and GIS framework was used, which eventually took shape of an open source application named Urban Morphology Extractor (UME). The study discusses the phases of application development and various components of UME. Further, UME is tested on a sample dataset and then deployed on the actual 3D database. For the computed parameters suitability analysis is performed and the selected parameters z_0 , z_d and Frontal Area Index (λ_f) are used to model and simulate the behaviour of winds for the study area. Identification of ventilation paths is one major output. The computed SVF values are used to identify the effect of building geometry and distribution on the ambient temperature at various locations. It was identified by the study that the ventilation paths had low temperature and higher wind speed. A negative correlation 0.71 was found between SVF and temperature. Finally, the results achieved are validated using ground measurements. The developed application, UME is tested and validated and can be used in future studies pertaining to urban microclimatic studies.

Keywords: Urban Roughness, Morphometric Methods, Urban Morphology Extractor (UME), Ventilation Paths and Sky View Factor (SVF)

Table of Contents

<u>CHAPTER 1: INTRODUCTION</u>	- 1 -
1.1 BACKGROUND	- 1 -
1.1.1 URBANIZATION	- 1 -
1.1.2 URBAN CLIMATE	- 4 -
1.1.3 URBAN ROUGHNESS	- 6 -
1.1.4 GEOSPATIAL TECHNOLOGIES	- 7 -
1.1.5 PYTHON FOR URBAN ROUGHNESS ESTIMATION	- 7 -
1.2 MOTIVATION	- 9 -
1.3 RESEARCH OBJECTIVES	- 10 -
1.4. RESEARCH QUESTIONS	- 11 -
1.5 PROBLEM STATEMENT	- 11 -
1.6 THESIS STRUCTURE	- 12 -
<u>CHAPTER 2: LITERATURE REVIEW</u>	- 13 -
2.1 URBANIZATION	- 13 -
2.2 URBAN ROUGHNESS PARAMETERS	- 13 -
2.3 METHODS OF ROUGHNESS PARAMETER ESTIMATION	- 14 -
2.3.1 ROUGHNESS VALUE BASED METHODS	- 15 -
2.3.2 MICROMETEOROLOGICAL METHODS	- 16 -
2.3.1 MORPHOMETRIC METHODS	- 18 -
2.4 URBAN MICROCLIMATIC ANALYSIS	- 24 -
2.4.1 WIND FLOW ANALYSIS	- 24 -
2.4.2 URBAN CANYON TEMPERATURE ANALYSIS	- 25 -
2.5 VENTILATION PATH IDENTIFICATION	- 27 -
<u>CHAPTER 3: MATERIALS AND METHODS</u>	- 29 -
3.1 STUDY AREA	- 29 -
3.2 DATA, SOFTWARE AND INSTRUMENTS USED	- 30 -
3.2.1 SATELLITE DATA	- 30 -

3.2.2 SOFTWARE USED	- 30 -
3.2.3 INSTRUMENTS USED	- 31 -
3.3 METHODOLOGY	- 32 -
3.3.1 3D DATABASE GENERATION	- 33 -
3.3.2 PYTHON AND GIS AUTOMATION FOR CALCULATION OF URBAN ROUGHNESS PARAMETERS	- 37 -
3.3.3 IDENTIFICATION OF VENTILATION PATHS	- 49 -
<u>CHAPTER 4: RESULTS AND DISCUSSION</u>	<u>- 51 -</u>
4.1 STEREO DATA PROCESSING	- 51 -
4.1.1 DEM AND ORTHOPHOTO GENERATION	- 51 -
4.2 3D BUILDING DATABASE	- 52 -
4.2.1 BUILDING FOOTPRINT SHAPEFILE GENERATION	- 52 -
4.2.2 3D HEIGHT MEASUREMENT	- 53 -
4.3 PYTHON AND GIS AUTOMATION	- 55 -
4.3.1 FRONTAL AREA COMPUTATION	- 56 -
4.3.2 HEIGHT-TO-WIDTH RATIO COMPUTATION AND VALIDATION	- 58 -
4.3.3 SVF COMPUTATION AND VALIDATION	- 59 -
4.4 IDENTIFICATION OF VENTILATION PATHS	- 62 -
<u>CHAPTER 5: CONCLUSIONS</u>	<u>- 80 -</u>
<u>REFERENCES</u>	<u>- 84 -</u>

List of Figures

Figure 1: The ten largest urban agglomerations in 2014 (Source: World Urbanization Prospects: The 2014 Revision)	- 2 -
Figure 2: Average annual rate of change of the percentage urban by major areas, 1950–2050 (Source: World Urbanization Prospects: The 2014 Revision)	- 3 -
Figure 3: Urbanization effects on the heat energy balance in the urban area (Image source: http://www.hko.gov.hk/climate_change/urbanization_e.htm)	- 5 -
Figure 4: Projection of building (S_B) from a surface element ΔA on a hemisphere centred at ΔA (Reproduced from Unger, 2009)	- 26 -
Figure 5: Geometrical parameters for SVF computation (H= Height, W=Width, β =Elevation Angle), Source: Oke (1987)	- 27 -
Figure 6: Study Area Location Map.....	- 29 -
Figure 7: GPS point collection from the field	- 31 -
Figure 8: Wind Rose generated from the field data collected using portable weather station. .	- 31 -
Figure 9: Field Weather Station Points	- 32 -
Figure 10: Methodology Flowchart.....	- 33 -
Figure 11: Cartosat-1 Stereo pairs.....	- 34 -
Figure 12: Flowchart of the python and GIS automation to compute various roughness parameters	- 37 -
Figure 13: The building area considered as frontal area exposed to the incoming wind.	- 38 -
Figure 14: GUI listing all wind directions.....	- 39 -
Figure 15: Windline creation in South-North direction.....	- 40 -
Figure 16:	- 40 -
Figure 17: Windline creation in the southwest to northeast direction	- 41 -
Figure 18: Windlines created for four wind directions.....	- 41 -
Figure 19: Frontal area calculation.....	- 42 -
Figure 20: Height- Width Ratio.....	- 44 -
Figure 21: Midpoint computation.....	- 46 -
Figure 22: Relationship between urban heat island intensity and height-to-width ratio identified by Oke (1981).....	- 46 -
Figure 23: Creation of Radial lines over a sample data.....	- 48 -
Figure 24: SVF Computation demonstration and definition of angle of elevation (β).....	- 49 -
Figure 25: GCP assignment in LPS	- 51 -
Figure 26: Building Footprint Shapefile.....	- 53 -
Figure 27: Building height measurement using LPS-Terrain Editor.....	- 53 -

Figure 28: Building height determination using distometer (Image Source: Yousef, 2010).....	- 54 -
Figure 29: 3D view of study area	- 54 -
Figure 30: Averaged Building heights for 50×50 grid cells	- 55 -
Figure 31: GUI listing of various sections of user input	- 56 -
Figure 32: Regular and irregular building group used as sample data.	- 57 -
Figure 33: Computed Frontal Area values for sample area at three different heights.....	- 58 -
Figure 34: Height-to-width ratio calculated results as a point features respective value mapped to the point feature in the attribute table.....	- 59 -
Figure 35: Fish eye photographs and respective threshold images used to compute SVF. The order of photographs is Location1, Location 2 and Location 3.	- 60 -
Figure 36: Radial lines and computed SVF and VF values displayed in the attribute table	- 61 -
Figure 37: Distribution of field observation points over the study area.	- 62 -
Figure 38: Z_0 distribution map.....	- 63 -
Figure 39: z_d distribution map	- 63 -
Figure 40: Frontal area index distribution map	- 64 -
Figure 41: Building height up to 6 meters.....	- 65 -
Figure 42: Building height between 6 and 15 meters.....	- 66 -
Figure 43: Building height between 15 meters and 24 meters	- 67 -
Figure 44: Building height greater than 24 meters	- 68 -
Figure 45: z_0 Classification	- 70 -
Figure 46: z_d Classification	- 71 -
Figure 47: z_d Classification Map	- 72 -
Figure 48: Relationship between temperature and ventilation classes.	- 77 -
Figure 49: Relationship between wind speed and various ventilation classes.	- 78 -
Figure 50: Relationship between SVF and Temperature.....	- 79 -
Figure 51: Relationship between SVF and ventilation classes.....	- 79 -

List of Tables

Table 1: Pattern and trend of urbanization in India 1901- 2001(Reproduced from Uttara et. al., 2012).....	- 4 -
Table 2: Devenport's Terrain classification. Reproduced from Wieringa, 1992.....	- 15 -
Table 3: Nomenclature of the Terminology used for different Morphometric Parameters.....	- 19 -
Table 4: Equations for Evaluating Different Morphometric Parameters, z_0 and z_d	- 23 -
Table 5: Procured data attributes.....	- 33 -
Table 6: Height-to-Width ratio standards suggested by various researchers.	- 45 -
Table 7: Comparative Analysis of UME computed and manually estimated frontal area values for regular building group and irregular building group	- 57 -
Table 8: Results of Height-to-Width ratio computed using UME for 6 well distributed points in 4 wind directions.	- 59 -
Table 9: UME and GLA computed SVF values and their difference.....	- 61 -
Table 10: Categories of height classification	- 64 -
Table 11: r^2 values for various relationships between identified geometric parameters	- 69 -
Table 12: Classification scheme for z_0 values	- 69 -
Table 13: Zd Classification	- 69 -
Table 14: The ground observation points, class they fall in and measured temperature values.-	76 -
Table 15: Average temperature in each ventilation class	- 77 -
Table 16: Average Wind Speed distribution in each Ventilation class	- 78 -

INTRODUCTION

Chapter 1: Introduction

1.1 Background

1.1.1 Urbanization

The world urban population is expected to increase by 84 per cent by 2050, from 3.4 billion in 2009 to 6.3 billion in 2050. By mid-century the world urban population will likely be the same size as the world's total population was in 2004 (*Source: Urban Agglomerations 2009 Wall Chart, UN Dept. of Social and Economic Affairs*). Level of urbanization increased from 27.81% in 2001 Census to 31.16% in 2011 Census. Today 54 % of urban population lives in urban areas and it is expected to reach 66% by 2050 and the 90% of increase is in Asia and Africa alone (*Source: www.un.org*). Urbanization refers to the increasing number of people that live in urban areas. According to UN report on World Urbanization Prospects, 2014, just the three countries India, China and Nigeria together are expected to account for 37% of the world's urban population. Urbanization can be closely associated with modernization, industrialization, and the sociological process of rationalization. Cities are the major drivers of economic activity and development activities and are thus considered as places of economic and social transformations. Cities are considered places of opportunities as there is a concentration of economic activity, commerce, governance, transportation and also act as a link to rural areas, places of national importance and international borders. These enhanced opportunities of social, cultural, economic and political participation leads to continuously increasing urban population. New Delhi is the world's second largest city in terms of population with 38 million people and Mumbai a prominent commercial hub of India is at fifth place with 21 million inhabitants. The issue of urbanization was raised in the 12th five year plan of Indian government, which termed urbanisation as an important and irreversible process. The plan considered urbanisation to be associated with growth. In 2001, India's urban population, living in approximately 5,200 urban agglomerations, was about 285 million. It has increased to almost 380 million in 2011. Projections are that by 2030, out of a total population of 1.4 billion, over 600 million people may be living in urban areas (Indian government 12th Five Year Plan).

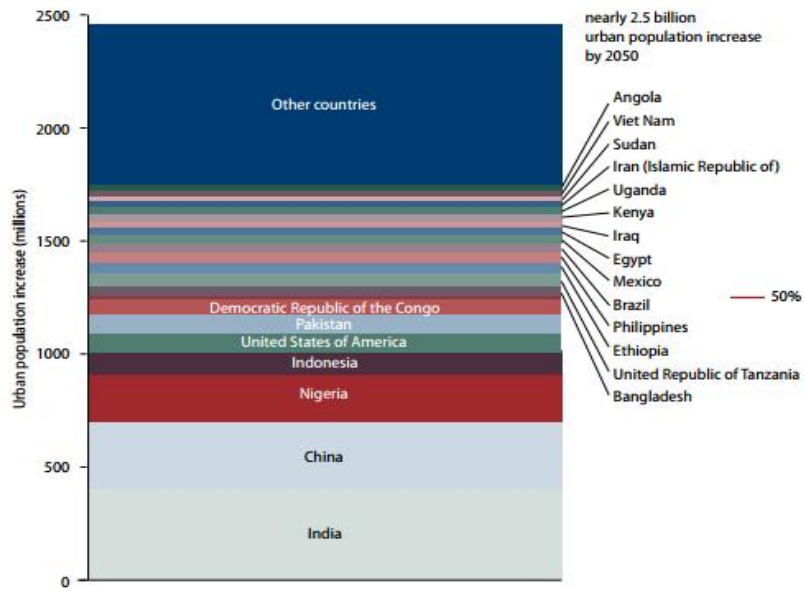


Figure 1: The ten largest urban agglomerations in 2014 (Source: World Urbanization Prospects: The 2014 Revision)

Urbanization is integrally connected to the three pillars of sustainable development: economic development, social development and environmental protection. The outcome of the Rio+20 United Nations Conference on Sustainable Development, “The future we want” (<http://www.un.org/en/sustainablefuture/>), recognized both the plight of the urban poor and the need for sustainable cities as matters of great urgency for the United Nations development agenda (Source: World Urbanization Prospects: The 2014 Revision). Accurate and timely data on global and regional trends of population and urban growth play a critical role in policy framework and accessing the current needs to implement inclusive urban development. The rate of urbanization, measured as the average annual rate of change of the percentage urban, is highest in Asia and Africa, where currently the proportion urban is increasing by 1.5 and 1.1 per cent per annum, respectively. Regions that already have relatively high levels of urbanization are urbanizing at a slower pace, at less than 0.4 per cent annually.

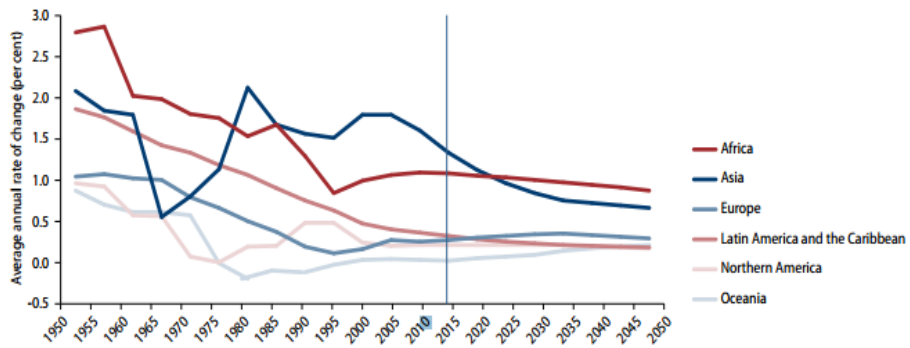


Figure 2: Average annual rate of change of the percentage urban by major areas, 1950–2050

(Source: World Urbanization Prospects: The 2014 Revision)

The cities also need to expand their access to better living conditions, access to services, healthcare, education and a sustainable environment to grow. Providing public transportation, as well as housing, electricity, water and sanitation must be the priorities of policy makers but a thought also needs to be given how these things will be provided, environment concerns and better living conditions must be well thought. India would have 1620 million populations by 2050. Due to uncontrolled urbanization in India, environmental degradation has been occurring very rapidly and causing many problems like shortages of housing, worsening water quality, excessive air pollution, noise, dust and heat, and the problems of disposal of solid wastes and hazardous wastes (Uttara et. al., 2012).

It would not be right to term urbanization as a necessary evil, as both positive and negative aspects can be associated with it. A planned and controlled urbanization can determine or at least influence the destiny of a city and may be a turning point for its existence and optimistic future, whereas in unstable and unplanned conditions, urbanization creates nothing but a real mess. A region or a country has an equal right to get developed, and cities are the centre of this growth. With this growth the inhabitants grow and the city grows in spatial as well as other social and economic aspects. Urbanization should resemble growth, growth in the urban area's infrastructure, services and utilities, economic and cultural aspects. And to let this growth happen, urbanization needs to be controlled and planned. Policy need to be framed, infrastructure and development activities should be carried at same pace as that of urbanization. And if urbanization is not planned, it leads to some catastrophic consequences.

Table 1: Pattern and trend of urbanization in India 1901- 2001(Reproduced from Uttara et. al., 2012)

Census Years	Number of Towns	Urban Population	Percent Urban	Annual Exponential Growth	Rate of Urbanization
1901	1916	25.9	10.8	-	-
1911	1908	25.9	10.3	0.0	-0.46
1921	2048	28.1	11.2	0.8	0.87
1931	2220	33.5	12.0	1.7	0.71
1941	2422	44.2	13.8	2.8	1.50
1951	3060	62.4	17.3	3.5	2.54
1961	2700	78.9	18.0	2.3	0.40
1971	3126	109.1	19.9	3.2	1.06
1981	4029	159.5	23.3	3.8	1.72
1991	4689	217.6	25.7	3.1	1.02
2001	5161	284.5	27.8	2.7	0.82

Environmental, social, cultural, liveability and climate are at stake if urbanization is not sustainable and planned. Slums, high pollution index, heaps of garbage, unemployment, environmentally unwanted events and unpleasant demographic events are some of the after effects of unplanned urbanization.

1.1.2 Urban Climate

Limiting ourselves to impacts of urbanization on urban climate, urban climate is defined by the set of climatic conditions that prevails in a large urban area and that differs from the climate of its rural surroundings. Urban climates are distinguished from rural climate by differences in there air temperature, humidity, wind speed, wind direction and amount of precipitation. One the characteristic that is attached to urban environments is presence of higher concentrations of pollutants such as carbon monoxide, oxides of sulphur, nitrogen, hydrocarbons, oxidants and particulate matter. Outdoor air pollution, both in cities and rural areas, prematurely killed 3.7 million people worldwide in 2012, according to the World Health Organization. The problem goes beyond respiratory health and quality of life: A recent study published in the Proceedings of the National Academy of Sciences found that in India, short-lived air pollutants such as ozone and black carbon, along with the changing climate, cut 2010 crop yields in half. Urban development, including land use changes, dense building developments, heat emissions, human activities, etc., has a great impact upon the local climate of a city. One of the best-known effects of urbanization is the urban heat island (UHI) effect, which develops when urban cooling rates are slower than rural ones. Materials like concrete asphalt and bricks absorb and reflect

energy differently as compared to soil and natural vegetation, as a result cities are warmer as compared to downtown areas. Urban heat island effect is more predominant during nights as rural areas are cooler as compared to urban areas.

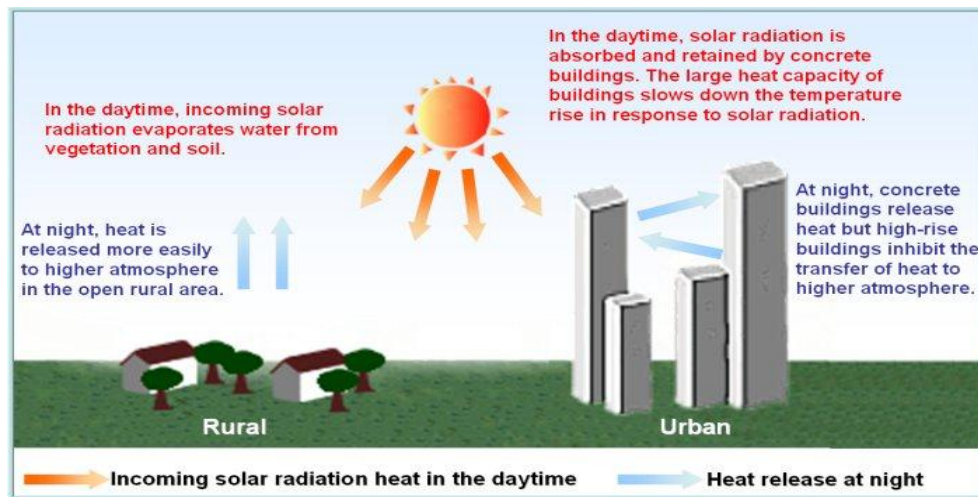


Figure 3: Urbanization effects on the heat energy balance in the urban area (Image source: http://www.hko.gov.hk/climate_change/urbanization_e.htm)

The increasing population has put an enormous pressure on land requirements for housing, commercial as well as official requirements. This has led to growth in all dimensions including the vertical dimension. The development and construction activities have led to an evolution of high rise structures due to which the surface geometry and characteristics have been changed. The cities are about the roughest surfaces; the enhanced drag effect of the urban surface on the air flow is one of their most important features (Gál and Unger, 2009). “In urban areas, buildings increase the roughness of the surface which modifies the near-surface flow field and promotes the vertical exchange of momentum between the surface and the atmosphere. The geometries of urban structures alter the flow phenomena within the urban street canyon in a variety of ways” (Burian et al., 2004). The flow of wind in urban areas is characterized by mean speeds of 20%-30% lower values as compared to mean wind speeds in the rural areas. The difference occurs as urban areas are rougher than rural areas. This increased roughness applies a frictional drag over the wind flowing in the urban areas. The flow of wind inside the urban area depends on its geometry and the amount of frictional drag imposed on the incoming wind depends on the urban structure’s height and density. The wind velocity decreases drastically from the topmost level to ground level and becomes highly turbulent due to roughness and varied topography of the urban area. Temperature differences between urban and rural areas are attributed to urban morphology – the size, shape, height and orientation of buildings and streets – and to the nature of materials used in building urban surfaces, their albedo, heat capacity, thermal conductivity, and wetness. The penetration of wind in an urban area has immense benefits to the

urban environment. The flow of wind between densely packed buildings enable reduction in overall temperatures, reduces humidity and thermal stress. A city is busy place with a large amount of anthropogenic activities that includes household works, industrial process, transportation and other utilities. All these activities generate a lot of heat and unwanted gases that are ventilated to the outside environment. This leads to excessive heat and pollution in the urban environment. If a city is planned and ventilated, the wind will flow inside and disperse off the accumulated pollution and also drain out the excessive heat.

1.1.3 Urban Roughness

Urban roughness mapping is of vital importance for sustainable development and for providing better living condition to the inhabitants of urban area. A numerous research exists to estimate urban roughness for studying dynamics of the wind flow inside an urban area. Urban roughness constitutes of elements of an urban area that introduce turbulence to the flow of wind. Urban roughness is defined by the set of attributes that are derived using the morphology of the urban area. Urban roughness is an aggregation of various parameters that include building plan area fraction (λ_p), zero plane displacement height (z_d), roughness length(z_o), frontal area density(λ_f), building area density($a_p(z)$), rooftop area density($a_r(z)$), complete aspect ratio(λ_c), height to width ratio(λ_s). Roughness length (z_o) and displacement height (z_d) are considered the most vital parameters to designate urban roughness. Frontal area one of the key building geometric parameter is required as an input parameter to compute z_o and z_d . The estimation of urban roughness parameters is often required in the areas of wind modelling, dispersion modelling, urban climatic studies and detection of ventilation paths. The roughness of the surface is often quantified in terms of the roughness length or the bulk drag coefficient and these values are strongly related to the size, shape and layout (morphology) of buildings in a neighbourhood. The morphology of the surface can be described quantitatively in terms of the building plan area index (λ_p) and frontal area index (λ_f). Accurate knowledge of the aerodynamic characteristics of cities is vital to describe, model and forecast the behaviour of urban winds, turbulence and the dispersion of pollutants at all scales. Broadly, the urban roughness mapping methods can be classified into following categories:

- Roughness value based methods
- Micrometeorological methods
- Morphometric methods

To approaches used to compute urban roughness and other required morphometric parameters have evolved drastically, however, the application of the computed parameters plays a key role in

selection of the approach used. Micrometeorological methods are considered as most accurate and efficient, as they completely depend on the in-situ measurements. But the site installation and operation are difficult and expensive. Also meteorological methods are not found suitable to model near surface wind flow. Morphometric methods on the other hand are less expensive and easy to operate. These methods are also identified suitable to understand wind flow near surface and inside the urban canyon. The GIS and remote sensing technologies have brought down the complexity of execution of these methods significantly.

1.1.4 Geospatial Technologies

Remote Sensing and GIS (Geographic Information System) comprise the most recent set of technologies that are now being utilised to compute roughness values. Several studies have proved the worth of using remote sensing and GIS in estimating urban roughness values (Su et al.,2008; Tian et al.,2011; Wong et al.,2011; Schaudta and Dickinson,2000; Yuan et al.,2014; Burian et al.,2002; Ratti et al., 2005; Gal and Unger,2009; Wong et al.,2010).

Deriving roughness parameter requires extensive network of in-situ measurements, hence application of micrometeorological methods is expensive and not feasible in urban area. On the other hand morphometric methods have a large potential due to availability of 3d urban database. However, the computation of frontal area is quite complex in urban areas and require automation.

Remote sensing imageries are now available in very high resolutions which are ideally suited for urban applications. In addition advent of new technologies like that of LiDAR (Light Detection and Ranging) has made the task of generating 3D databases and urban models hassle free. High resolution stereo datasets are also available which coupled with photogrammetric techniques are useful for computing the third dimension of urban area. GIS is a magnificent platform that integrates the unique geographical data to the highly useful platform of information technology. GIS is a complete package that allows processing of remotely sensed satellite data, allows to perform analysis and also helps in map generation. GIS has support for programming languages, one of the common language supported by many GIS platform including ESRI is python. The support for programming language allows user to customize GIS operations and also build a standalone application that performs GIS tasks. Gal and Unger (2009) developed an avenue script in ArcView 3.2 for estimating the roughness values. Use of remote sensing and GIS has unleashed all-new potential for performing multi-dimensional studies such as the one of urban roughness mapping for urban microclimate studies.

1.1.5 Python for Urban Roughness Estimation

Python is a strong and powerful language and was founded by Guido van Rossum in late 1990s. Python is a general purpose, by not being specific to an application domain and is a multi-

paradigm language: procedural, object oriented and functional. Python is both a programming language and a scripting language and is frequently referred to as object oriented scripting language. Python is relatively lightweight as compared to other programming languages and is also platform independent. Python is interpreted as a byte code created by python virtual machine. The latest version of python in use is python 3.4. Python provides integrated development environment (IDLE), when it is installed fresh. IDLE allows to write python codes. Python has two windows a python shell and a python script window. The python shell is used for output and error messages generated by the script and python script window is the place to write the script files. Python supports a variety of data types that include lists, dictionary, numbers, strings, tuples, files, sets etc. Python language is dynamically typed i.e. it does not require the user to specify the data type.

Python is useful for accomplishing real-world tasks—the sorts of things developers do day in and day out. It's commonly used in a variety of domains, as a tool for scripting other components and implementing standalone programs. Python has a variety of libraries that can be used in variety of applications that include scientific and non-scientific applications. One of the fields that have benefited with the use of python is remote sensing and GIS. Python is an open source programming language. It doesn't have anything to do with GIS itself, but has become one of the key languages to use for GIS. This is mainly because it's very commonly available and integrates well with the C++ code which forms the basis of a lot of GIS functionality (GEOS, Mapnik, and OGR are written in C++). Most of the software's involved in analysis and processing of remote sensing data and GIS supports python. Python support is available for a variety of open source and commercial GIS processing software, that include ArcGIS versions starting from 9.0, QGIS and many other software platforms support python customization and programming.

Python has a very strong support for geospatial applications. The following section details out some of the most used modules used extensively by Python GIS developers.

GDAL/OGR: Geospatial Data Abstraction Library is a python library that is used to work with raster geospatial data. OGR was initially made as a separate library to work with vector data but is now partially merged with GDAL. GDAL and OGR together make the most strong geospatial library for reading and writing geospatial data. GDAL can read raster files in 81 different formats and write in 41 different formats. OGR supports reading data in 27 formats and can write in 15 different formats.

PyProj: Pyproj is python wrapper class around another library called pyproj.4. This library is used to handle projections of geospatial data.

Shapely: Shapely is a python package for the analysis and manipulation of 2 dimensional geospatial data. As GIS input data works with geometric features so shapely acts a vital platform for processing geospatial data.

Mapnik: Mapnik was originally developed for C++ platform but bindings are now available for it to work with python. Mapnik is freely available tool for mapping applications. Mapnik imports data from PostGIS, shapefile and other GDAL/OGR supported file formats to render it into good looking maps and images.

ArcPy: ArcPy is python module that provides a set of tools and a geospatial environment for working with geographic data. ArcGIS has inherent support for python for all the new versions starting from version 9.1.

1.2 Motivation

India would have 1620 million populations by 2050..Projections are that by 2030, out of a total population of 1.4 billion, over 600 million people may be living in urban areas (12th Five Year Plan). Urbanization if planned and controlled has a positive implication and if not planned leads to disastrous consequences. Urban planning is being practised in India from way long back but rapid urbanization has led to somehow planning not meeting the pace with the urban process. The 12th five year plan addresses the issue of urbanization and policy framework to tackle it. In India not much heed is being paid to the concept of sustainable development. Sustainable and planned development incorporated urban planning is the call of time. New Delhi is one of the biggest cities of the world and was also declared the most polluted city in the world (*World Health Organization, Ambient Air Pollution Database*). Increasing levels of pollution can be associated with the deteriorated geometry, both in vertical and horizontal dimensions which has led to no inflow of wind and hence no pollution dispersion. Urban roughness estimation is a prerequisite for understanding urban climate, pollution dispersion and wind flow dynamics in the urban area. Studies and research for estimation of urban roughness are nonexistent for Indian scenario. With the pace with which urbanisation is undergoing studies like these need to be conducted regularly.

India has a very successful and impressive series of remote sensing satellites. Indian satellites provide datasets with a resolution ranging from 0.8 meters stereo panchromatic data to 5.8 meters of multispectral data. This availability of high resolution data promotes studies like these. Remote Sensing and GIS can prove handful in automating the task of extraction of these values using a GIS database which was otherwise a very complex and computational task. GIS

environments support a variety of computer programming languages using which the repetitive task of computation of the roughness parameters can be standardized and automated.

Remote Sensing and GIS facilitates spatial analysis which is a set of analytical methods. Geographic information systems (GIS) and remote sensing techniques can provide alternative solutions by adopting simplified assumptions and numerical approximations [6].

A detailed 3D database can be generated efficiently using a GIS environment. Remote sensing images and GIS can be used to generate thematic maps that can be further exploited to act as input data for estimation of urban roughness parameters. In a GIS environment support for various programming languages exist, that allow customization and mathematical computation over a 3D database generated initially. Thus remote sensing and GIS can together be coupled to estimate aerodynamic potential of urban area.

The need of study explained precisely by the following key points.

- Availability of high resolution satellite data and GIS together makes the highly computational task of studying urban morphology more effective.
- A few studies have been conducted on GIS automated generic morphological parameter extraction.
- Urban morphological studies are nonexistent in Indian scenario.
- Adaptation is required as per changing climate scenarios and Wind circulation needs to be integrated with urban development.

1.3 Research Objectives

The aim of study is to estimate urban roughness parameters for microclimatic analysis. To fulfil this objective the following sub-objectives are required to be attained:

- Development of a 3D database with attribute set most effective for roughness value determination.
- Automate the task of roughness parameter estimation using open source computer programming platform.
- To identify the potential ventilation paths using the estimated roughness values.

1.4. Research Questions

- Can a semi-automatic approach be deployed to generate a 3-Dimensional database of an urban area?
- How to automate the task of estimation of urban morphometric parameters?
- What are the set of morphometric parameters and the criteria's that can be utilized to perform microclimatic analysis?

1.5 Problem Statement

Climate change is one of the major concern of today's world. Climate change is a bigger phenomenon which results from various smaller and long term phenomena. Urbanization and anthropogenic activities play one of the role in climate deterioration. To understand this affect, urban microclimatic analysis is usually performed. The key factors that are required to determine urban climate include wind, temperature and humidity. To understand the behaviour of wind, knowledge of urban roughness plays a key role. Urban roughness constitutes of various urban features like buildings, vegetation, terrain and various other land use and land cover classes. z_0 and z_d are two vital parameters used to designate urban roughness. To understand inside canopy and near surface wind flow for an urban area morphometric methods are preferred. However, the computation of these parameters is complex and cumbersome and therefore requires automation.

The aim of current research is to generate an automated approach to compute urban morphometric parameters that are required to perform microclimatic analysis of the study area. Very few such applications have been developed in the past, which are either not available or are outdated in terms of technology. 3D urban databases are also not available for majority of Indian cities. The current study attempts to delineate a methodology to generate one such database, using remote sensing data and GIS technologies. When we talk of urban microclimatic analysis for Indian cities, such studies are nonexistent with no standard parameters and criteria set defined. The present study identifies the applicability of morphometric parameters used in studies having different urban characteristics and also identify the criteria set to perform microclimatic analysis.

1.6 Thesis Structure

Thesis comprises of five chapters and a brief essence of the chapters is provided in the following section.

Chapter 1: This chapter gives introduction to the research topic, motivation and problem statement, research objectives and research questions. An introduction to the urbanization process, urban climate, urban roughness, geospatial technologies, and python is given in this chapter.

Chapter 2: This chapter provides an intensive review of the literature available. This chapter gives details of all the roughness estimation methods that have been used as late as 1930 to the modern methods of GIS and remote sensing. Within each specific method of estimating urban roughness, all the works and studies found in literature are reviewed and their respective pros and cons are summarized.

Chapter 3: Chapter 3 details the methodology adopted to conduct the study. This chapter explains the approach followed to execute the three major components of study: 3D Building database generation; Python and GIS Automation; Urban Microclimatic Analysis. The very details of each individual step are discussed. The chapter attempts to present a thorough understanding of adopted methodology using text, figures, tables and flowcharts.

Chapter 4: In this chapter the results achieved at various stages of the study are presented and discussed. This chapter provide insights about the accuracy with which the outputs were generated and also the error with which the outputs were accepted. The chapter provide factual data about the accuracy and error about various components that include: Field survey validation, automation validation and results analysis. The output in the form of maps, tables and charts have been presented in this chapter.

Chapter 5: Chapter 5 talks about the general conclusions that have been drawn after the successful completion of the study. The chapter highlights both the strong points and the weak points that were encountered while the study was being conducted. The chapter discusses the conclusions that were derived from the achieved results.

LITERATURE REVIEW

Chapter 2: Literature Review

2.1 Urbanization

The urban population is large and increasing. Today 54 % of urban population lives in urban areas. It is expected to reach 66% by 2050 of which the 90% of increase is in Asia and Africa alone (*Source: www.un.org*). This increase in urban population has led to haphazard expansion of urban area in three dimensions. There is a strong need to incorporate environmental and climatic data with urban planning. For establishing better living conditions within urban area urban planners, environmentalists and engineers need to come at a same platform and address the issue of climate friendly urban planning. Increasing population has very catastrophic implications on an urban environment. To accommodate this big population the whole urban geometry has changed, an evolution of high-rise structures has come up. Urban roughness is constituted of the changed morphology which holds the key of urban microclimate. The geometry of urban area greatly influences the flow of wind inside the urban area. Wind flow is a vital microclimate parameter that helps to surpass a variety of human induced harmful effects in the urban environment. Urban roughness parameters are estimated to find the movement of wind inside the urban environment. The surface roughness length of cities is of worldwide interest and has applications to air pollution, the surface energy balance and the vital urban heat island effect (Macdonald et al., 1998). Morphology is the roughness feature of urban area and it is identified by various parameters of which z_0 and z_d are estimated most frequently (Liang et al., 2009).

In the current urban scenario a lot of technologies have come up in the field of satellite remote sensing using which a 3D urban database can be easily generated. A remote sensing data and GIS tools can prove very handy in estimation of urban roughness parameters which was earlier a very computationally intensive task. High resolution stereo satellite data such as the one captured using Cartosat, IKONOS and Pleiades, can be used effectively to generate a detailed urban database of the urban area. GIS environment supports customization using a number of computer scripting languages which can be used further to enhance the task of parameter estimation.

2.2 Urban Roughness Parameters

Urban roughness parameters are estimated to study the effects of urban structures on the movement of wind. Urban roughness parameters can be utilized to study some important urban phenomenon like detection of urban ventilation paths, dispersion modelling and heat flux exchange in an urban area. Several methods and parameters have been suggested for overall

estimation of urban roughness: Zero-Plane Displacement Height (z_d) and the Roughness Length (z_o) (Lettau, 1969) Plan Area Density (λ_p), Frontal Area Index (λ_f) (Grimmond and Oke, 1999; Burian et al., 2002, Wong et al., 2010), Frontal Area Density (Yaun et al., 2014), Depth of the Roughness Sub-layer (z_r) (Bottema, 1997; Grimmond and Oke. 1999) and the Effective Height (h_{eff}) (Matzarakis and Mayer, 2008) etc. One of the important parameter is Frontal Area Index and this is said to have parameter has strong relationship with Surface Roughness (z_o). Frontal area index is suggested as a good indicator for mesoscale meteorological and urban dispersions models (Burian et al., 2002).

Burian et al. (2004) gave a comprehensive list of building morphological parameters: Height Statistics, Building Plan Area Fraction, Building Area Density, Rooftop Area Density, Frontal Area Index, Frontal Area Density, Complete Aspect Ratio, and Building Surface Area to Plan Area Ratio, Height to Width Ratio, Roughness Length and Displacement Height.

2.3 Methods of Roughness Parameter Estimation

History of roughness estimation goes well back to 1930's when Nikaradse (1933), studied the flow of fluid inside pipes. The fluid flow inside the pipe was roughened with grains of sand, from measurements he found that the roughness length, $z_0=h/30$, where h is the roughness height of pipe. Later Jensen's (1958), Ariel and Kliwchnikova (1960) and Hanna (1969) made their contribution to surface roughness evaluation however some of these studies lacked inclusion of zero plane displacement height and for some studies like that of Jenson (1958) surface roughness length of study area Copenhagen was abnormally high. However the more recent studies (Dong and Sullivan, 1992; Blumberg and Greeley, 1993) question the approach used by Nikaradse (1933) as the urban surfaces are much complex as considered according to these new authors, surface attributes and topography also needs to be considered. Studies on aerodynamic parameters z_0 and z_d for urban arrays with various geometry conditions have been carried out through various methodologies, including wind tunnel experiments and numerical simulations for several decades (w et al., 2014). From then, till today a lot of advancements have been made in the estimation of roughness parameters that includes technological advancements, methodological advancements and also there has been a considerable increase in the number of parameters that are today used to denote roughness of an urban area.

Methods to estimate roughness parameters can be broadly generalized in three categories: Roughness Value Based, Micrometeorological (Anemometric) and Morphometric (Geometric) (Grimmond and Oke, 1999).

2.3.1 Roughness Value Based Methods

Roughness value based methods use land use information based evaluation of the predetermined roughness values of each land use class for estimation of overall roughness areas. These methods were identified suitable for a larger scale estimations and can be used to quantify roughness values of a whole city. At the most primitive stage roughness values were suggested by Davenport (1960). Davenport (1960) to estimate surface roughness values visually or from maps used for the wind profile data that was well exposed for a wide range of varying terrain. Davenport (1960) classified the terrain into eight roughness classes where the terrain was supposed to be open and moderately rough as listed in Table 1. Wieringa (1992) validated Davenport (1960) eight classification techniques. Wieringa (1992) used data from 60 good field experiments to extend the range of classes from 8 to 10 which added smooth terrain and open water to classification scheme.

Table 2: Devenport's Terrain classification. Reproduced from Wieringa, 1992

Terrain category	Class	Surface	Landscape Description	$Z_0(m)$
1	1	Sea	Open sea, fetch at least 5 km	0.0002
1	2	Smooth	Mud flats, snow, little vegetation, no obstacles	0.005
2	3	Open	Flat terrain: grass few isolated obstacles	0.03
3	4	Roughly open	Flat terrain: grass few isolated obstacles	0.03
3	5	Rough	High Crops: scattered obstacles	0.25
3	6	Very Rough	Orchards, bushes: numerous obstacle	0.5
4	7	Closed	Regular large obstacle coverage (suburban area, forest)	1.0
4	8	Chaotic	City centre with high and low rise building	>2

Various studies (Ramli et al., 2009; Wever, 2012) have been inspired by Davenport classification method. Wever (2012) estimated the roughness values for many stations using Bottema (1997) in the Netherlands and compared them with the Davenport classifications for the year 1962, 1981 and 2009 for the Netherlands. Ramli et al. (2009) used quantitative information (NDVI) from Landsat satellite image and used land use information to determine z_o value.

Roughness values by Davenport (1992) were identified for broad categories of classes, so his method could be successfully utilized for mapping the roughness values of a larger area. But

including frontal area index, height, width and density of roughness elements (Grimmond and Oke, 1999). Frontal area index and z_0 is said to have strong relationship with wind flow in urban area. Morphometric methods have the advantage that values can be determined without need of tall towers and instrumentation. Morphometric methods have a disadvantage as these methods are based on empirical relationships derived from a wind tunnel experiments where there are idealized flows such that the flows are constant in direction, normal to the roughness elements and the array of elements is regular. However, these kind of situations are totally different from real urban areas where roughness elements are in all shapes and also the wind direction is constantly changing (Grimmond and Oke. 1999). But now advent in technology and large computation capabilities helps to generate simulation which very closely represent real scenarios.

Table 3: Nomenclature of the Terminology used for different Morphometric Parameters

S. No.	Parameter	Parameter Description
1	\bar{h}	Mean Building Height
2	s_h	Standard Deviation of Building Height
3	h_i	Height of Building I
4	N	No. of Buildings
5	\bar{h}_{AW}	Mean Building Height
6	A_i	Plan Area
7	λ_p	Building Plan Area Fraction
8	A_p	Plan Area of Buildings at Ground Level
9	A_T	Total Plan Area
10	$a_p(z)$	Building Plan Area Density
11	Z	Specified Elevation Above Ground
12	z_{ref}	Logarithmic Height Range
13	Δz	Height Increment
14	$a_r(z)$	Roof Area Density
15	$L(z)$	Building Area Index
16	h_c	Canopy Height
17	λ_f	Building Frontal Area Index
18	A_{proj}	Area Projected to Wind
19	Θ	Wind Angle
20	$\overline{L_y}$	Mean Breadth of Roughness Elements

21	\bar{H}	Mean Roughness Element Height
22	ρ_d	Roughness Element Density
23	$A(\theta)_{proj(\Delta z)}$	Area Projected to Wind at Θ Direction at a Height Increment Z
24	a_f	Frontal Area
25	λ_c	Complete Aspect Ratio
26	A_c	Combined Surface Area of Buildings and Ground Exposed
27	A_R	Roof Area
28	A_G	Area of Exposed Ground
29	A_W	Wall Surface Area
30	λ_B	Building Surface Area to Plan Area Ratio
31	λ_s	Height to Width Ratio
32	H_1	Height of Upward Building
33	H_2	Height of Downward Building
34	z_d	Displacement Height
35	z_0	Roughness Length
36	f_d & f_0	Empirical Coefficients: $f_d=0.5$ & $f_0= 0.1$, for Urban Areas
37	c_{d1}	Free Parameter ($c_{d1}=7.5$)
38	ψ_k	Roughness Sub Layer Influence Function
39	u_*	Frictional Velocity
40	U	Large Scale Wind Speed
41	c_s, c_r	Drag Coefficients; $c_s=0.003$, $c_r=0.3$
42	K	Von Karman's Constant (K=0.4)
43	α	Empirical Coefficient (4.43 For Staggered Array)
44	β	Correlation Factor for Drag Coefficient (1.0 for Staggered Array)
45	C_D	Drag Coefficient (1.2)
46	C_{dh}	Drag Coefficient Dependent On Obstacle Shape
47	S_{12}	Distance Between Building 1 And Building 2

The Lettau (1969) relationship has been used for almost three decades by meteorologists and wind-tunnel engineers to estimate surface roughness from the geometry of regular arrays of roughness elements. Lettau (1969) in his study discussed various problems that micrometeorological applications deal with. Like the masts used for measurements were itself acting like a roughness element. The determination of roughness values using wind profile measurements is troublesome as the instrumental errors need to be eliminated and major problem

Automatic estimation of Urban Roughness Parameters for Microclimatic Analysis

arises when the true reference point log law is not known in prior, making determination of z_d in addition to z_0 . Lettau (1969) proposed analytical model that relates surface roughness to z_0 .

$$z_0 = \frac{0.5hA_f}{A} 5$$

where h is average height of roughness elements A_f is Frontal area within area of interest A . Later Marshall (1971) used a homogeneous array to estimate roughness values using computed values of frontal area of the roughness elements. Counehan(1971) used a relation using the area of interest and roughness elements to estimate roughness length using velocity profiles, he measured for cubic elements in a wind tunnel.

$$z_0 = h^* \left[1.08 \frac{A_r}{A} - 0.08 \right] 6$$

where A_r is total plan area of roughness elements, A is area of interest and h^* is average height of roughness elements.

Raupach (1994) estimated roughness values for a vegetated area based on the canopy height (h) and area index (A). He analysed the behaviour of z_0/H with roughness density where roughness elements were of varying heights.

Macdonald (1998) analysed the methods used by Lettau (1969), Counehan (1971), Raupach (1994) and used their fundamentals principle to derive a new approach. Macdonald (1998) tried to address the different issues such as Lettau (1969) used homogeneous array of roughness elements and similarly Couhenan (1971) also tested his methods against homogeneous arrays in a wind tunnel. The method yields z_d and z_0 using the below mentioned equation:

$$\frac{z_d}{z_h} = 1 + \alpha^{-\lambda_p} (\lambda_p - 1) 7$$

$$\frac{z_0}{z_h} = \left(1 - \frac{z_d}{z_h} \right) \exp \left\{ - \left[0.5\beta \frac{C_D}{k^2} \left(1 - \frac{z_d}{z_h} \right) \lambda_F \right]^{-0.5} \right\} 8$$

where α is an empirical coefficient, C_D is a drag coefficient , k is von Karman's constant, and β is a correction factor for the drag coefficient (the net correction for several variables, including velocity profile shape, incident turbulence intensity, turbulence length scale, and incident wind angle, and for rounded corners). λ_p is plan areal fraction, λ_F is frontal area Z_d/Z_h is height normalized value of zero plane displacement and Z_0/Z_h is height normalized roughness length.

As discussed above a number of empirical formulas have been suggested to compute the urban roughness parameters directly. The only limitation is that these methods become computation intensive as the area of study increases. But with the advent of higher computation capabilities, advent of new technologies like that of Remote Sensing, GIS and availability of 3D

urban databases has led to an easy estimation of roughness values. However these much recent techniques rely on the algorithms using drag force and force around buildings (Ratti et al., 2005).

As height data for many urban areas is not available so many studies (Su et al., 2008; Tian et al., 2011; Wong et al., 2011; Schaudta and Dickinson, 2000; Yuan et al., 2014) used remote sensed data for estimation of roughness values of an urban area. Using remote sensing technologies such as Photogrammetry and GIS the height of urban features was estimated, and then a detailed urban database was generated which was further used to calculate urban roughness elements. However some of the researchers (Burian et al., 2002; Ratti et al., 2005; Gal and Unger, 2009; Wong et al., 2010) used existing building datasets.

Burian et al. (2004) gave a comprehensive review of various roughness parameters and also demonstrated calculation for the sample area of downtown Los Angeles, CA. 3D urban database, DEM and Land Use/ Land Cover (LULC) data was used and analyzed in a GIS environment. Ratti et al. (2005) computed λ_f , λ_p and Z_H using a Digital Elevation Model. Shadow casting and sky view factors were obtained using basic Image processing techniques. Gal and Unger (2009) divided the study area of Szeged, Hungary in irregular polygons and applied modified Bottema (1995) equation for irregular building groups. The final results were achieved by developing an avenue script for ArcView 3.2 software by using the assign proximity function of the spatial analyst module. Although this tool is freely available but to use that extension commercial software is required. Su et al. (2008) used high resolution ortho photos for deriving the height of urban structures in Vancouver, Canada. Land Use regression models were used to finally compute morphological parameters. Wong et al. (2011) proposed a GIS based technique to investigate urban roughness along the coast of Kowloon peninsula of Honk Kong. Using a building database on a grid of 100m urban structures were analysed and roughness values were computed by developing a customized program in Arc GIS, however the program needs access to commercial software and has also some technology glitches. Later using Least Cost Path Analysis (LCP) on GIS platform ventilation pathways was found. Wong et al. (2011) also performed scenario analysis for validating the wall effect by removing the frontal building of the area.

Now climatic studies and urban studies require a multi-disciplinary approach. The support for different programming and scripting language in various GIS platforms have change the strategy adopted earlier for roughness parameter estimation. Extensive use of computer programming language to automate the task of urban roughness estimation which was once a computation intensive task is frequently used by researchers today.

Table 4: Equations for Evaluating Different Morphometric Parameters, z_0 and z_d

S. No.	Equation	Equation Definition	Equation Source
1	$\bar{h} = \frac{\sum_{i=1}^N h_i}{N}$	Mean Building Height	Burian et al. (2004)
2	$s_h = \sqrt{\frac{\sum_{i=1}^N (h_i - \bar{h})^2}{N - 1}}$	Standard Deviation of Building Height	
3	$\bar{h}_{AW} = \frac{\sum_{i=1}^N A_i h_i}{\sum_{i=1}^N A_i}$	Average Building Height weighted by Building Plan Area	
5	$a_p(z) = \frac{\lambda_p(z)}{\Delta z}$	Building Plan Area Density	
6	$a_r(z) = \frac{A_p \left[z - \frac{\Delta z}{2} \right] - A_p \left[z + \frac{\Delta z}{2} \right]}{A_T \cdot \Delta z}$	Roof Area Density	
7	$L(z) = \int_z^{h_c} a_r(z') dz'$	Building Area Index	
8	$\lambda_f(\theta) = \frac{A_{proj}}{A_T}$	Building Frontal Area Index	
9	$\lambda_f = \overline{L_y} \overline{H} \rho_a$	Building height characteristics	
10	$a_f(z, \theta) = \frac{A(\theta)_{proj(\Delta z)}}{A_T \Delta z}$	Frontal Area Density	
11	$\lambda_c = \frac{A_C}{A_T} = \frac{A_W + A_R + A_G}{A_T}$	Complete Aspect Ratio	
12	$\lambda_B = \frac{A_R + A_W}{A_T}$	Building Surface Area to Plan Area Ratio	
13	$\lambda_s = \frac{H_1 + H_2/2}{S_{12}}$	Height to Width Ratio	

14	$z_d = f_d \bar{z}_H$ $z_0 = f_0 \bar{z}_H$	Displacement height Roughness Length	Gimmound and Oke (1999):
15	$\frac{z_d}{z_H} = 1 - \left\{ \frac{1 - \exp[-(c_{d1} 2 \lambda_f)^{0.5}]}{(c_{d1} 2 \lambda_f)^{0.5}} \right\}$ $\frac{z_0}{z_H} = \left(1 - \frac{z_d}{z_H}\right) \exp(-k \frac{U}{u_*} + \psi_k)$ $\frac{u_*}{U} = \min \left[(c_s + c_R \lambda_f)^{0.5}, \left(\frac{u_*}{U}\right)_{max} \right]$	Height Normalized Zero Plane Displacement Height Height Normalized Roughness Length	Raupach (1994)
16	$\frac{z_d}{z_H} = 1 + \alpha^{\lambda_p} (\lambda_p - 1)$ $\frac{z_0}{z_H} = \left(1 - \frac{z_d}{z_H}\right) \exp \left\{ - \left(0.5 \beta \frac{C_D}{k^2} \left(1 - \frac{z_d}{z_H}\right) \lambda_f \right)^{-0.5} \right\}$	Height Normalized Zero Plane Displacement Height Height Normalized Roughness Length	Macdonald et al. (1998)
17	$z_0 = (z_{ref} - z_d) \exp \left(- \frac{k}{\sqrt{0.5 \lambda_f C_{dh}}} \right)$	Roughness Length	Bottema (1997)
18	$z_0 = (z_{ref} - z_d) \exp \left(- \sqrt{\frac{0.4}{\lambda_f}} \right)$	Roughness Length	Gal and Unger (2009)

2.4 Urban Microclimatic Analysis

2.4.1 Wind Flow Analysis

Estimation of roughness parameters is complex and computationally intensive task. The process of estimation is numerical and considers a lot of assumptions. Micrometeorological studies use rigorous field measurements, hence not feasible in urban areas. Roughness value based methods can incorporate GIS and remote sensing in the stages of classification of land use but these methods are suitable for estimating roughness values on a coarser scale. Morphometric methods require information of the morphology of urban area. Remote sensing and GIS can be used very efficiently to compute the required geometric parameters, which can be used by morphometric methods to estimate urban roughness. GIS and remote sensing techniques have the ability to provide solutions with simplifying assumptions and numerical approximations (Wong

et. al, 2010). Wong et al. (2010, 2011) used GIS based tool for estimating frontal area, one of the important parameter for analyzing meso-scale wind flow dynamics. GIS based data models provide various opportunities and improved execution approach for urban modelling. These advantages include: spatial analysis tool, model builder, support for various globally used geographic data formats and support for a computer programming environment (Skelhorn et al., 2012).

Yuan et al. (2014) used a high-resolution (1m X 1m) building height database and developed a program embedded as a VBA script in the ArcGIS system was applied to calculate the frontal area density. Gal and Sumeghy (2007) used the existing database of the earlier studies for his study area of Szeged, Hungary and aggregated the building polygons to lot areas using assign proximity function available in ArcView 3.2 software. Later Gal and Sumeghy (2007) constructed a simple Avenue script for calculation of footprint area and other roughness parameters. Chun and Guldmann (2012) studied urban heat island effect in built up environments and used built up geometries for his cause. They developed the 3D database using LiDAR data, developed building footprints in a GIS environment and constructed a DTM to derive terrain information. Defense Threat Reduction Agency (DTRA) a US agency has developed an Urban Geographic and Environmental Database Information System (GEDIS) that provides a platform for automated urban morphology extraction which is further used by a range of hazard assessment, dispersion and prediction models (Fry et. al, 2004). Chen and Ng (2011) computed sky view factor and frontal area density using an ArcGIS embedded computer program for mapping quantitative urban climate. Ng et al. (2011) used a high-resolution (1m×1m) three-dimensional building database with building height information and digital elevation model (DEM) and later developed a program embedded as a VBA script in the ArcGIS system for calculating frontal area density. However, these extensions require access to commercial GIS software and are also written in some outdated programming languages

Based on the literature surveyed for estimation of urban roughness parameters, the estimation of urban roughness parameters using geospatial technologies can be disintegrated into two parts: Three Dimensional database preparation of urban area which includes height and development of a computer program to compute roughness parameters using the urban database.

2.4.2 Urban Canyon Temperature Analysis

Sky View Factor (SVF) is considered as one of the vital parameter to understand the effect of building geometry and building spatial distribution on the urban ambient temperature. SVF is defined as SVF, that is, the ratio of the radiation received (or emitted) by the ground

- e) The edges of ventilation paths should be comparatively smooth.
- f) The width of the obstacles in a ventilation path should not be greater than 10% of the width of the ventilation path.
- g) The height of the obstacle in a ventilation path should not be greater than 10 m.
- h) Obstacles within a ventilation path should be oriented in such a way that their greatest width is parallel to the axis of the ventilation path.
- i) Single obstacles within a ventilation path should have a ratio of height to horizontal distance between two successive obstacles of 0.1 for buildings and 0.2 for trees.

Applying the above criteria a ventilation path can be identified. The same criterion set was later used by Gal and Sumeghy (2007) to identify ventilation paths for Szeged, Hungary.

Wong et al. (2010) gave a comprehensive outline for Least Cost Path (LCP) analysis method for detection of ventilation paths. LCP compared wind pathways generated in different wind directions. Pathways represented high potential ventilation zones. Wong et al. (2010) described the underlying principle of LCP as identifying the path with minimum resistance, the resistance denotes the assigned path cost that was frontal area index (λ_f). Higher frontal area index implied higher friction values. Wong et al. (2010) exported the map to IDRISI v.14.02 (Clark Labs., Worcester, MA, USA). The λ_f pixel values were reclassified into 5 classes and each class was given a weight as friction. And using the IDRIS COST module the cost surfaces were created, which later led to identification of ventilation paths.

MATERIALS AND METHODS

Chapter 3: Materials and Methods

3.1 Study Area

To conduct the current study Dwarka Sub-City area, New Delhi, India was selected. Dwarka is a planned development located in the western side of the national capital. Dwarka covers a total geographical area of 56.48 km². Dwarka has a total population of 1,100,000 with a density of 19000/km².

Dwarka is Asia's largest housing colony. Dwarka has a large presence of high rise structures with height varying from 6m to 33m. The study area encompasses buildings of various geometries distributed all over the study area. Dwarka has a lot of open areas and vegetated areas. Dwarka being an upmarket and most sought after residential areas faces an immense pressure of huge population.

The limitations of satellite data used and presence of high rise structure were major reasons for selecting Dwarka, New Delhi to conduct the current study.

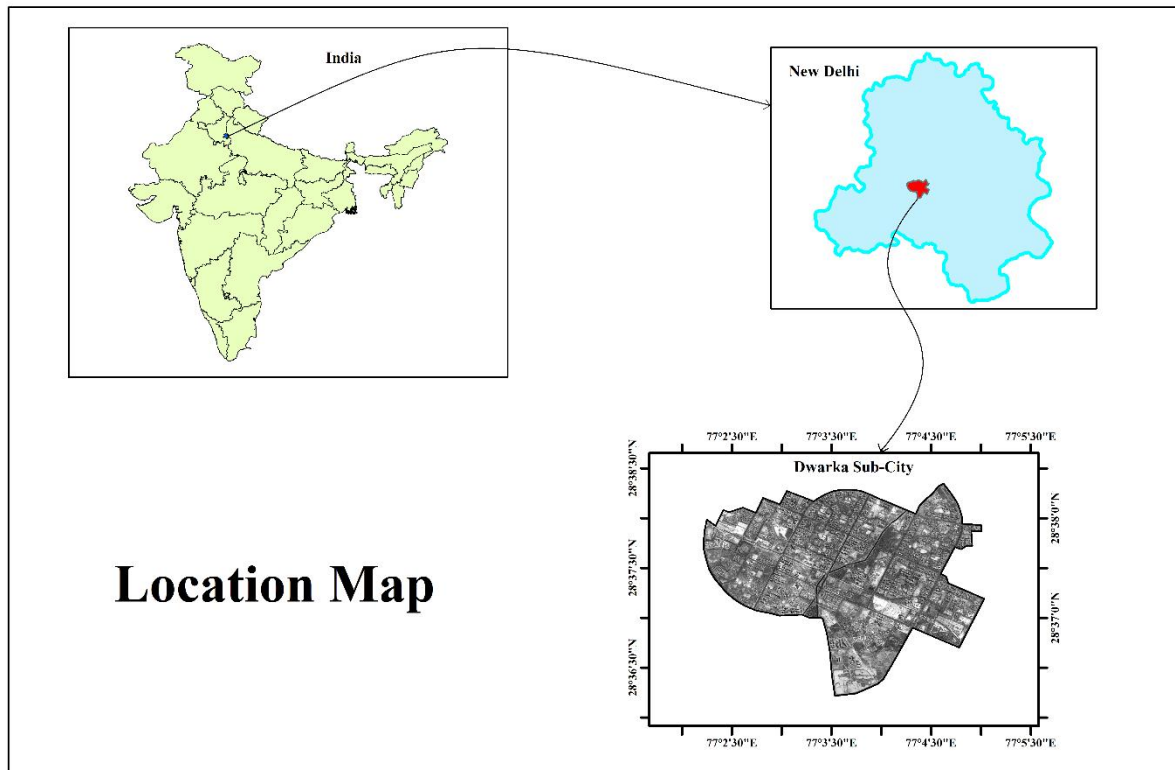


Figure 6: Study Area Location Map

3.2 Data, Software and Instruments Used

3.2.1 Satellite Data

Cartosat-1 Orthokit was the input satellite data used. The procured imagery included two scenes Aft scene and Fore scene. The satellite data is a panchromatic imagery of 2.5m resolution.

3.2.2 Software Used

- a) Erdas 2013: ERDAS 2013 is commercial image processing software that is used for the manipulation and analysis of remote sensing acquired imagery. Leica Photogrammetry Suite (LPS) is a package of ERDAS that was used to do the processing of Cartosat stereo data. The software package was used to triangulate imagery, generate Digital Elevation Model (DEM), orthorectify the image and also the epi-polar images were used to measure building heights in 3D.
- b) ArcGIS 10.1: Arc GIS was used to perform GIS operations and visualization of various GIS datasets. 3D Building database was generated using ArcGIS which included Building footprint shapefile digitization and adding to the database measured building heights.
- c) Google Earth: Google Earth was used to validate the digitized building footprints and also as an aid for the identification which were not clearly identifiable in the Cartosat imagery.
- d) Python 3.3: Python is an open source programming language and is also a preferred of GIS professional. It has a huge support in the form of inherent and additional packages for scientific and GIS data processing. Python was used as a computer programming language for automating computation of morphometric parameters.
- e) QT and PyQt: QT is an interactive user friendly software application that provides a graphical way of designing application interfaces. PyQt is QT binding for python and both packages were used to generate a complete user interactive application to compute urban roughness parameters.
- f) Gap Light Analyzer (GLA): GLA is image processing software which is used to process hemispherical images to compute various gap light transmission indices inside an urban canopy. In current study GLA was used to compute Sky View Factor (SVF) from hemispherical photographs.

3.2.3 Instruments Used

- a) Trimble R7 GNSS: To ortho rectify the procured satellite data a DGPS survey was conducted using Trimble R7 GNSS. Trimble R7 GNSS system is a high accuracy GPS receiver and UHF radio combined in one unit.



Figure 7: GPS point collection from the field

- b) Leica Distometer: Leica Distometer is a hand held instrument which makes use of a laser beam to compute fast and precise measurements between two points. The device was used in the current study to collect building heights from field and was then used to validate the height measured in the 3D environment.
- c) Portable Weather Station: Hoboware data logger was coupled with various sensors that included sensors to measure wind speed, wind direction, air temperature, humidity and pressure. These all sensors were part of portable weather station that was used to collect field data required by the current study.

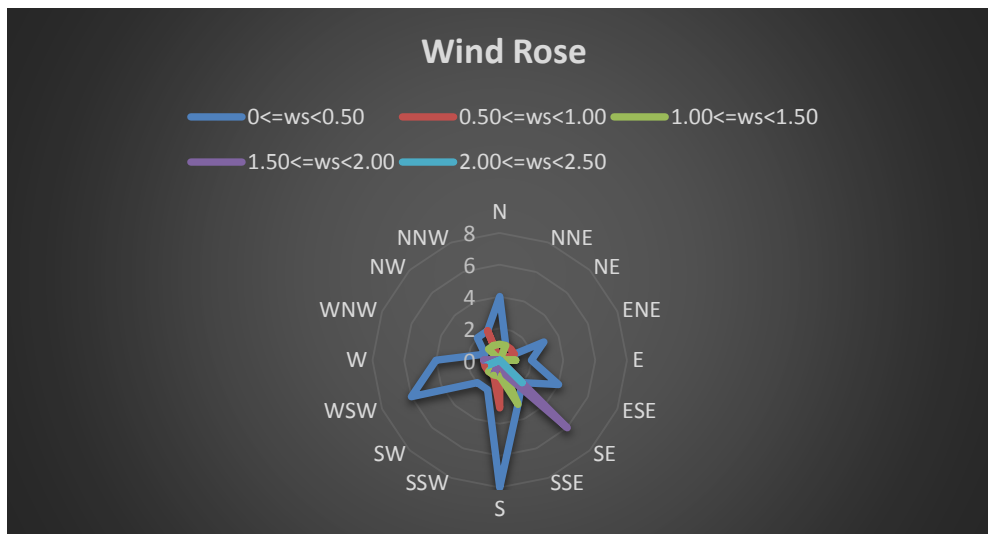


Figure 8: Wind Rose generated from the field data collected using portable weather station.



Figure 9: Field Weather Station Points

- d) HemiView- Canopy Image Analysis System: HemiView is a camera system that processes hemispherical photographs, originally to provide information about plant canopy geometry and sky obstruction. However, in this study this system was used to gather information about sky obstruction by buildings in an urban area. A Nikon Coolpix 5400 camera equipped with Nikon Fisheye Converter FC-E9 0.2X lens was used to capture hemispherical at various observation points. The fisheye images were captured to compute and validate an important geometric parameter called Sky View Factor (SVF).

3.3 Methodology

The overall execution of research work can be categorised into three major methodological blocks.

- 3D Database Generation
- Python and GIS automation for frontal area computation
- Identification of ventilation paths

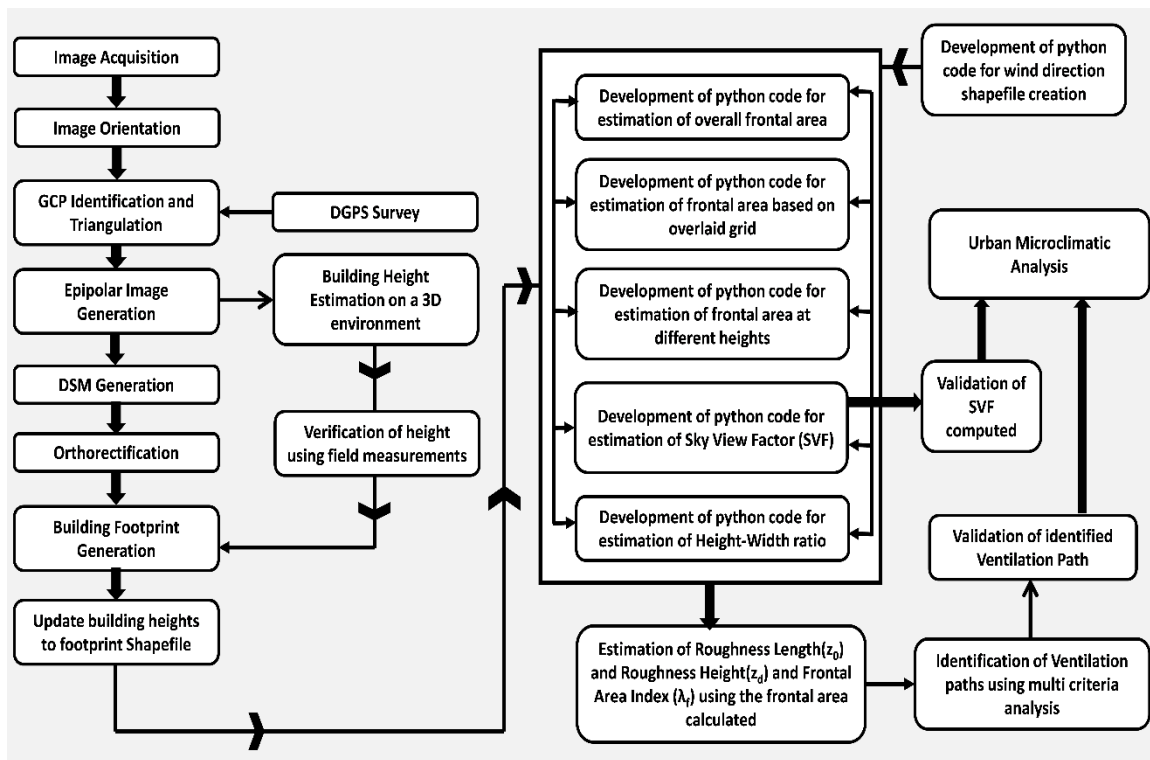


Figure 10: Methodology Flowchart

3.3.1 3D Database Generation

Cartosat stereo data was obtained and processed with the aim to use the stereo pair to generate 3D urban database and building footprints of the study area. All the image processing was conducted in Leica Photogrammetry Suite (LPS) and Arc GIS

a) Image Acquisition

Cartosat Stereo dataset was procured to conduct the study with specifications mention in table 5.

Table 5: Procured data attributes

Image	Altitude	Head	Incidence	Roll	Pitch	Yaw	Processing Level	Date of Pass
AFT	623.66	192.3	28.57	1.26	-21.08	3.03	STD	21/04/11
FORE	624.04	192.3	5.62	1.26	-21.08	2.92	STD	21/04/11

The procured images were evaluated for usability that addressed the issues pertaining to the image quality. The two images were very similar in terms of radiometry and sharpness. In the images there was no major radiometric artifact and also

the image was free from saturation, streaking, banding and noise. This type of image quality is prerequisite before using the stereo data. There was a slight difference in the sharpness of the two images which can be due to the different viewing angles, atmosphere and different Ground Sampling Distance.

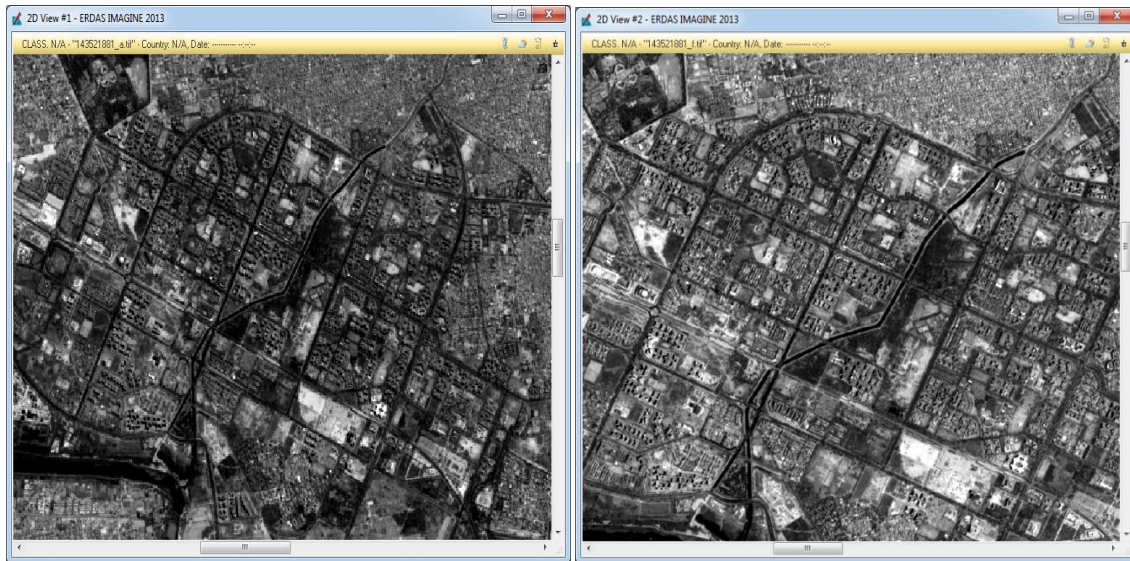


Figure 11: Cartosat-1 Stereo pairs

b) Ground Control Point Collection

A Differential Global Positioning System (DGPS) survey was conducted for collection of Ground Control Point's (GCP). A DGPS is a superior GPS with improved accuracy. DGPS system comprises of two separate GPS devices one of which is a base receiver and other one is a rover receiver. The Base receiver is placed at a precisely known location. The base station computes correction by comparing with the data it receives from the satellites and the known location. These computations are then applied to the roving GPS receiver which enhances the readings. The DGPS instrument used for the survey was Trimble R7 GNSS. A well distributed set of 9 points were identified in the satellite imagery as well as on the ground. The survey was conducted over a period of three days and the base station which was set at a known location, was operational for the whole period. GPS data for the rover receiver were collected for over an hour at each respective point. No real time processing was done as the distance between the two receivers was large. The data was collected and later processed in a Trimble data management utility named Trimble Business Centre

c) Block File Generation

A block file was generated using LPS project manager. A block file is a binary file that contains stereo images, Ground control points, orientation parameters, image coordinates and projections (Rajpriya et al., 2014).The geometric model category used was Rational Functions and geometric model used was Cartosat RPC. The reference coordinate system is assigned as UTM and horizontal units in meters. Spheroid and datum are in WGS 84. The UTM zone specified is 43 in the northern zone. The stereo images are supplied in Tiff format. For input images pyramid layers are created which allows faster processing.

d) Image Orientation

The geometry of orthoimage is proportional to the accuracy of orientation during epipolar image generation, accurate ground control points, geometric quality and quality of used DEM (Bhardwaj, 2013). The product procured is an orthokit which comes bundled with the Rational Polynomial Coefficient (RPC). RPC's relate the normalized pixel coordinates with the normalized ground coordinates. The task of image exterior orientation is achieved using aerial triangulation or block triangulation which is a process of finding a mathematical relationship between images, camera or sensor model and the ground. The orientation of images was carried out using RPC files. Even if ground control points are not available, GCP's can be derived using the RPC file. However availability of GCP's will refine the process. In the present study the interior orientation and exterior orientation were automatically performed using the RPC supplied with the scenes. The photogrammetric processing was done using Leica Photogrammetric Suite (LPS). The image matching was done using tie points which were automatically generated and GCP's collected. Using LPS the Cartosat-1 stereo data was triangulated. The output of triangulation was later used for image orthorectification.

e) GCP Identification and Tie Point generation

Point measurements were done using classic point measurement tool from LPS. Point measurement tool allows defining Ground Control Points (GCP's). All the nine points collected from the field using DGPS were added using this utility. All the points were full i.e. had x, y and z values and were used as control points. Point measurement utility further allows automatic tie point generation which generates the possible tie points automatically. This utility was used which generated 30 tie points which were used along with control points for triangulation of the stereo imagery.

f) Epi-polar Images and DEM Generation

Epi-polar images were generated during the DEM editing process. Epi-polar images enable stereo vision as the epi-polar images are re-projected such that images have a common orientation, appear to be along the same horizontal axis and also have similar matching features. The epipolar image generation consistency is validated by the eATE module of LPS. eATE is Enhanced Automatic Terrain extraction module that uses Triangular Irregular Network (TIN) model for the surface realization. Sample points are overlaid irregularly all over the epi-polar images and then these mass points are used to generate TIN network. The points are checked for being on the surface or below the surface. This whole process results into the generation of DEM.

g) Orthorectification

Orthorectified images are true images, true in the sense that the ground objects are represented in their true, real world x and y positions. The input requirements for ortho image generation are fore and aft images, RPC files, GCP's and DEM. The aft scene of the Cartosat-1 data is used for generation of ortho rectified image as it has a better GSD of 2.2 meter as compared to 2.5 meter fore scene.

h) Building Height Measurement

The epi-polar images were used to estimate building heights using LPS Terrain Editor utility. The building heights were measured in a 3D environment which comprised of a 3D enabled monitor, infrared emitter, 3D glasses and leica topomouse. Leica topomouse is capable of moving the cursor in all three dimensions which helped in measuring the building top and bottom values from mean sea level, which further furnished calculation of building elevations. All the building heights were computed in a similar manner.

i) Building Footprint Generation

A building footprint shapefile was produced using the orthoimage generated from the Cartosat stereo data. Building footprint is a polygon which outlines the total area of the building as it is perceived in the satellite imagery. The footprints were manually digitized in Arc GIS software platform. The footprint shapefile comprises of a total of 2000 building polygons of various geometries. To each respective building footprint the measured and validated heights were added as attributes under a separate field which led to the finalization of the complete building 3D database.

3.3.2 Python and GIS Automation for Calculation of Urban Roughness Parameters

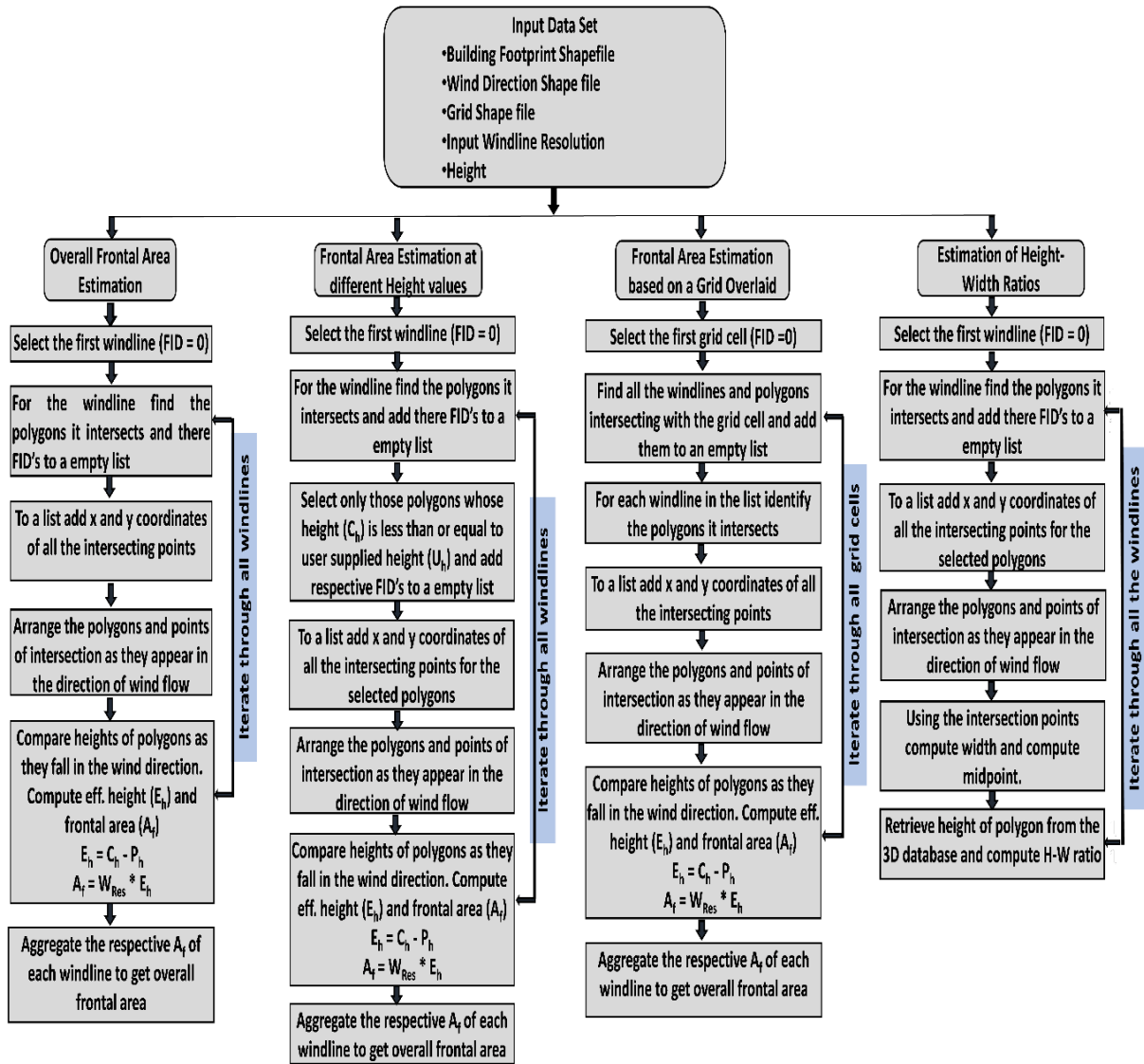


Figure 12: Flowchart of the python and GIS automation to compute various roughness parameters

a) Wind Direction Shapefile Creation

Morphometric methods use the various urban geometric parameters to estimate urban roughness of an urban area and understand the flow of wind inside the urban area. Calculation of frontal area is wind dependent as it is defined as the building area exposed to the wind.

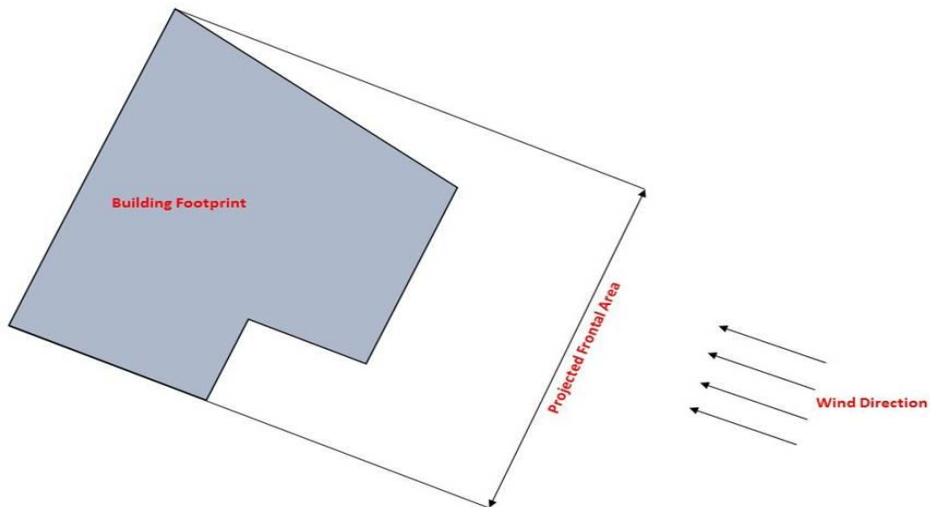


Figure 13: The building area considered as frontal area exposed to the incoming wind.

The direction of wind flow plays pivot role in frontal area determination. For an urban area wind direction can be categorized as dominant and non-dominant. The dominant wind can be identified by analysis of meteorological data. Also there may be a situation where an urban area may have more than one dominant wind directions. So it is always better to explore all the possible wind directions. The current application considers eight wind directions: South-North, Southeast-Northwest, East-West, Northeast-Southwest, North-South, Northwest-Southeast, West-East and Southwest-Northeast.

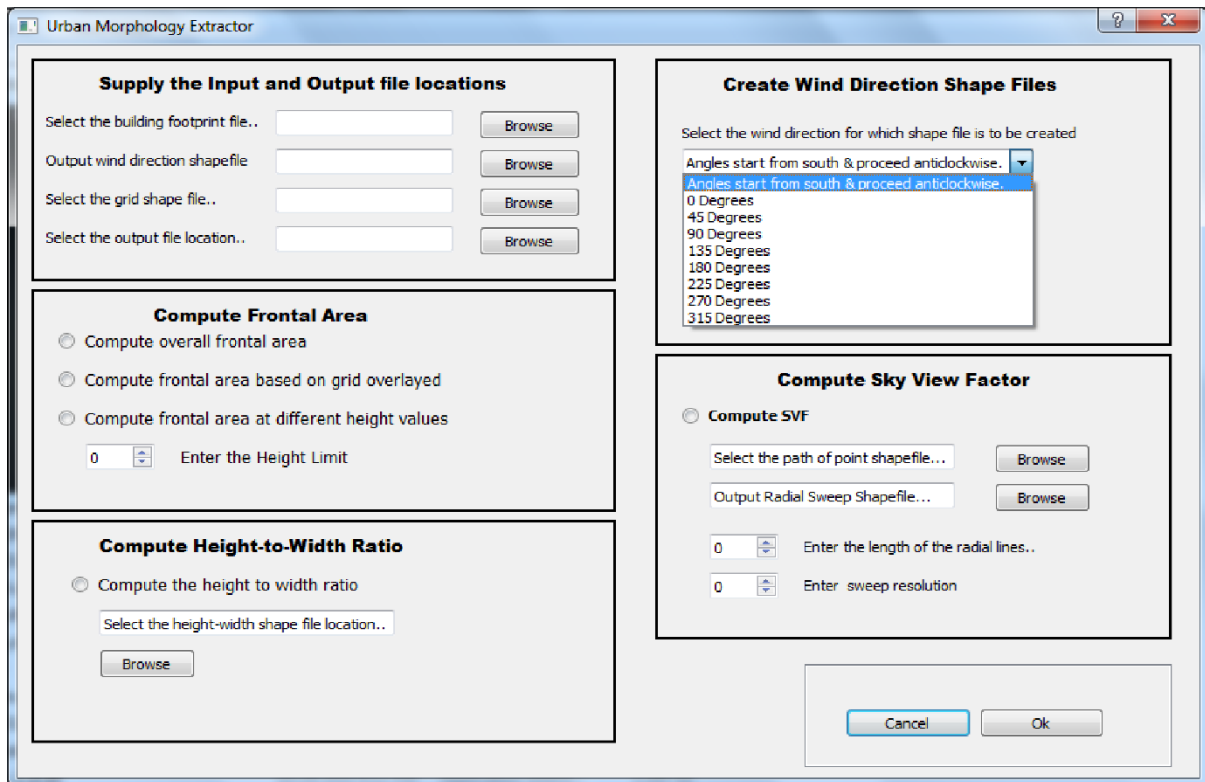


Figure 14: GUI listing all wind directions

Wind flow is continuous and anisotropic, to create such a physical process in a simulated environment is difficult. The wind is simulated as straight line with some separation between subsequent lines. This separation is termed here as windline resolution. The lower the resolution value, lower is the error that creeps in. The windline resolution is accepted as user input. The python GDAL/OGR library's GetExtent() method provides the extent of the input shape file. This method gives the coordinates of the four corners of the shape file. These four corner point coordinates are later used to generate windlines. Line type geometry requires two point coordinates for creation. The corner point is available and the separation between respective lines is known. While moving in x-axis direction from the bottom-left corner, if we add the windline resolution value to the x coordinate and keep the y coordinate as it is we can get the first point of windline. Repeating the same step at the top-left corner will give us the second windline point. Using both points we will get our first windline in the direction from south to north. Repeating the process till the bottom-left x-coordinate is equal to the bottom-right x-coordinate will give the windlines spread all over the study area shapefile. The very similar approach can be used to create windlines from East-West direction. Once the windlines are generated for the South-North and East-West, the windlines if flipped will give the windlines in North-South and West-East respectively.

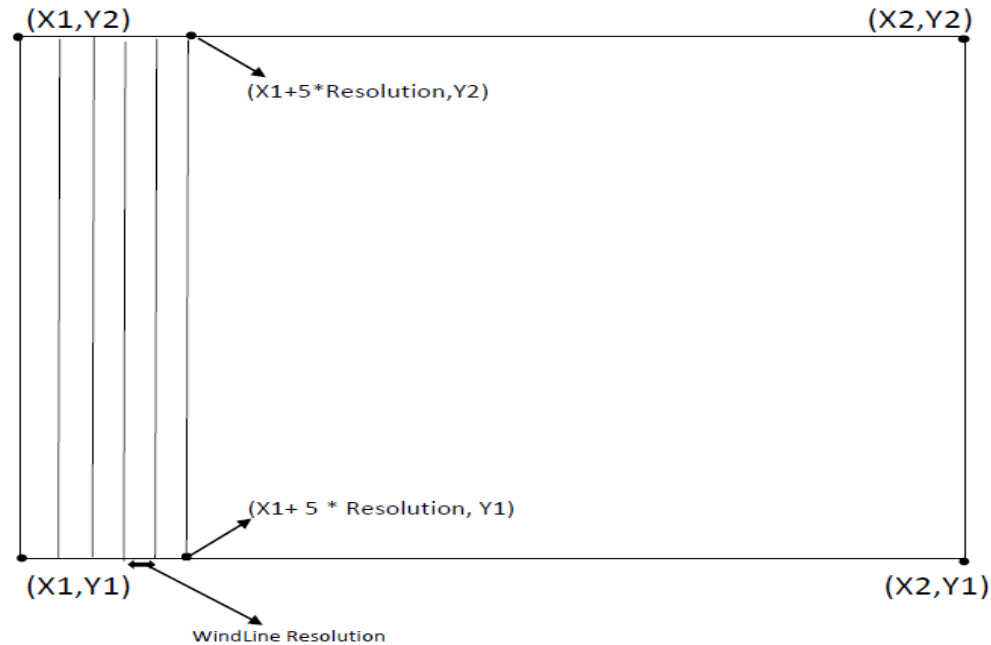


Figure 15: Windline creation in South-North direction

Figure 16:

The windlines for the remaining wind directions which include southeast-northwest, northeast-southwest, northwest-southeast and southwest-northeast were generated using a slightly modified approach. The numbers of windlines to be generated were identified by dividing the diagonal distance of the respective wind direction with the windline resolution. Next the respective points in the x-axis and the y-axis were supplied for creation of windline. The each line generated was separated by the windline resolution value as supplied by the user. The point in the x-axis varied only for the x value while the y-value was constant for each point. In the y-axis only a varied y value was supplied while the x-value was constant for each line. This approach was followed for generation of windlines in three remaining directions. The only difference was in the selection of subsequent points used for line feature creation.

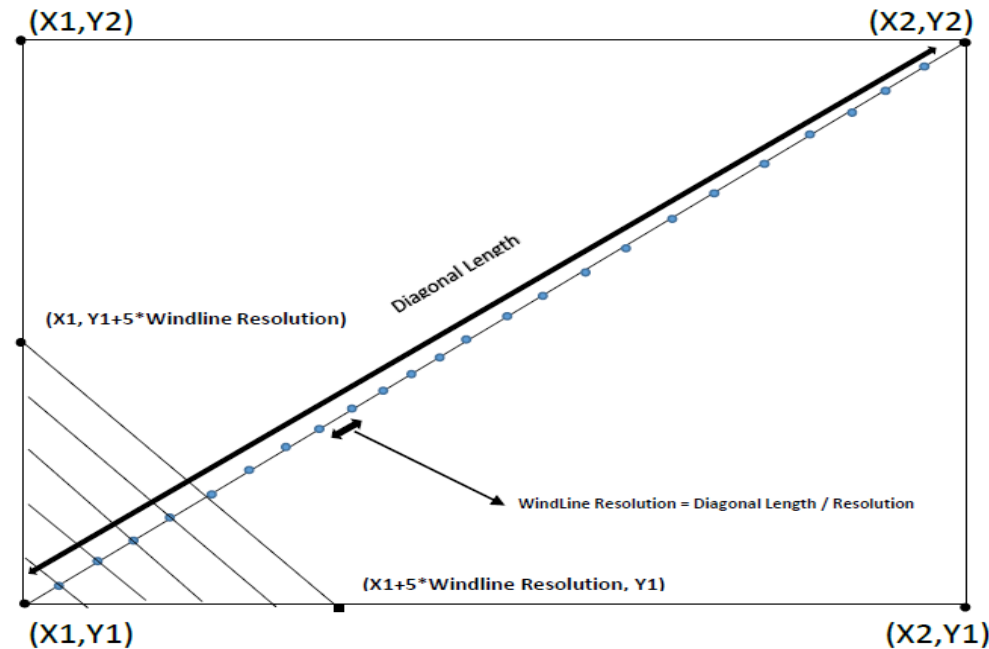


Figure 17: Windline creation in the southwest to northeast direction

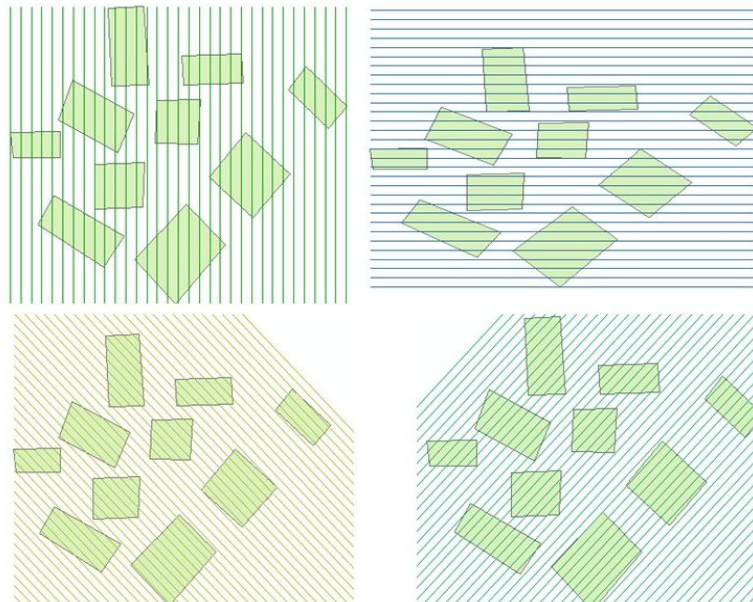


Figure 18: Windlines created for four wind directions.

b) Frontal Area Computation

Frontal area represents precisely the area of a building that is exposed to the wind flowing in a particular direction. Urban areas are usually complex in terms of their shape, height and density. In Indian scenario urban areas mostly do not follow a regular pattern of development and urban areas are marked by high density, varying orientation, different shapes and structures. To estimate urban roughness parameters frontal area is considered

as a vital parameter. The computation of frontal area involves interaction of point, lines and polygons, all the geospatial database entities. Computation of frontal area only considers the areas that are exposed to the wind and act as an obstruction. In urban areas several building blocks are shadowed by the building in front of them and such cases are not considered. Wind flow is a continuous phenomenon and to realize wind flow inside an urban area windlines are generated. Windlines are generated at a specific resolution. The resolution defines the separation between the windlines generated. The accuracy of frontal area calculated highly depends on the resolution at which windlines are generated. The GUI allows the user to input the resolution of his choice.

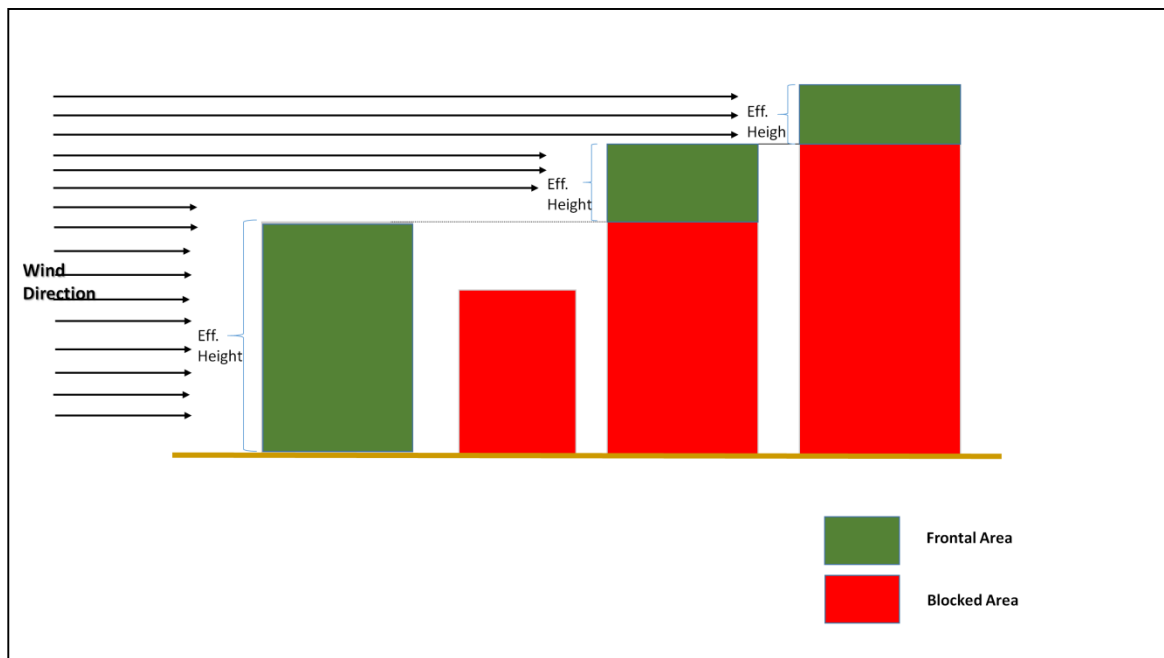


Figure 19: Frontal area calculation

To compute the frontal area the input requirement is a building footprint of the area under consideration and a wind direction shapefile. The underlying concept of computation of frontal area is to count the number of windlines that intersect a building polygon and multiply the count with the windline resolution value. The resultant value is the frontal area of the particular building. Similarly frontal area can be calculated for all the buildings in the area under consideration. But the frontal area computed using this method also considers the buildings that might fall in the shadow region of the preceding buildings. For the ease of issue encountered a slightly different approach is adopted. For each windline the building polygons that it intersects are discovered. In a python and GDAL/OGR programming environment this can be accomplished using the ‘intersect’

Table 6: Height-to-Width ratio standards suggested by various researchers.

Height –to-Width Ratio	
Alexander et al.	1:1 ideal
Hedman	1:1 - 1:2 ideal
Lynch and Hack	1:4 minimum 1:2 - 1:3 ideal
Duany and Plater-Zyberk	1:6 minimum
A. Jacobs	1:2 minimum 1:1 ideal

The flow of wind inside the urban canyon is also affected by the spacing between the building blocks. For large building spacing building wakes do not interfere (isolated obstacle flow) and low spacing the wakes form higher buildings affect the flow around the lower height buildings (Ratti et al., 2005). Height to width ration can be utilized to identify the urban areas with good and poor ventilation. Oke (1981) used a variation of his formula to study urban heat island effect based on street aspect ratio.

The application is capable of computing height-width ratio in all the eight wind directions. The application creates a point shapefile where each point is the midpoint of the distance between respective buildings. The value of height-width ratio estimated is updated to a new field that the application adds to the newly created point shape file shapefile. The estimation of height to width ratio follows the same hierarchy as discussed in the above mentioned processing options. For each windline the intersecting polygons are identified and then polygons are sorted as they appear on the direction of wind flow. Initially we create a shapefile onto which we will add the midpoints and also update the height-width value. Using the Intersect() method of python GDAL/OGR the intersecting points of windline and polygon are identified. The intersecting points are updated to a list as their respective sequence of intersection. For the first polygon encountered we require only the second point of intersection, which can be selected from the updated list of points. Select the second point compute the distance between the points, which is the width between the points and also calculate the midpoint and finally write midpoint as point geometry to the shape file that was created in the earlier steps. The step is repeated for the subsequent pairs of points in the point list. From the sequence of intersecting polygons, the height values are fetched for the first building polygons from building footprint shapefile. The average height is calculated and using the width value calculated

in the earlier steps, height- width value is calculated. The height-width width value is finally written to the point shapefile subsequent to the point feature.

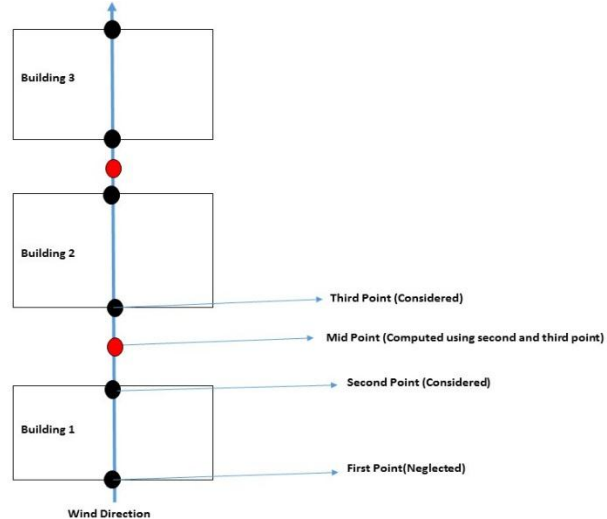


Figure 21: Midpoint computation

The relationship between height-to-width ratio and urban heat island intensity is positive which was observed by Goh and Chang (1999). Oke (1981) conducted a study on the phenomenon in Singapore and he found a positive correlation between urban heat island intensity and the height-to-width ratio.

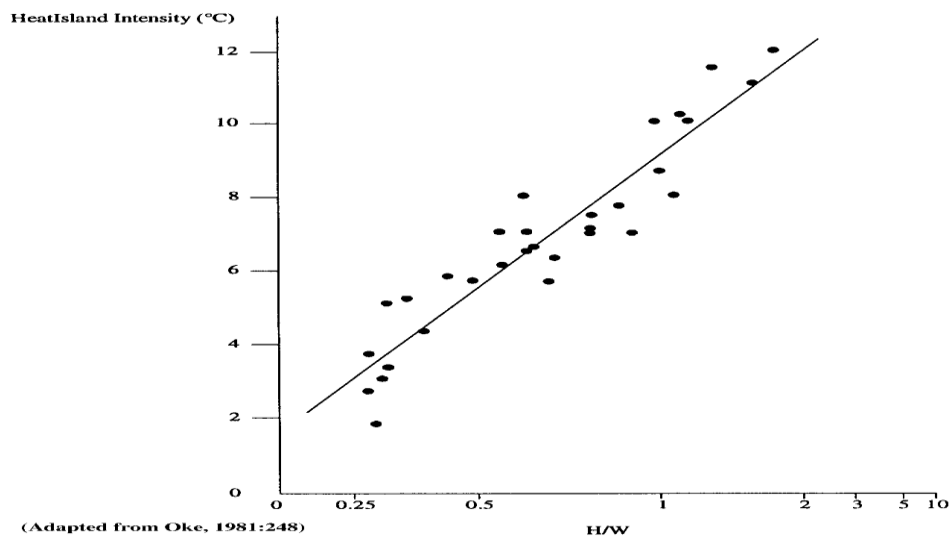


Figure 22: Relationship between urban heat island intensity and height-to-width ratio identified by Oke (1981)

e) Frontal Area Calculation at different Height Values

Variation in height refers to different layers of the urban environment. Urban Boundary Layer (UBL) can extend from ground to around 1 kilometre. Urban boundary

layer is constituted of three distinct sub layers: Outer Urban Boundary Layer (OUBL), Inertial Sub-layer (ISL) and Roughness Sub-layer (RSL). The RSL is influenced by the urban built up structures, the geometry and layout play a vital role on the depth of RSL. Inside RSL lies Urban Canopy Layer (UCL), which extends to the average built-up and obstacle heights (Padhra, 2010). A large urban area is composed of built-up units that are completely different from each other in terms of shape, size and height so the determination of average height for a heterogeneous urban area is difficult. For simplicity of this the roughness values can be computed at different height values, a height value representing average height for some part of the urban area and another height value denoting average height of some other section of the study area.

The application can compute the frontal area at different height values which can be later used to estimate roughness values. The application allows the user to supply the height value up to which the frontal area of building is to be considered. The application exclusively computes the frontal area till the specified height value and neglects the remaining frontal area. The underlying principal of execution is same as the one discussed under the heading frontal area computation. The slight modification is the calculation of effective height. For each building if its height is greater than the height limit supplied by the user than effective height is the difference of the buildings height and user supplied height. And if the height is less than the user supplied height then the same height is considered for frontal area computation.

f) Computation of SVF

To compute SVF a python code was written which utilized python package for GIS processing GDAL/OGR and another package for geometry based computation Shapely. The SVF computation required user to provide a building footprint shapefile containing height values and a point shapefile which identified the points at which the SVF is to be computed.

To compute the SVF the defined algorithm generates a series of radial lines covering the whole 360° angular span. The algorithm allows creation of radial lines at a user assigned angular difference and of a user specified length. The length of radial lines is to be assigned based on the built-up density of the area of the area under consideration. The angular separation of the radial lines plays a pivot role in the accuracy quotient of the algorithm, as the lower is the accuracy the more is the accuracy of discovering the blocked area of the sky. Figure 18, displays the created radial lines from the observation points, the created radial lines are at a resolution of 10° .

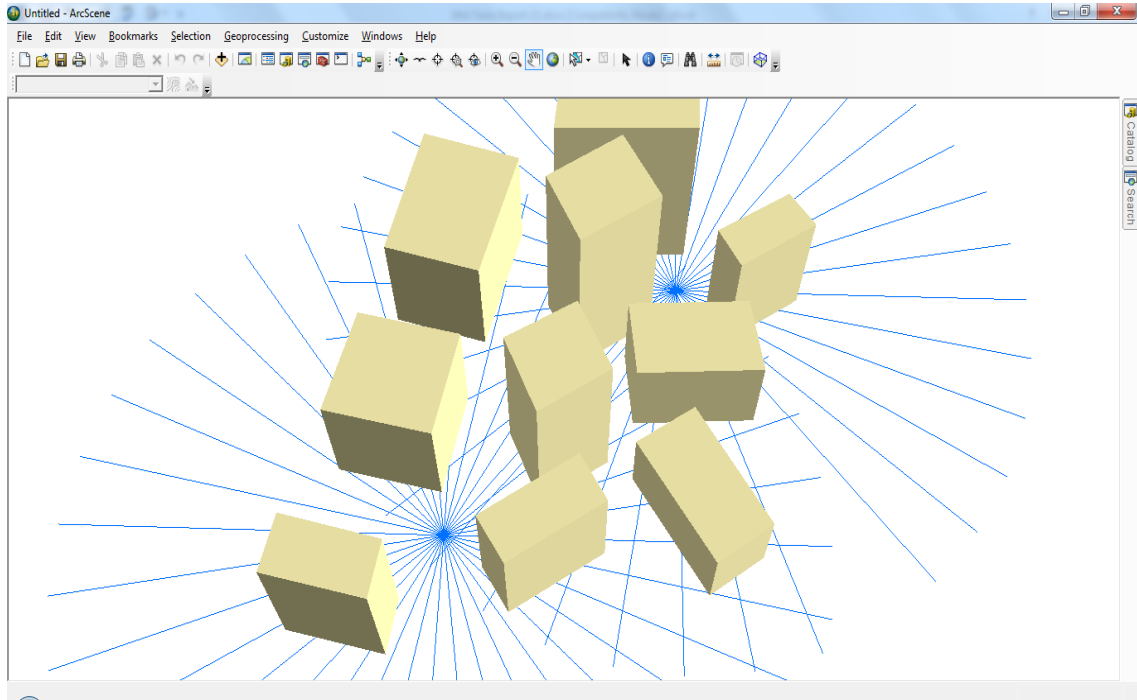


Figure 23: Creation of Radial lines over a sample data

The radial lines that intersect a building account for the blocked sky and the radial lines that pass through represent the sky openness. This whole computation is in 2 dimensions and the 3rd dimension is introduced by utilizing the ‘Height’ attribute from the 3D database. An automated approach is used to calculate the width between the point of observation and the first point of intersection with each building polygon the radial line intersects. Utilizing the calculated width and the database retrieved height the angle of elevation (β) is computed. The β is computed for each building and the maximum beta is the one selected, as this value represents the building that blocks the most of sky in that particular direction. The above discussed approach is applied to a single annuli and is repeated for 360° space.

edges, roughness elements height not greater than 10m, orientation of roughness elements should be along the axis of path. Another study by Wong et al. (2010) used only frontal area index (λ_f) to identify ventilation paths. In the current study three criteria were found suitable to be used for identification of ventilation paths. The criterion applied were: z_0 less than 0.5, z_d less than 3 and path identified with a length of 1000 m to be designated as ventilation paths.

To fulfil the requirements of criteria's selected for identification of ventilation paths a regular grid of 50m×50m size, was overlaid over the 3D building footprints. Using a developed application, UME, the required urban morphometric parameters were computed for each individual grid cell. This automated approach computed values of z_0 , z_d , frontal area and λ_f and updated these values to the GIS database.

For identification of ventilation paths the grid cells with roughness length greater than 0.5 m or height values of zero plane displacement greater than 3 m were selected. The path lengths were taken to be more than 1000 m

The values computed were then used to generate raster images of the study area based on each listed parameter. By applying multi-criteria analysis over the three input images ventilation paths were identified.

b. Validation of Ventilation Paths

Ventilated paths are the areas in urban area where there is significant flow of wind i.e. wind speed should be higher as compared to non-ventilated areas and also the temperature values should be lower in the ventilated areas as compared to non-ventilated areas. Field measurements were taken and values of temperature and wind speed were captured in a series of points that were well distributed over the whole study area. The whole study area was divided into various ventilation classes: Ventilated, Partial ventilation and Weak Ventilation. The distribution of observation points was observed for the various ventilation classes and based on the measured temperature and wind speed values the ventilation paths were validated.

RESULTS AND DISCUSSION

Chapter 4: Results and Discussion

4.1 Stereo Data Processing

4.1.1 DEM and Orthophoto Generation

The procured satellite Cartosat stereo pair was used to generate DEM and orthorectified image using the Rational Coefficient File (RPC) which was shipped with the data package. However when triangulation was performed a Root Mean Square Error (RMSE) of 15.58 was found, which was beyond acceptable limits. So a Differential GPS survey was planned and the Cartosat satellite imagery was registered using collected ground control points. Nine points were identified in the satellite imagery which were well distributed and were clearly identifiable in the imagery as well as in the ground.

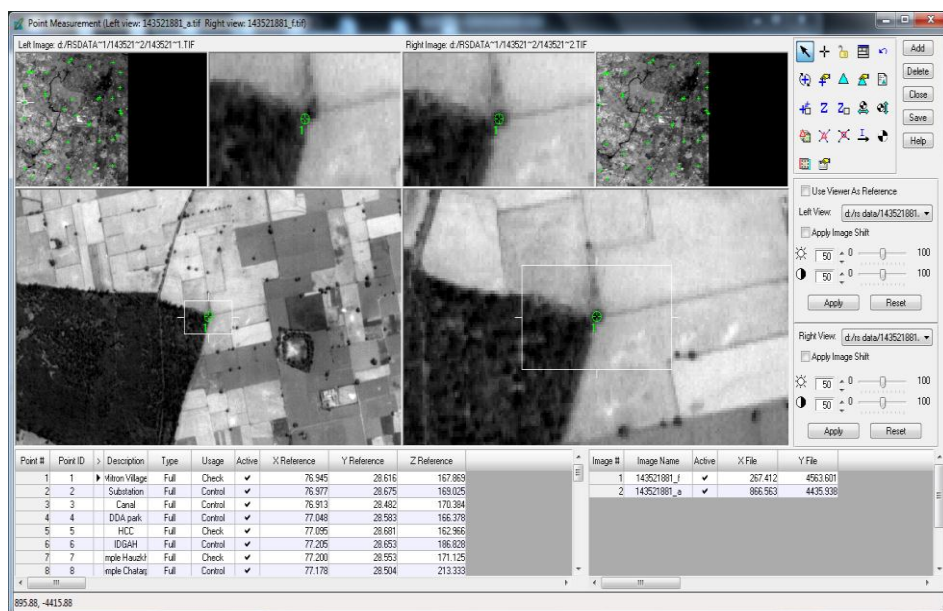


Figure 25: GCP assignment in LPS

The collected Ground Control Points were then used as tie points and control points, based on which the stereo pair was triangulated again.

A Root Mean Square Error (RMSE) was found to be 0.412 which was within acceptable limits. The RMSE error drastically reduced as compared to the RPC based registration. The points were rechecked for positional accuracy but the attained accuracy remained the same. The triangulated

imagery was accepted with the error found and was further used for generating Digital Elevation Model and orthorectified image.

The triangulated imagery was then used to generate digital Elevation Model and orthorectified image.

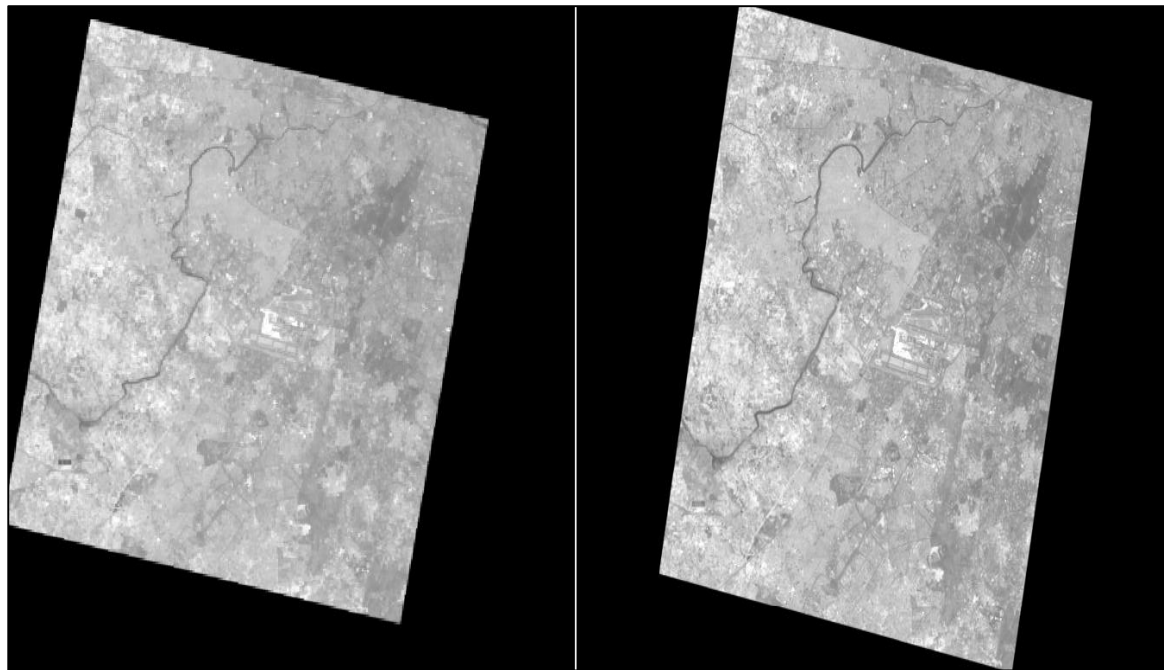


Figure 22: Ortho Images generation for Aft and Fore scenes of Cartosat data.

4.2 3D Building Database

4.2.1 Building Footprint Shapefile Generation

The registered Cartosat satellite image was used to generate a Digital elevation Model which was further used to generate an orthorectified image. The orthorectified image was used to generate building footprint shapefile. The building footprints were manually digitized using Arc GIS 10.1 software. Overall 1953 building were identified in the Cartosat image and were subsequently digitized. Measured and validated building heights were added to the building database as entries to a new field named 'Height'.

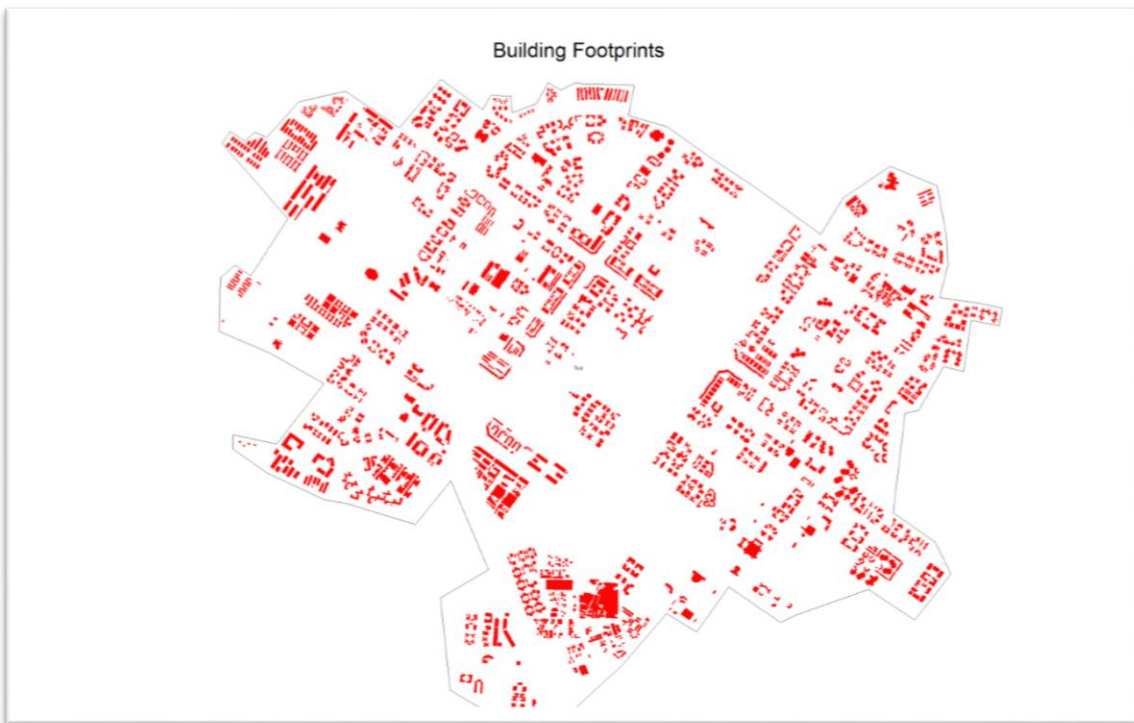


Figure 26: Building Footprint Shapefile

4.2.2 3D Height Measurement

The registered Cartosat stereo pairs were used to generate epipolar images. And the epi-polar images were used in ERDAS terrain editor utility to perform 3D measurements. Heights were measured for 1953 buildings.

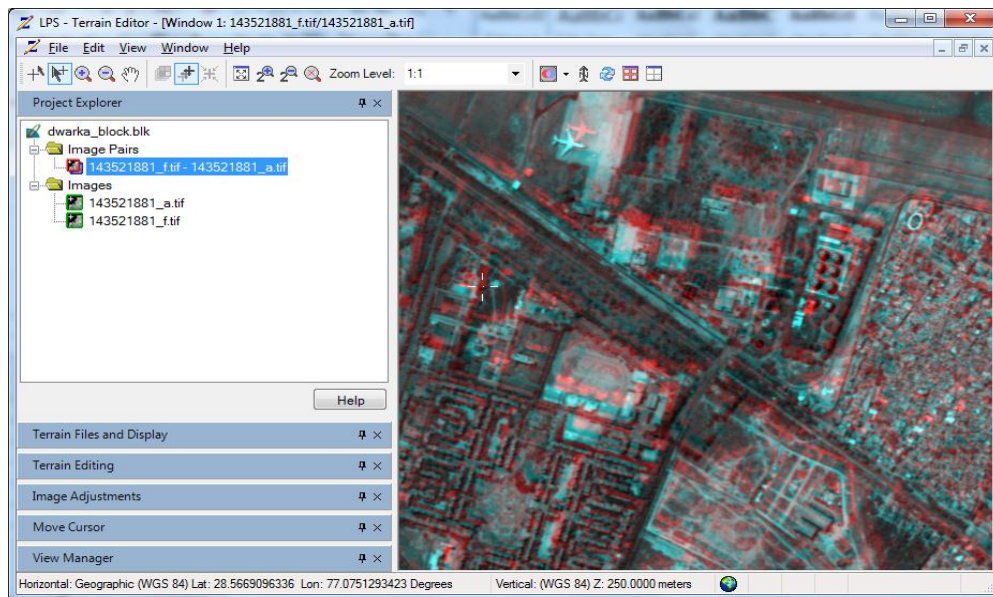


Figure 27: Building height measurement using LPS-Terrain Editor

To find the accuracy of measured heights a field visit was planned in which heights were measured at several well distributed locations using Leica Distometer.

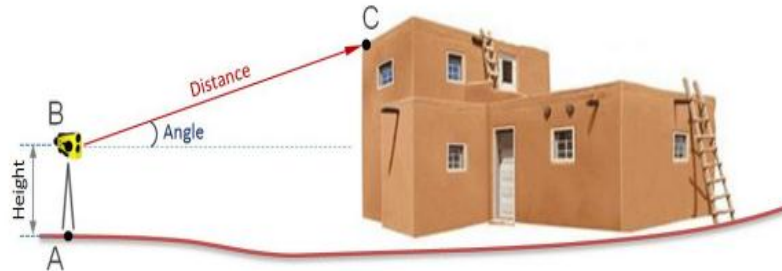


Figure 28: Building height determination using distometer (Image Source: Yousef, 2010)

Overall 576 building heights were measured in the field which ranged from 9 meter to 33 meters. A Root Mean Square Error (RMSE) was computed for the stereo measured heights and heights measured from field. The error computed was 1.41.

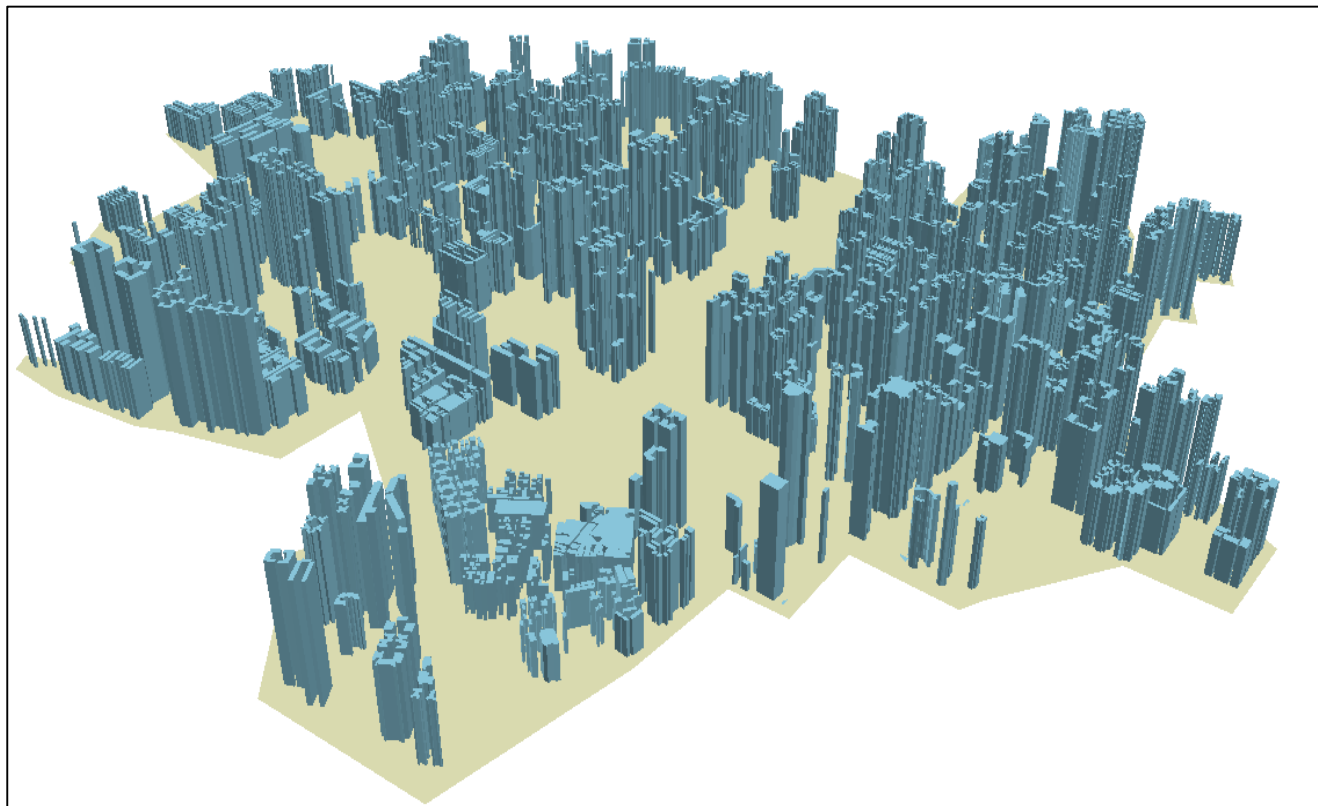


Figure 29: 3D view of study area

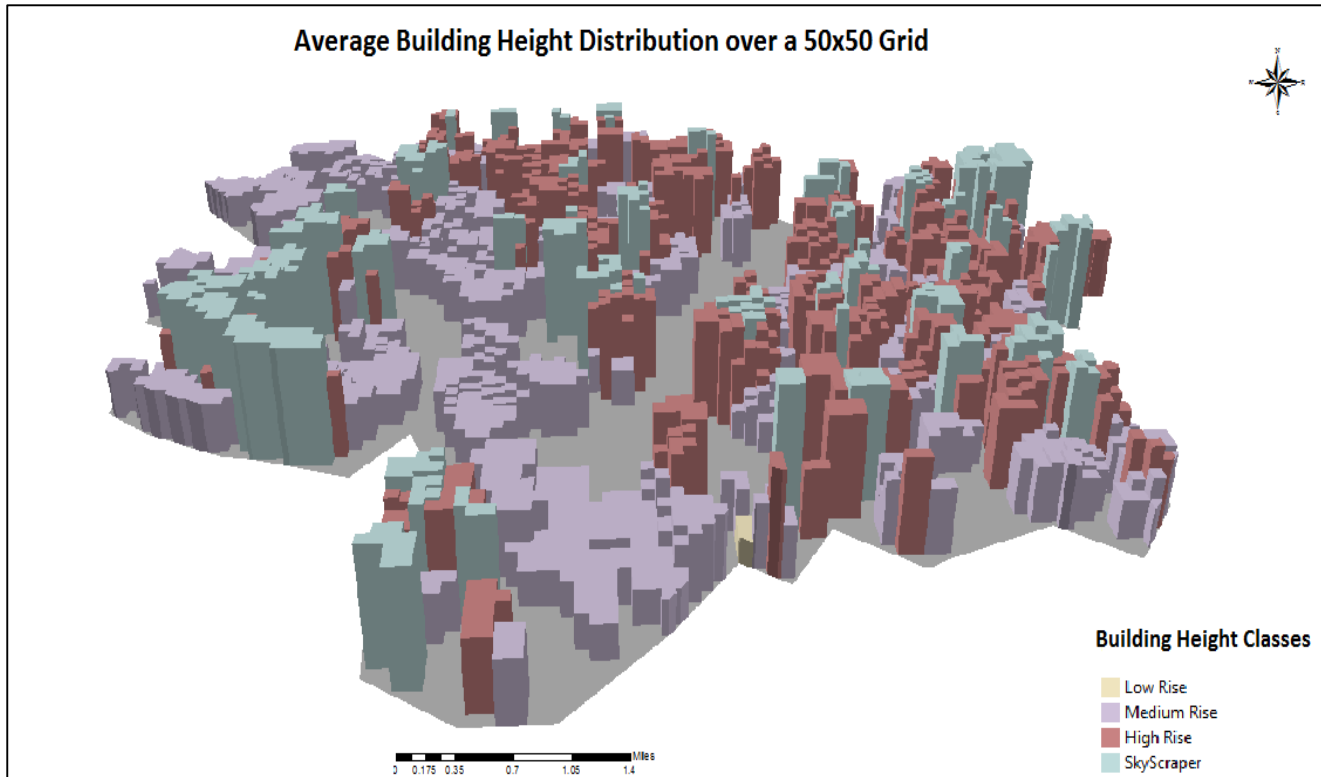


Figure 30: Averaged Building heights for 50×50 grid cells

4.3 Python and GIS Automation

To compute various urban morphometric parameters a python and GIS based open source application was developed which was named as Urban Morphology Extractor (UME). UME takes all the inputs in shapefile (.shp).

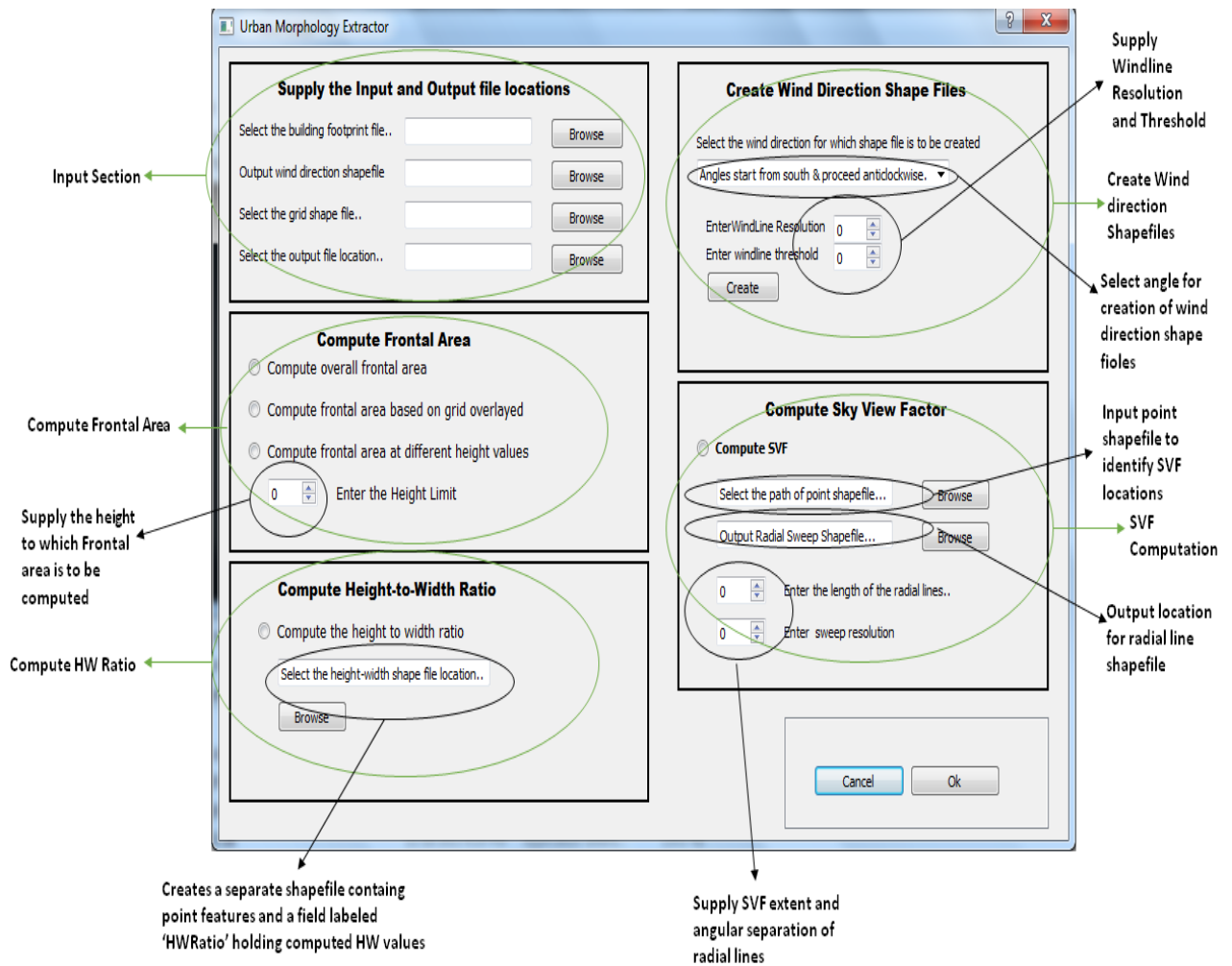


Figure 31: GUI listing of various sections of user input

4.3.1 Frontal Area Computation

Before deployment of UME over the actual study area it was validated over a sample dataset. The sample dataset contained ten polygons which were aligned both to orthogonal and non-orthogonal directions. The polygons were well distributed and were of different shape and varying plan area. The computations were done based on a regular grid and a non-regular grid for all the eight wind directions.

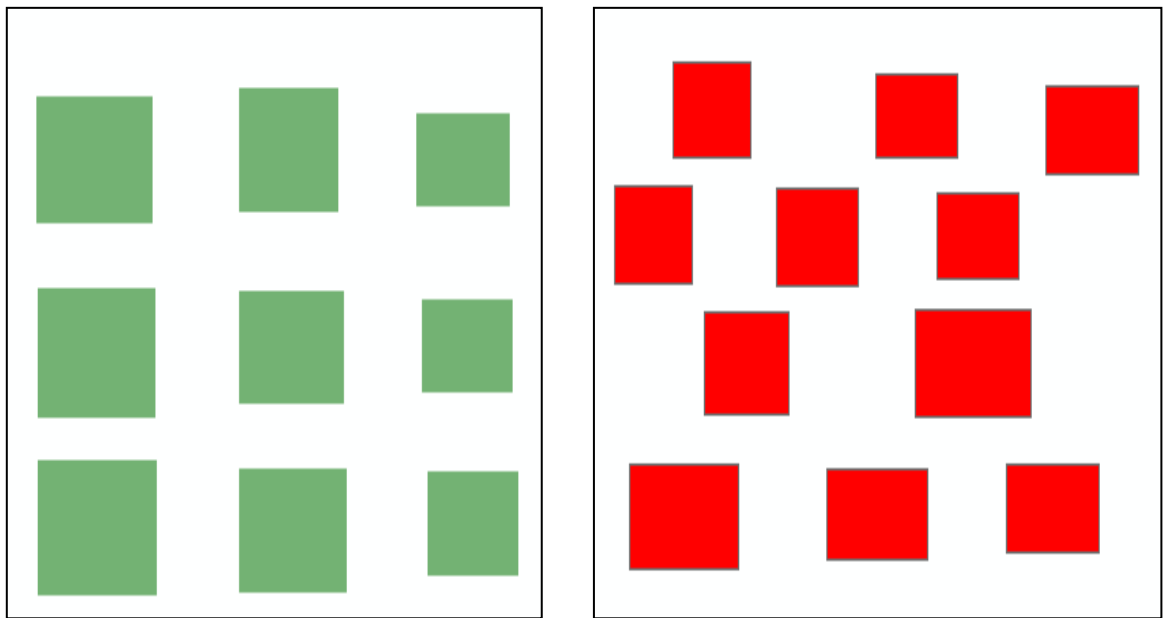


Figure 32: Regular and irregular building group used as sample data.

Frontal area was computed for all the three wind directions for a regular building array and an irregular building array. Table 6 lists out the frontal area values that were computed for the regular building groups and irregular building groups for three different directions. And it is evident that the frontal area computed using UME and manually estimated have an average difference below 3%.

Table 7: Comparative Analysis of UME computed and manually estimated frontal area values for regular building group and irregular building group

Wind Directions	Regular Array		Irregular Array	
	UME Computed	Manually Computed	UME Computed	Manually Computed
South-North	1162	1122	1830	1848
Southeast-Northwest	1652	1638	2485	2468
East-West	834	812	1004	1157
Difference	2.85%		2.89%	

The frontal area was also computed at 5 m, 10m and 14m to validate one of the other utility of UME i.e. to compute frontal area at different user supplied height values. Figure 30, displays the computed frontal area values for the eight wind directions. The computed frontal area value increases as the height increases and also it was observed that for non-orthogonal directions frontal area was significantly higher which can be attributed to the larger area exposed in the direction of the wind.

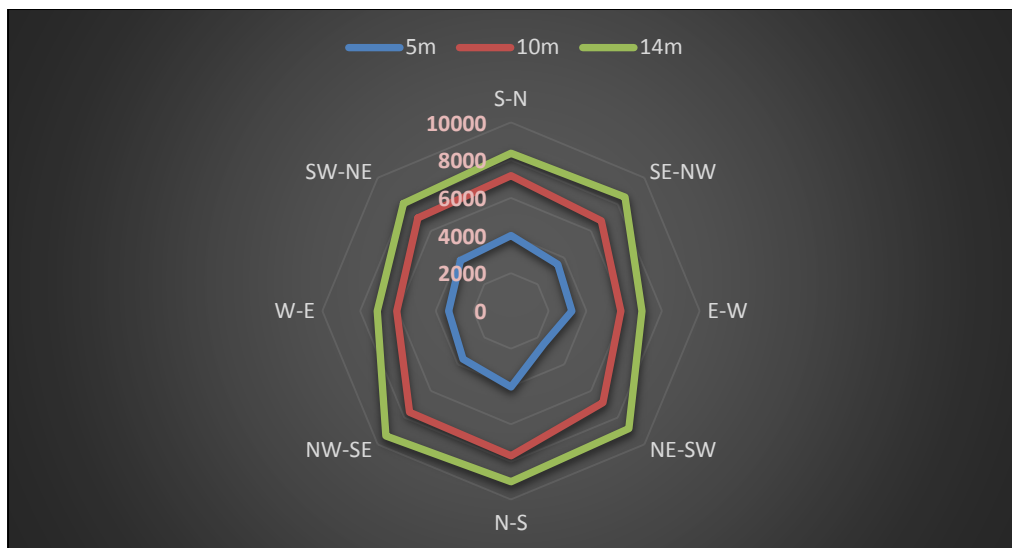


Figure 33: Computed Frontal Area values for sample area at three different heights

4.3.2 Height-to-Width ratio Computation and Validation

One of the other very important morphometric parameter that UME is capable to computes is Height-to-Width ratio. Height-to-width ratio can be computed in each of the eight wind directions and the computed values are automatically updated to a point shape file which is the output of this utility of UME.

Height to –Width ratio was computed using UME for all the eight wind directions which resulted in an output shape file with various point geometries, to each point geometry the value of respective height-to-width ratio was mapped. As the number of point geometries was large enough, so sampling was performed, for each direction a set of five points were identified well distributed over the sample data set and height-to-width ratio was manually measured.

Table 8: Results of Height-to-Width ratio computed using UME for 6 well distributed points in 4 wind directions.

Point ID	Height-to-Width Ratio Direction Wise UME Computed				Height-to-Width Ratio Direction Wise UME Manually			
	S-N	SE-NW	E-W	NE-SW	S-N	SE-NW	E-W	NE-SW
8	0.627	0.331	0.808	4.492	0.654	0.401	0.801	4.444
30	0.871	0.513	0.614	4.114	0.869	0.512	0.611	4.145
53	0.722	0.917	0.640	3.904	0.698	0.916	0.586	3.897
76	0.308	0.586	1.502	3.688	0.310	0.498	1.671	3.876
94	0.401	0.442	2.865	3.541	0.403	0.437	2.867	3.546
129	3.057	0.220	0.218	0.161	2.998	0.221	0.225	0.178

An overall error percentage of 0.90% was found between the height-to-width values computed using UME and values manually measured.

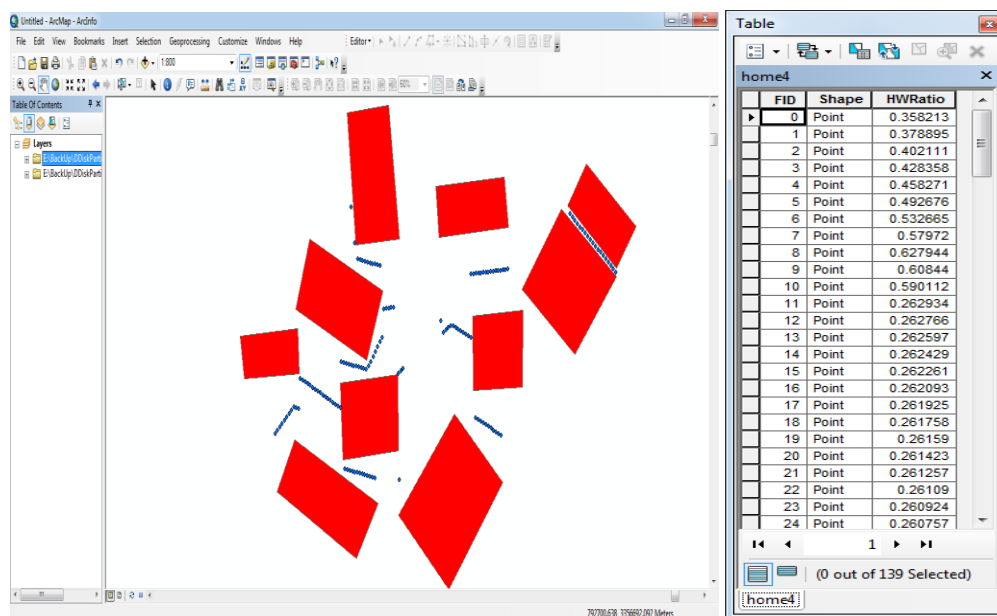


Figure 34: Height-to-width ratio calculated results as a point features respective value mapped to the point feature in the attribute table.

4.3.3 SVF Computation and Validation

SVF is another key urban geometric parameter that UME can be used to compute. The input requirement for SVF computation is a point shapefile, using which the designated points for computation are identified. The validation of SVF computed was done using another application named Gap Light Analyser (GLA). GLA is imaging software used to extract forest canopy and gap light transmission indices from true color hemispherical photographs.

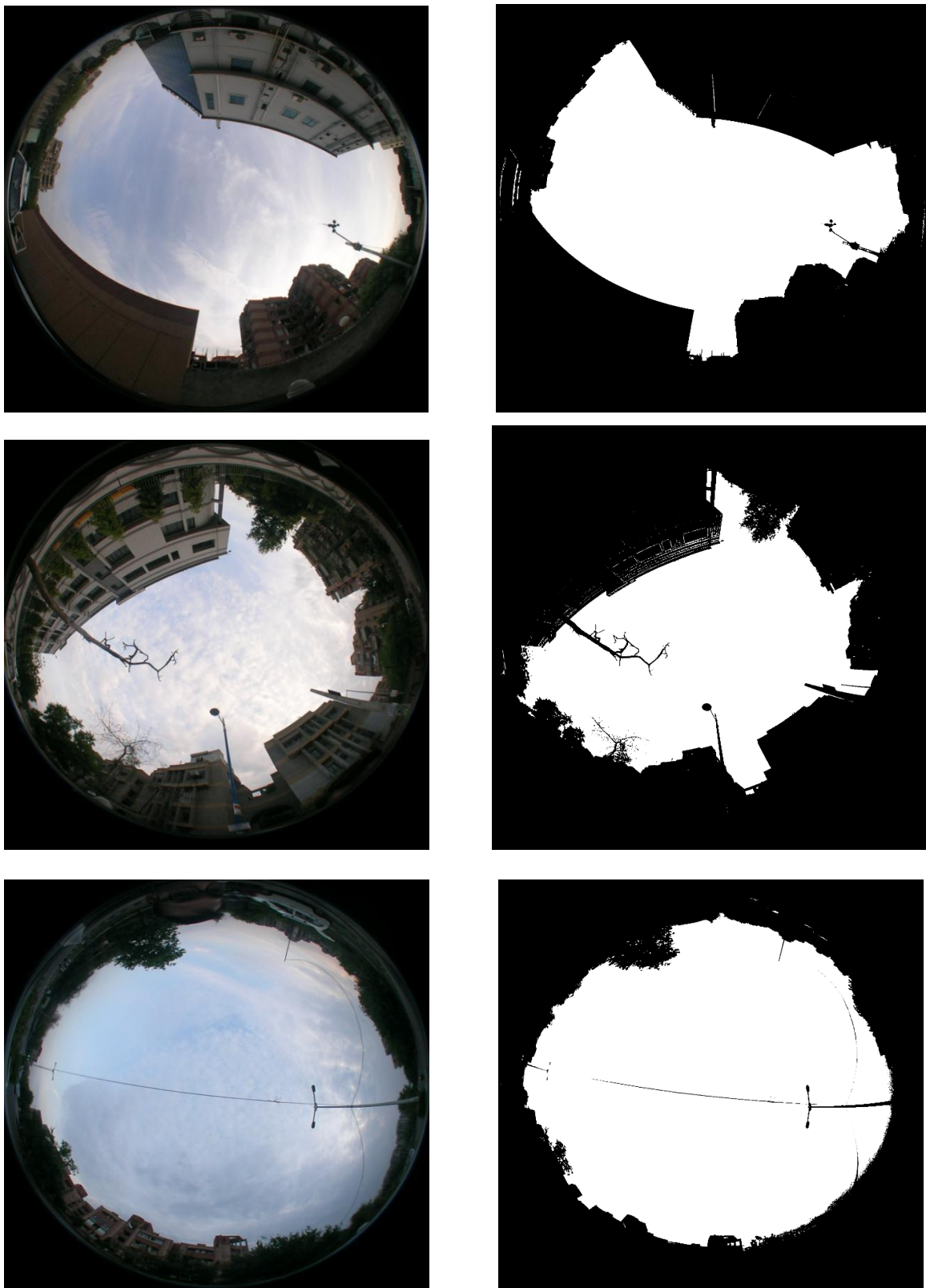


Figure 35: Fish eye photographs and respective threshold images used to compute SVF. The order of photographs is Location1, Location 2 and Location 3.

Three hemispherical fish eye photographs were used to compute the SVF using GLA and at the same points UME based automated approach was utilized to compute SVF. All the radial line or stereo net were generated at a resolution of 1° . Table 8 list the results of computation.

Table 9: UME and GLA computed SVF values and their difference.

Point Id	UME Computed	GLA Computed	Error %
Location 1	0.6808	0.7176	3.68
Location 2	0.5123	0.4887	2.36
Location 3	0.9402	0.9192	2.10

The average difference between SVF computed using UME and SVF computed by GLA is 2.77%.

The use of fish eye photographs is not suitable for SVF calculations of large urban areas. GIS and automated approach are very much required in such scenarios. However the efficiency of the SVF estimation hugely depends on the resolution of stereo network or network of radial lines. The lower is the value between the lines the better is the SVF estimation.

Access to open sky is one of major cause for urban heat island effect. In the current study a field survey using a portable weather station was conducted, temperature was measured for a set of locations which were well distributed and varying locations based on urbanization patterns and built-up density. At the same locations SVF was also computed using UME. Figure 48 demonstrates the relation between SVF and temperature.

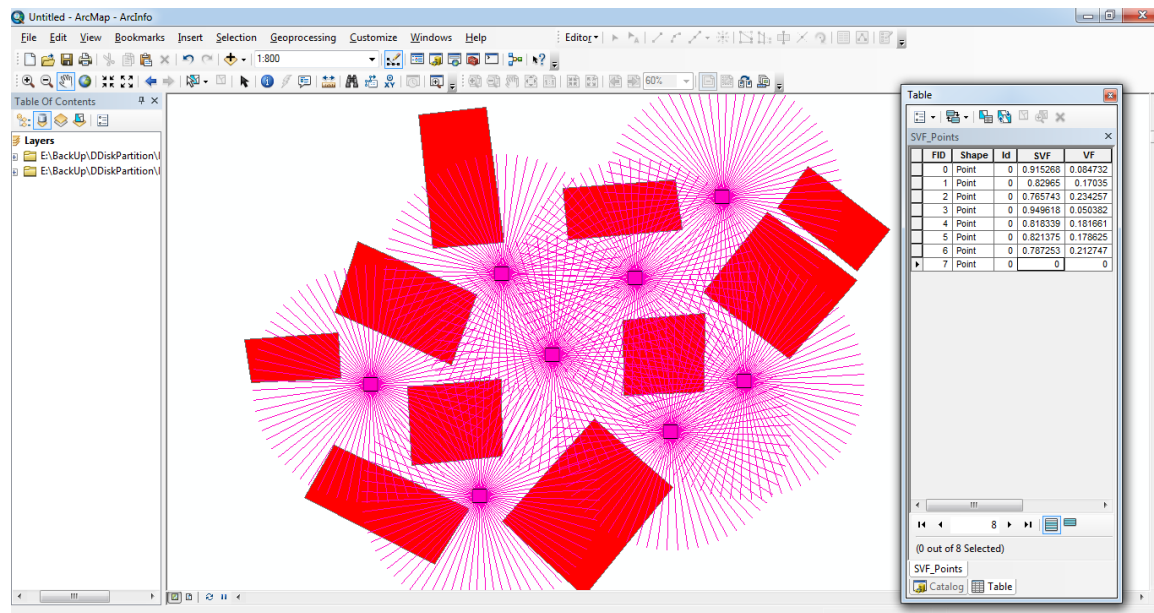


Figure 36: Radial lines and computed SVF and VF values displayed in the attribute table

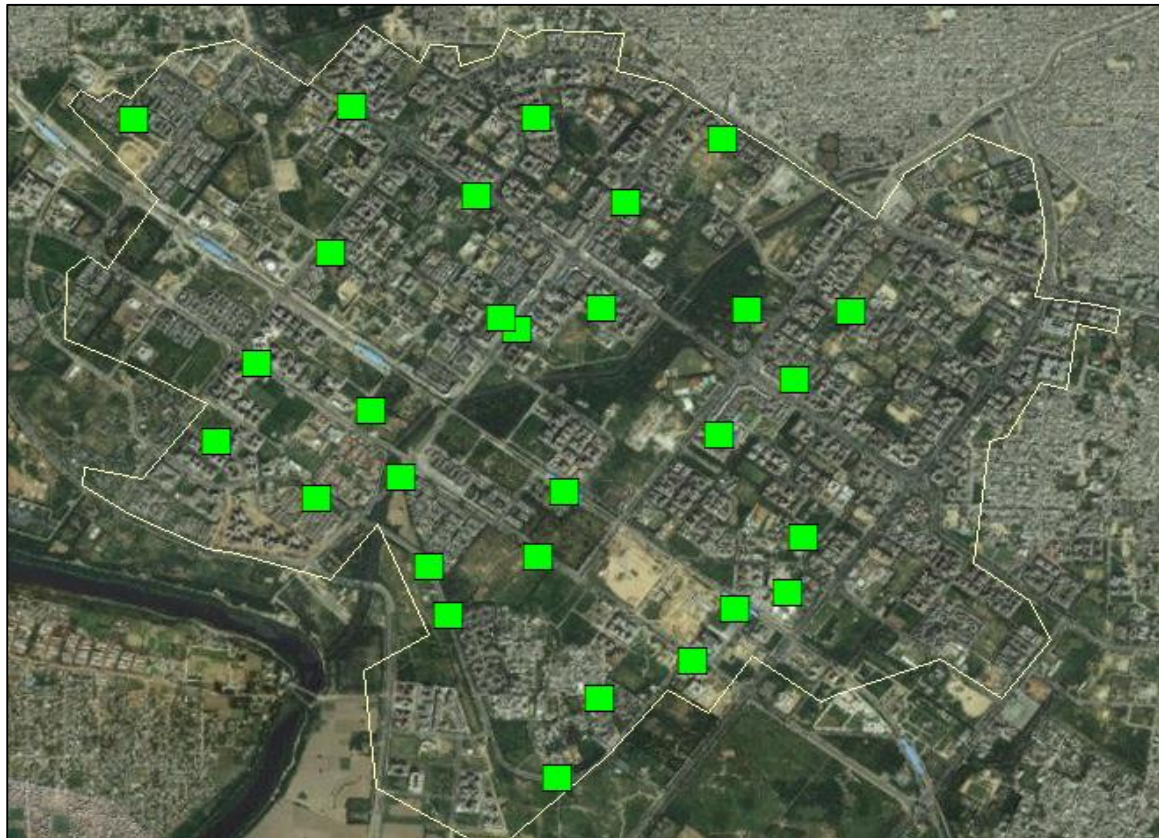


Figure 37: Distribution of field observation points over the study area.

4.4 Identification of Ventilation Paths

The identification of ventilation paths was based on a combined approach adopted by Gal and Unger (2009) and Wong et al. (2010). The parameters used for delineation of ventilation paths included z_0 , z_d and λ_f . All the parameters were computed for each wind direction using UME and were updated to building database. Figures 35-37 displays the distribution of average value of z_0 , z_d and λ_f computed using UME for all the eight wind directions.

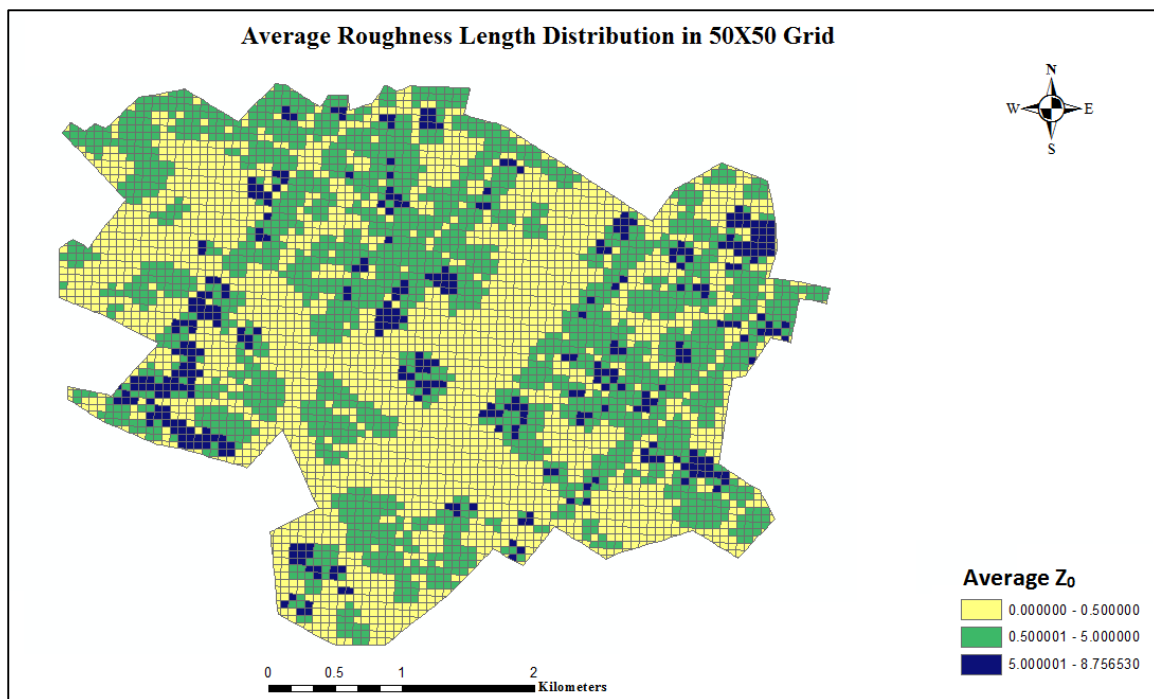


Figure 38: Z_0 distribution map

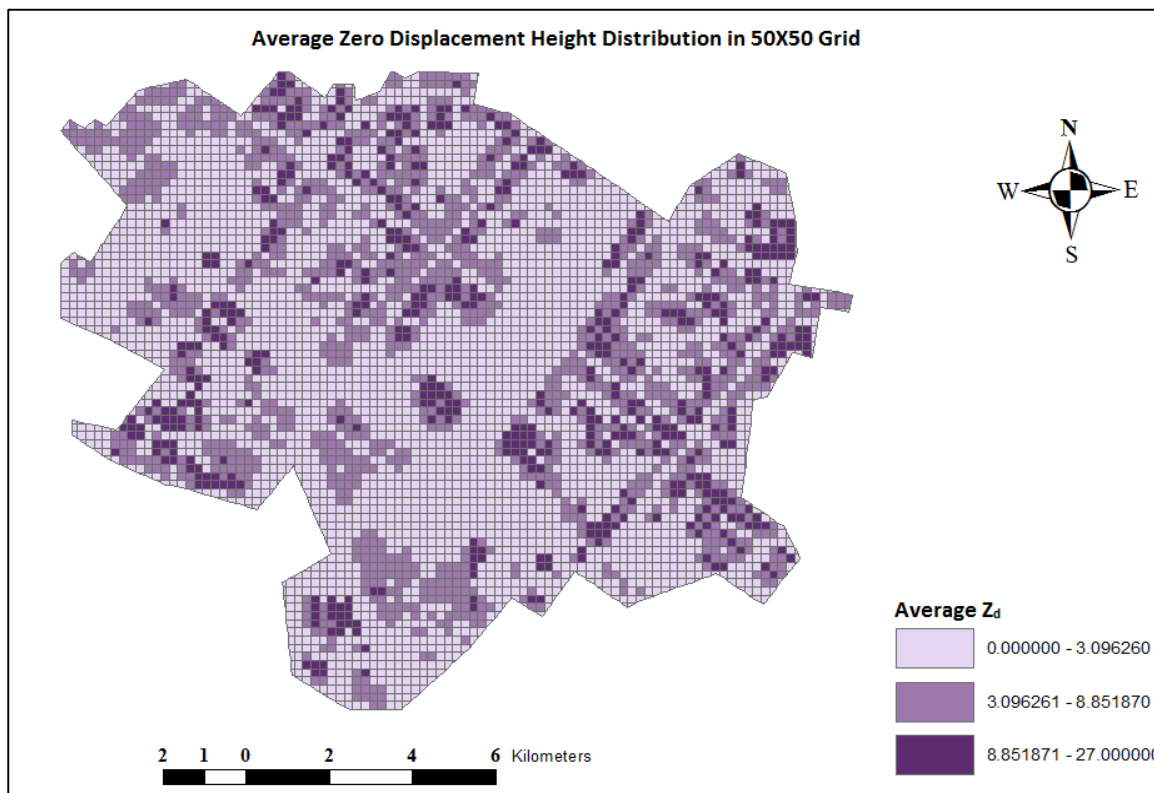


Figure 39: z_d distribution map

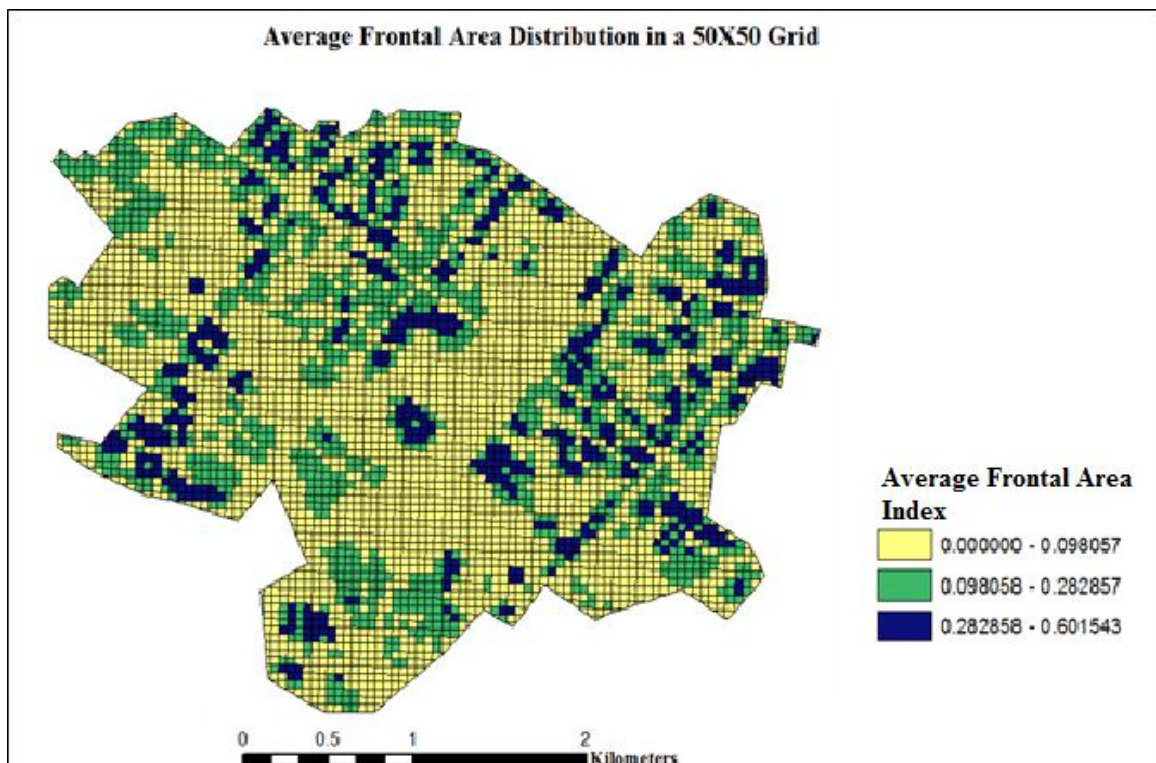


Figure 40: Frontal area index distribution map

Buildings were categorised based on Delhi master plan 2021, the various categories are listed in table 10.

Table 10: Categories of height classification

Height	Category
Height \leq 6 m	Low Rise
6 < Height \leq 15	Medium Rise
15 < Height \leq 24	High Rise
Height > 24	Skyscraper

Based on the classification scheme, the buildings were grouped to their respective classes and the values of z_0 , z_d and λ_f were computed for each building group. Figure 9 –Figure 11 shows relationship between various morphometric variables that have been used in detection of ventilation paths.

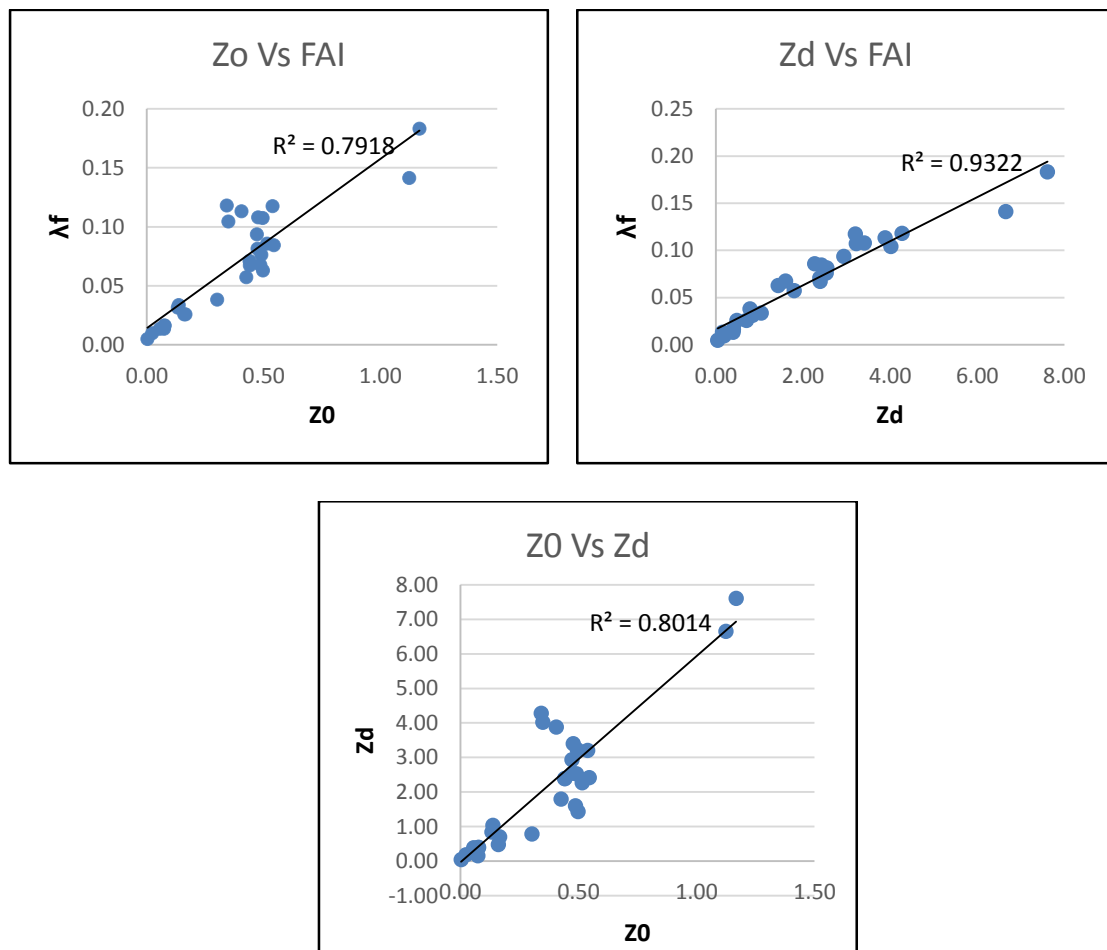


Figure 41: Building height up to 6 meters

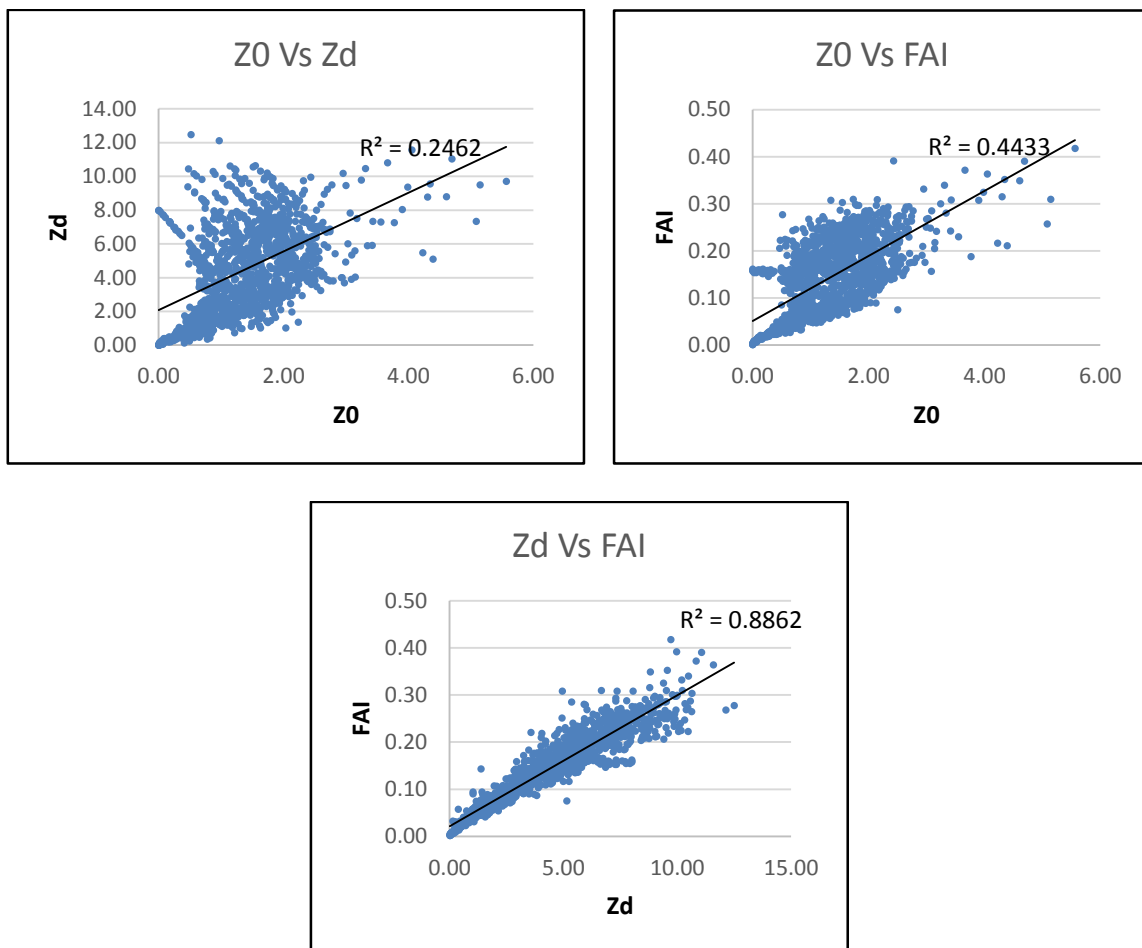


Figure 42: Building height between 6 and 15 meters

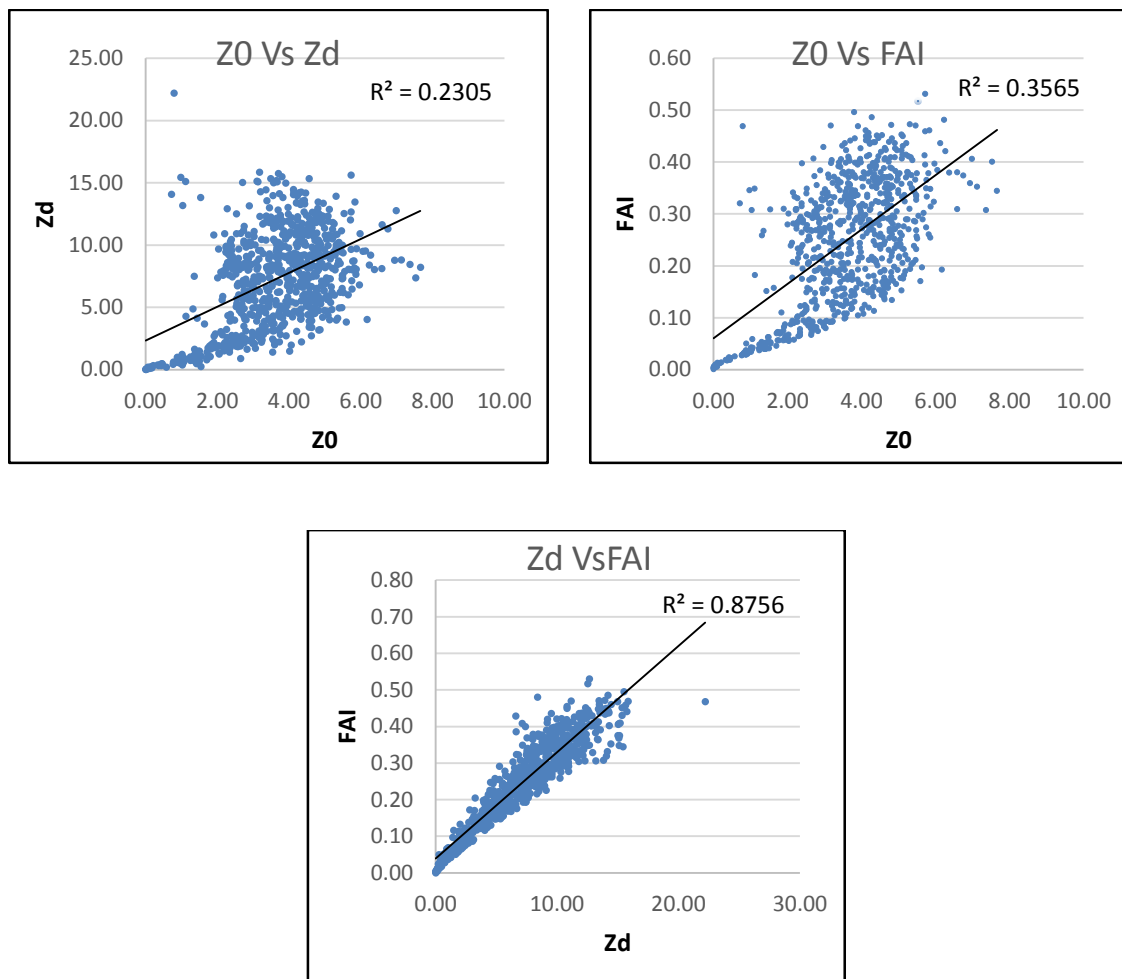


Figure 43: Building height between 15 meters and 24 meters

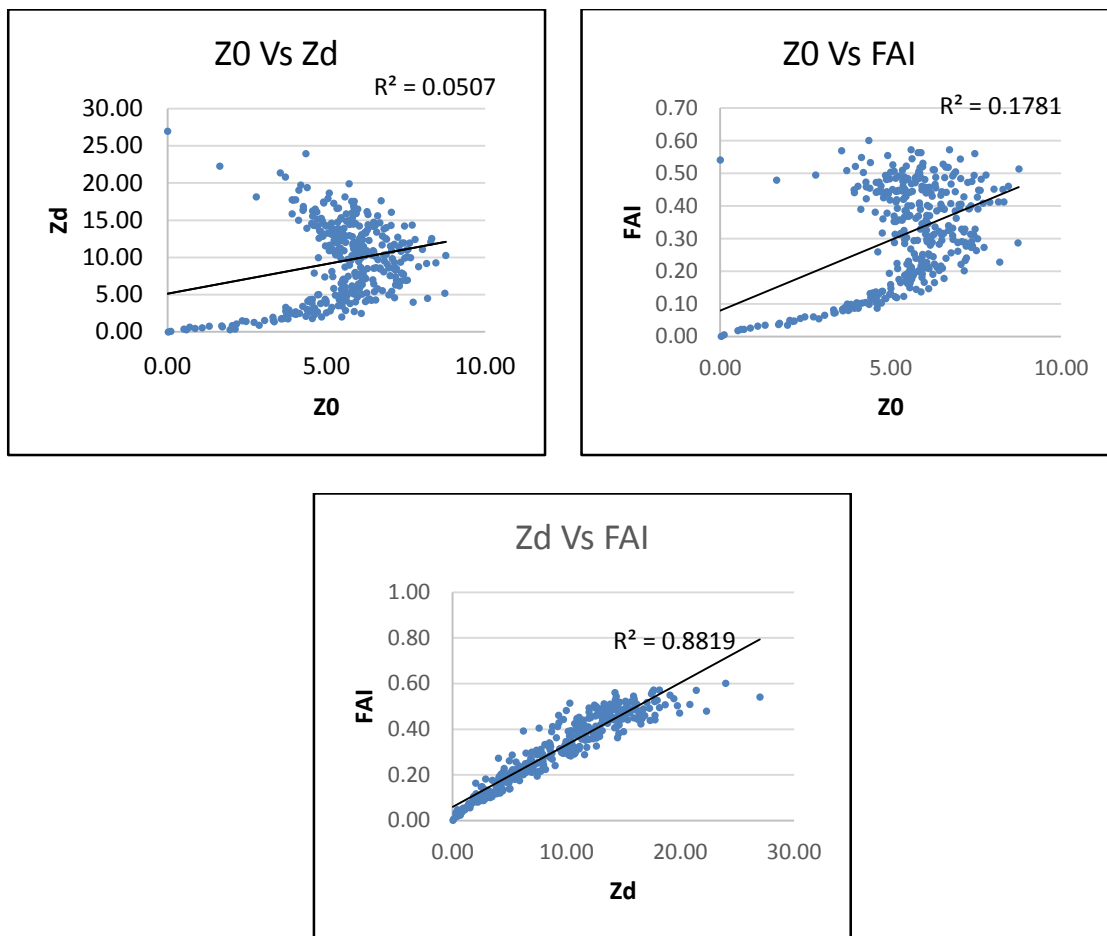


Figure 44: Building height greater than 24 meters

Based on the results achieved and using the r^2 values it is evident that, only for the low rise buildings there exists a strong relationship between different parameters as listed in table 10. However as the building height increases the relationship between the variables cease to exist, the only strong relationship that sustains with increase in height is the relation between Zero Displacement Height (z_d) and Frontal Area Index (λ_f). This strong relationship is justified as both λ_f and z_d depend exclusively on the height of building.

Table 11: r^2 values for various relationships between identified geometric parameters

	Zd vs Zo	Z0 vs FAI	Zd Vs FAI
Low Rise	0.8014	0.7918	0.9322
Medium Rise	0.2462	0.4433	0.8862
High Rise	0.2305	0.3565	0.8756
Skyscraper	0.0507	0.1781	0.8819

For identification of ventilation paths raster based criteria analysis was done. Raster images were generated based on criteria's mentioned below.

- $Z_0 < 0.5$
- $Z_d < 3$
- Length > 1000 m
- Path width > 50 m

λ_f was not used in the determination of ventilation paths as a very strong correlation exists between z_d and λ_f . Using any of the two parameters led to similar results. The raster images were generated from the grid database which contained the averaged values of each parameter associated with each grid cell. The raster images were produced with a pixel size of 50. The raster image for z_0 criteria was reclassified into three classes as mentioned in table 11.

Table 12: Classification scheme for z_0 values

Value Range	Class Name
$z_0 \leq 0.5$	Ventilated
$0.5 < z_0 \leq 1$	Partially Ventilated
$z_0 > 1$	Blocked

Table 13: Zd Classification

Value Range	Class Name
$Z_d \leq 3$	Ventilated
$Z_d > 3$	Blocked

Based on a classification scheme a raster image was generated for the distribution of all the z_0 and z_d values. The z_d image was used with its original classes. The two images were later combined which resulted in an image with six classes. Giving priority and weightage to z_0 values the resultant image was reclassified into three final classes: Ventilated, Partially Ventilated and Weakly Ventilated. The final map was designated as ventilation map.

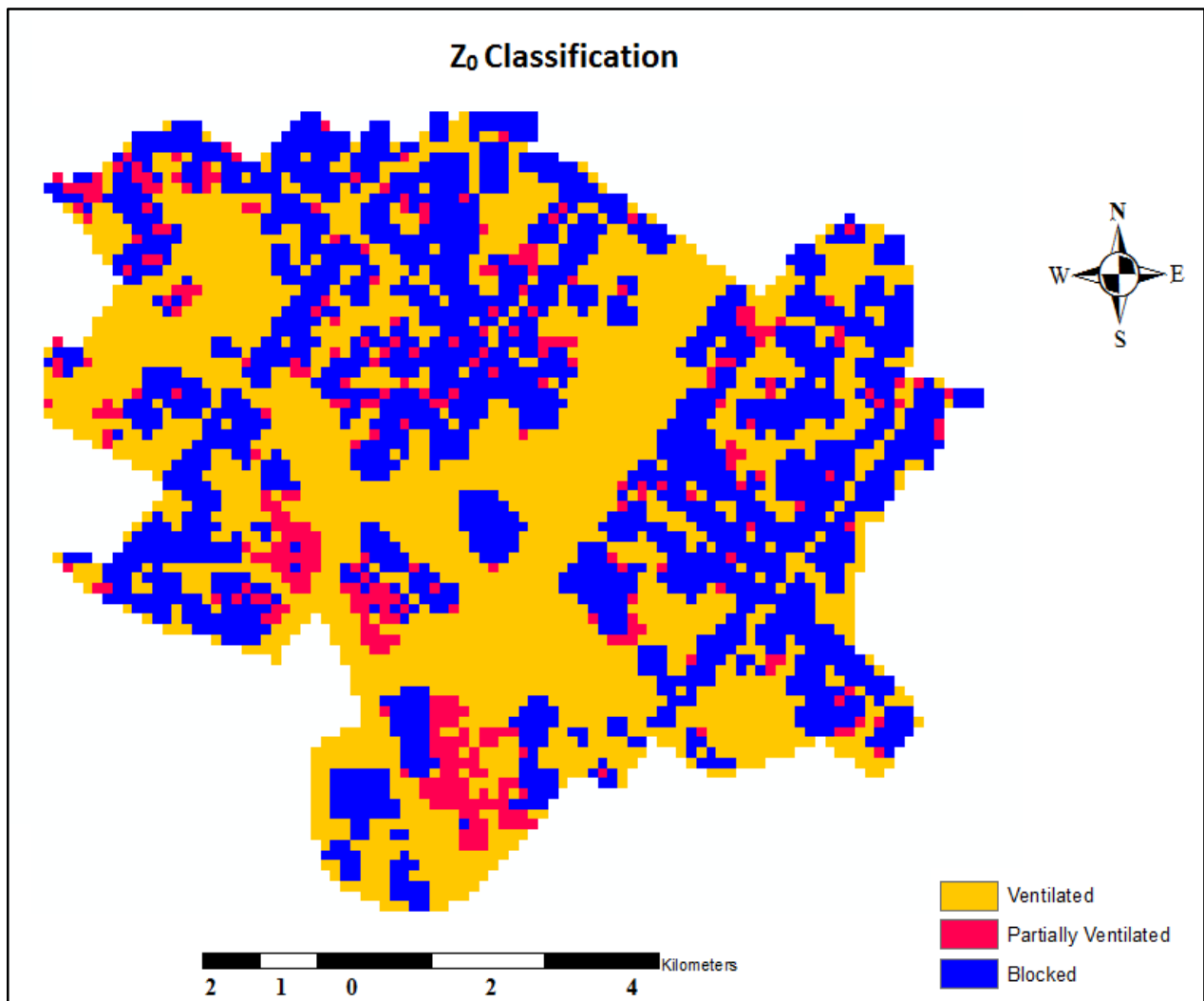


Figure 45: z₀ Classification

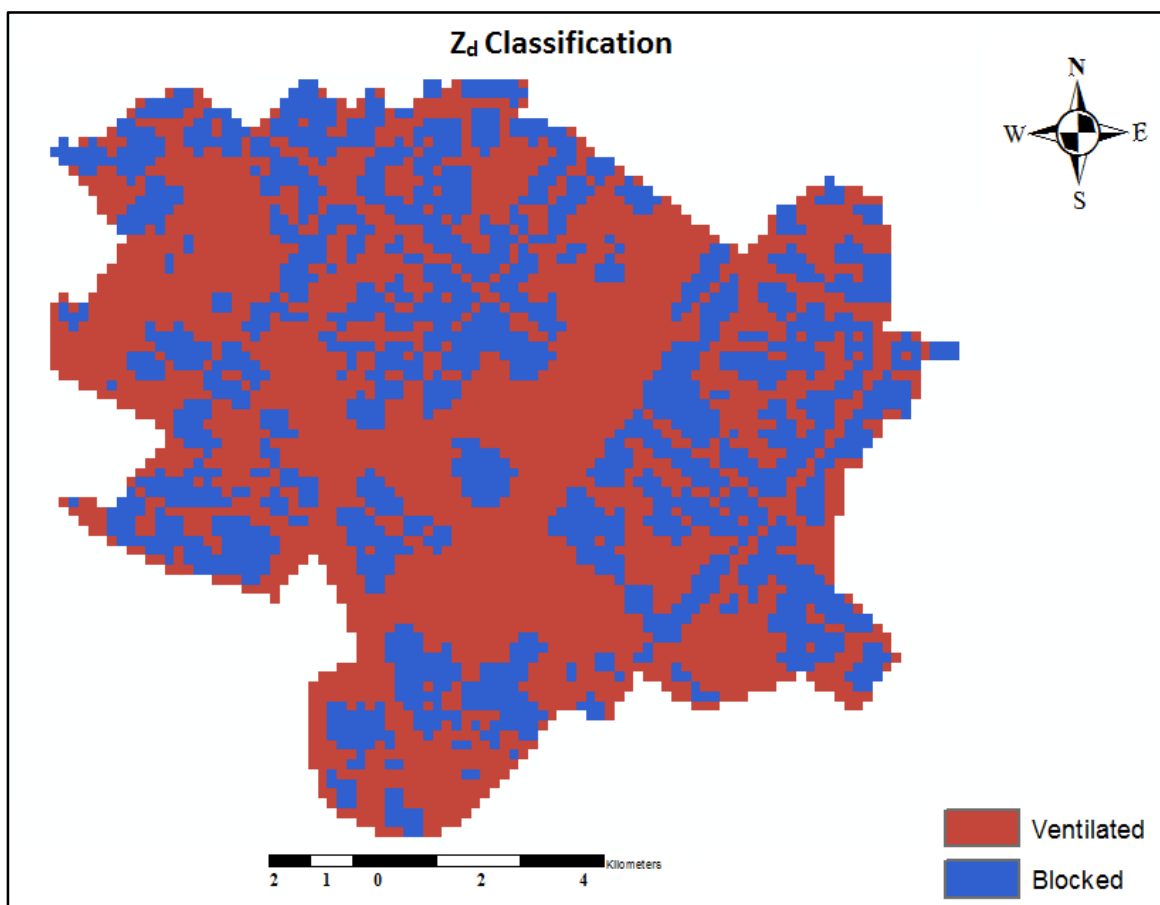


Figure 46: Z_d Classification

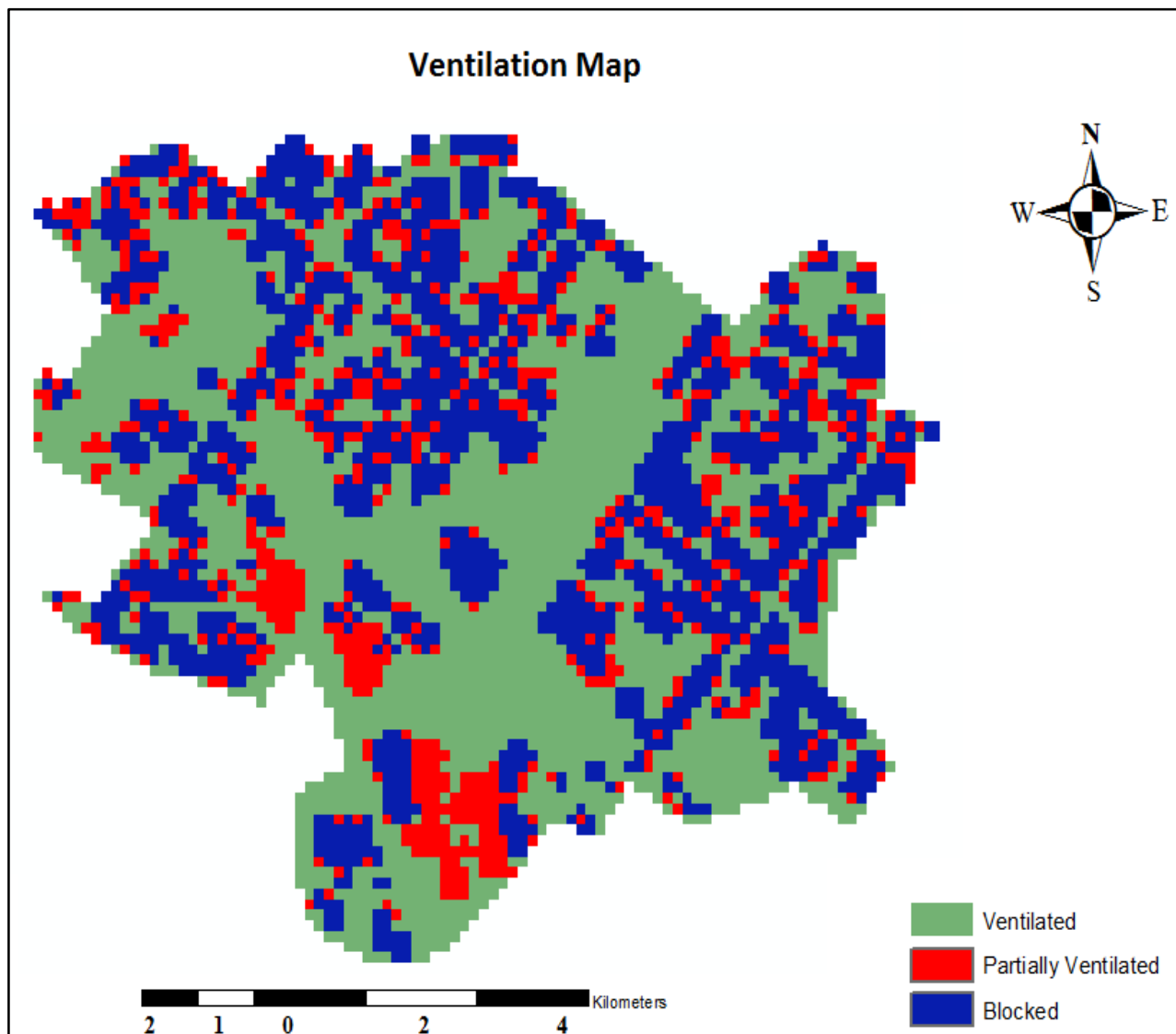


Figure 46: Ventilation Map

Analysis and classification of ventilation map led to identification of ventilation paths. The identified ventilation paths were categorised as:

- **Major Ventilatuion Paths**
- **Minor Ventilation Paths**

The major ventilation paths were identified as the one having length greater than 1000 m and width greater than 50 m. The minor ventilation paths were identified as the one with length less than 1000 m or width less than 50 meters. . Two major corridors of ventilation were identified, the first ventilation corridor 3199 m long, ran along Northeast-to-Southwest direction and the second one extended along Northwest-to-Southeast to a length of 3685 m. Both ventilation corridors had sufficient width greater than 50 meters and ran along the whole lengths of study area and hence were designated as major ventilation paths.

Various other ventilation paths with a lesser length and width were also delineated. These ventilation paths had a local presence i.e. did not compete the whole directional lengths and congregated into the major ventilation corridors.

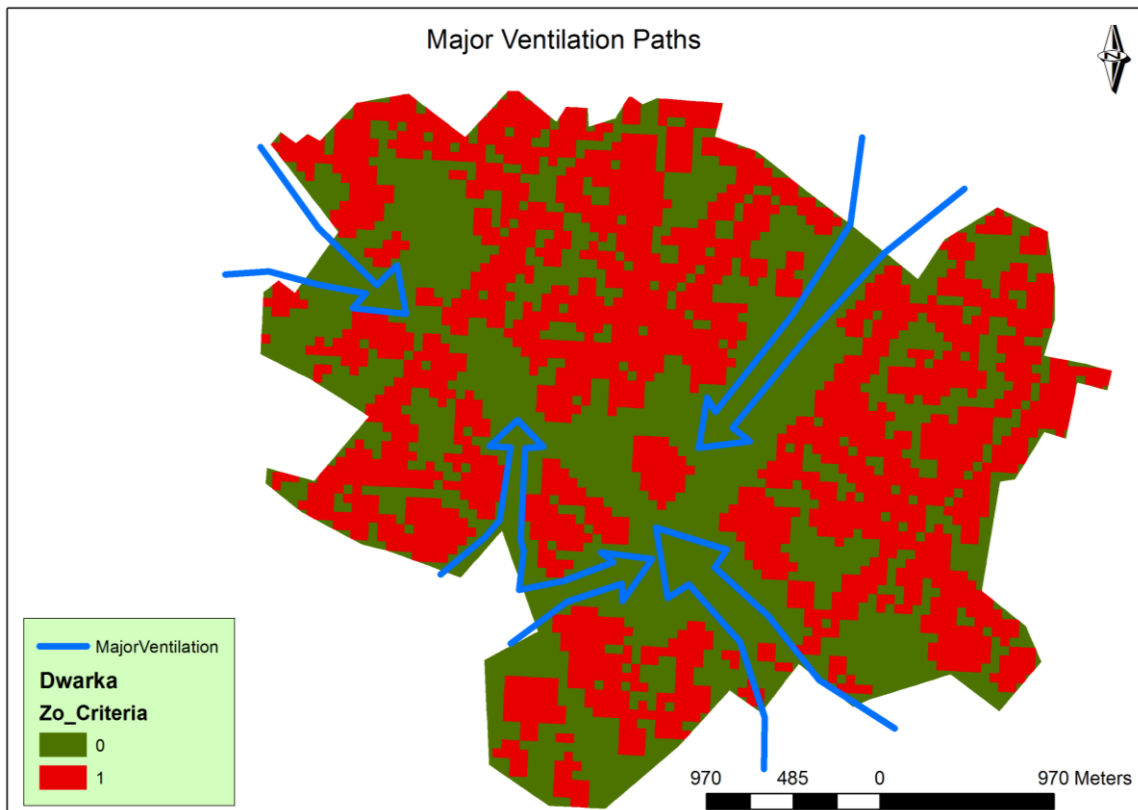


Figure 47: Identified Major Ventilation Paths

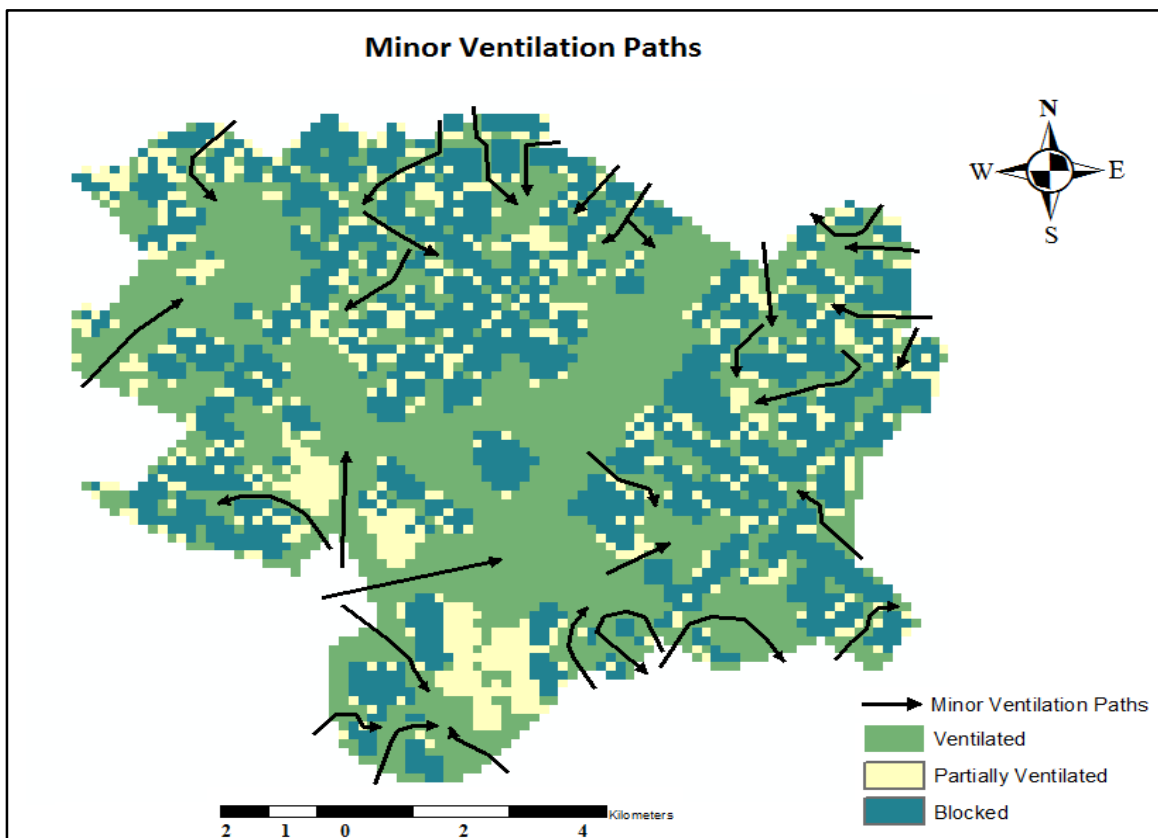


Figure 48: Identified Minor Ventilation paths

To validate the identified ventilation paths temperature values were measured at different locations well distributed in all the three classes of ventilation map.

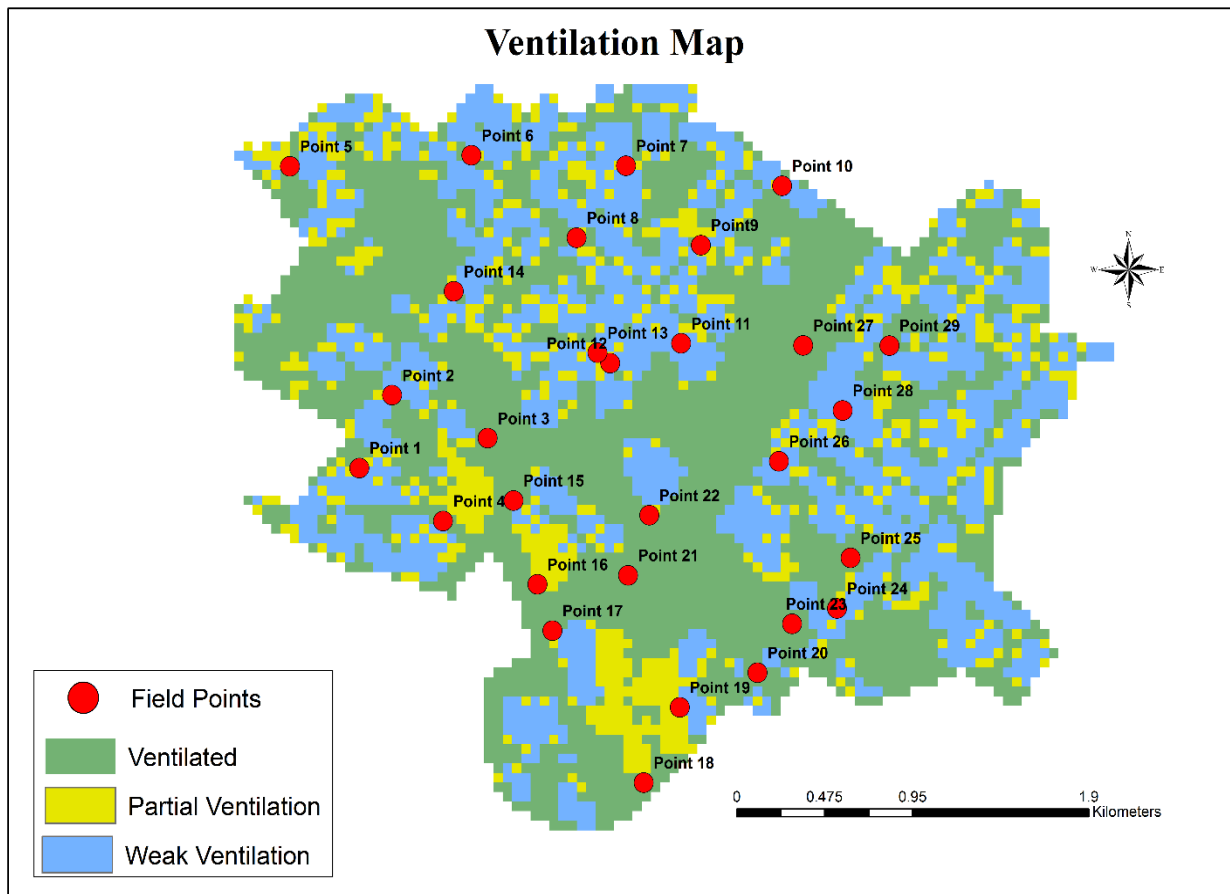


Figure 49: Ground observation points distributed over various ventilation classes

Table 14: The ground observation points, the class they fall in and measured temperature values.

Point ID	Class	Temperature
1	Ventilated	25.78
2	Weak Ventilation	26.00
3	Ventilated	24.82
4	Ventilated	24.29
5	Weak	25.10
6	Ventilated	23.94
7	Partial	24.83
8	Weak	26.53
9	Weak	26.82
10	Partial	25.91
11	Partial	25.10
12	Ventilated	24.82
13	Partial	25.33
14	Partial	25.42
15	Ventilated	24.78
16	Ventilated	24.77
17	Partial	24.97
18	Ventilated	23.50
19	Weak	25.01
20	Ventilated	25.01
21	Ventilated	24.99
22	Ventilated	23.93
23	Ventilated	23.83
24	Weak	25.10
25	Ventilated	24.88
26	Weak	24.69
27	Ventilated	26.41
28	Weak	25.74
29	Ventilated	24.53

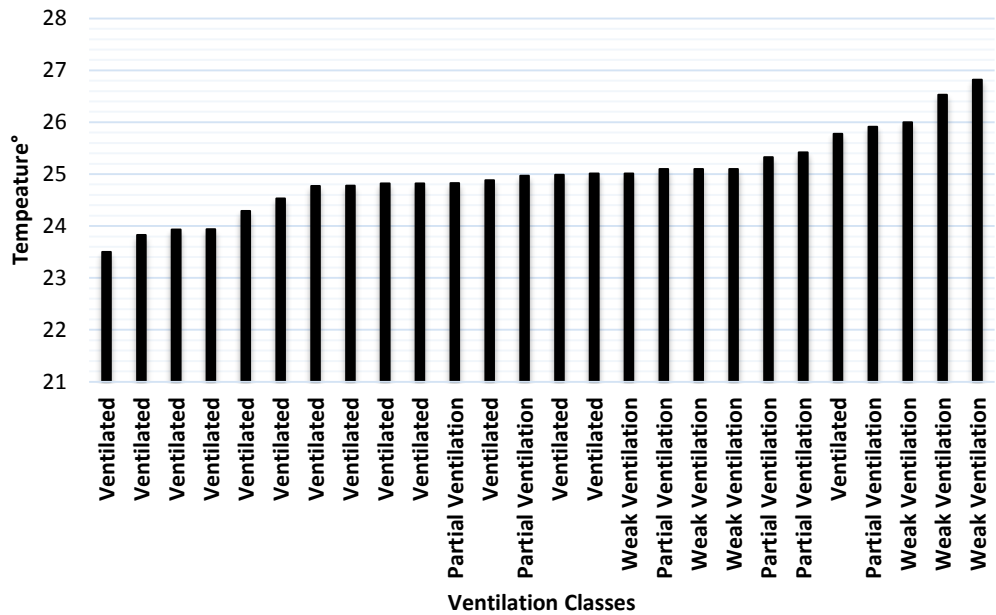


Figure 48: Relationship between temperature and ventilation classes.

Table 13 details out distribution of points in various ventilation classes and the in-situ measured temperature value. The values varied form 23.5° to 26.82° and the average values of temperature for each class were:

Table 15: Average temperature in each ventilation class

Ventilation Class	Average Temperature (Degree Celsius)
Ventilated	24.00
Partial Ventilation	24.96
Weak Ventilation	26.07

From the results attained it is evident that ventilation of an urban area affects the ambient temperature of urban area. As the ventilation of an area is obstructed it will lead to increase in surrounding temperature.

Wind speed, another important microclimatic parameter was used to validate the identified the potential ventilation paths. In-situ wind measurements of wind varied form 0 m/sec to 2.36 m/sec. The observations that were taken in the ventilated paths showed higher wind speed as compared to partially ventilated and weakly ventilated areas. Even zero wind speed was also observed in some of weakly ventilated areas. Figure 45 illustrates this relationship between wind speed and various ventilation classes.

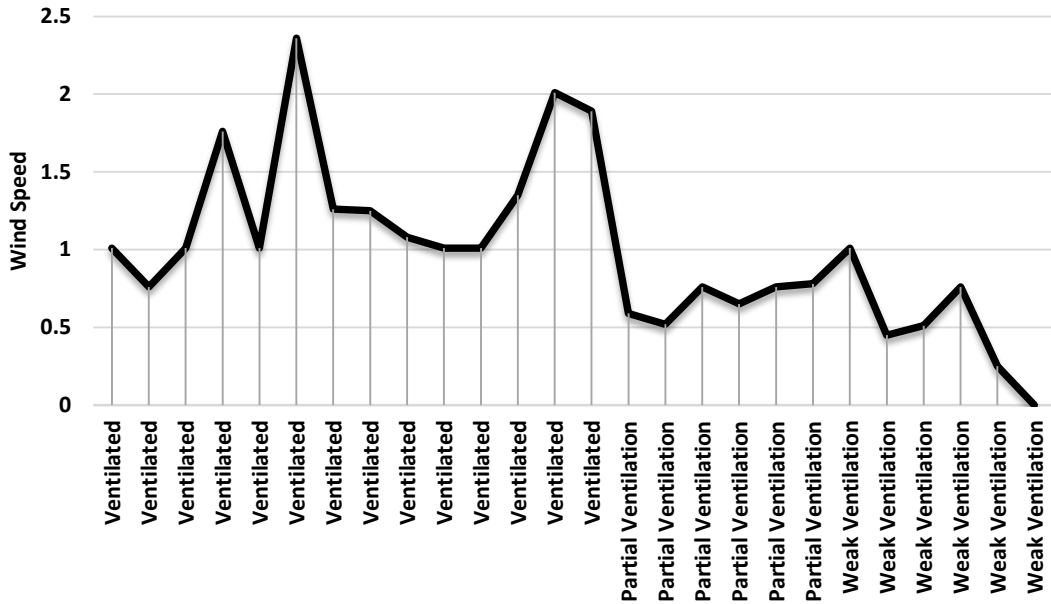


Figure 49: Relationship between wind speed and various ventilation classes.

Average values of wind speed for each ventilation class are listed in table:

Table 16: Average Wind Speed distribution in each Ventilation class

Ventilation Class	Average Wind Speed
Ventilated	1.3407
Partial ventilation	0.6767
Weak ventilation	0.4967

SVF is a vital parameter to understand the effect of building geometry and building distribution on the ambient temperature. SVF for all the observation points was computed using newly developed automated approach and validated using fish eye photographs as discussed in section 3.2.6.

The computed SVF values were compared with the respective field measured temperature values and it was found that there existed a negative correlation between the two parameters. As the SVF value increased, temperature values descended. Figure 46 demonstrates this relationship between temperature and SVF.

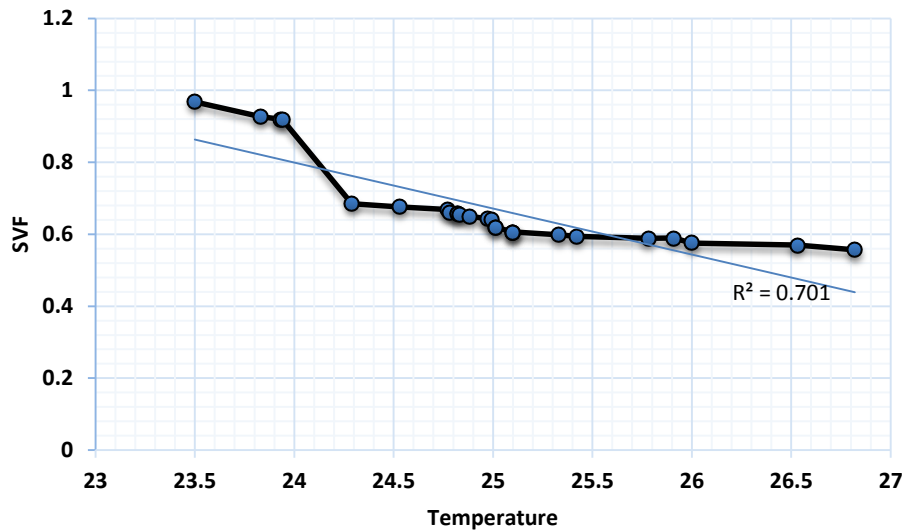


Figure 50: Relationship between SVF and Temperature

The computed SVF values were further compared with the ventilation class, they fall in. SVF values ranged from 0.96 to 0.55. The ventilated class contained the SVF points with largest values and the lowest values were located in the weakly ventilated class. The relationship is shown in figure 47.

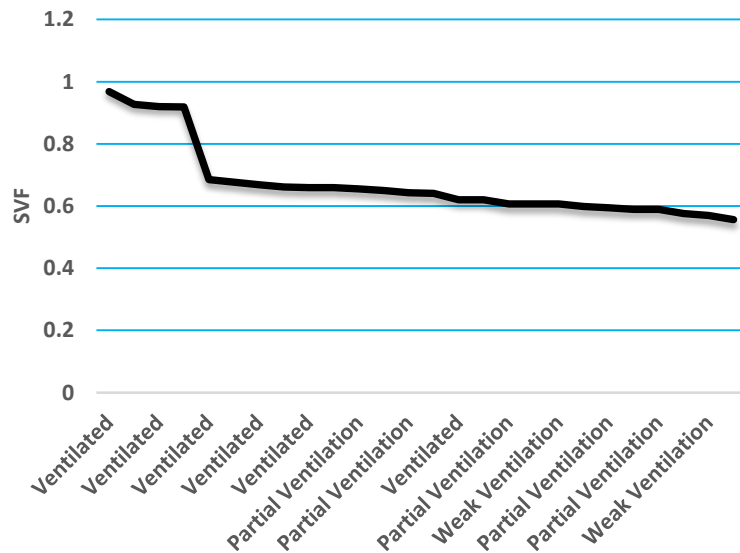


Figure 51: Relationship between SVF and ventilation classes

CONCLUSIONS

Chapter 5: Conclusions

General Conclusions

The study aimed at carrying out microclimatic analysis of an urban area using building morphometric characteristics which were to be computed automatically from a 3D building database. It was an evident observation that the triangulation based on Rational Polynomial Coefficient (RPC), alone is not sufficient to orthorectify a Cartosat stereo pair as the RMSE value is quite high. However, GCP assignment during triangulation significantly decreased the RMSE, to acceptable limits.

To generate 3D building database heights were measured from Cartosat stereo data in a 3D environment. Sample heights were also measured from field and it was found that the heights computed in the 3D environment slightly varied from the actual heights. Hence it can be said that use of Cartosat imagery to measure heights using a 3D setup is an efficient approach and the slight error that is introduced can be accepted, as it is time consuming and tedious task to measure all building heights from the field itself.

As part of automating the computation of urban morphometric parameters, a comprehensive, open source standalone application was developed named UME. UME has several components which were tested on a sample dataset. The error percentage that was computed based on manual calculations of frontal area were well within acceptable limits and proves the efficiency of frontal area computed using UME. UME was also tested for regular and irregular grid and the results achieved were encouraging. The height-to-width ratio computed using UME was next to the actual value the error percentage was 0.90%. One of the other parameter that UME can compute is SVF. The validation of computed SVF was done on an actual area, for which fish eye photographs were captured. Gap Light Analyser (GLA) an established application to measure light transmission indices was used to compute SVF values. The UME computed SVF value closely matched the value computed using GLA with a slight difference of 2.77%. Thus, it can be concluded based on the results achieved on a sample data set and fish eye photographs, that UME is effective enough to be deployed to compute various urban morphometric parameters. UME was used to identify

Using computed morphometric parameters and applying multi criteria's, ventilation paths were identified. Based on the achieved results it was noticeable that when the height was below 6 m, all

the parameters namely z_0 , z_d and λ_f showed high values of correlation but as the height increased the relation between the computed parameters deteriorated. The only relationship that sustained with increasing height was relationship between z_d and λ_f . This can be accounted due the building distribution, the existence of immense open spaces and the dependence of parameters, z_d and λ_f on height of buildings. Hence it can be concluded that for a study area like Dwarka, New Delhi, where the only relation that exists is between z_0 and z_d . The criteria set: $z_0 > 0.5$ and $z_d < 3$, based on which the ventilation paths were identified successfully delineated the wind paths which were also validated using field data. Hence applicability of computed morphometric parameters and the designated criteria set are fully competent to simulate and model the flow of the wind in the urban area. The effect of building geometry in the temperature values inside the urban canyon was determined by another morphometric parameter, SVF. SVF was computed for various points distributed evenly in the whole study area, which included ventilated and non-ventilated areas. It was found that a strong negative relationship prevail between SVF and temperature and based on the results obtained we can conclude that as the SVF value rises the temperature decreases. In the current study only buildings in an urban area were considered for modelling winds, however the effect of vegetation also plays a significant role in the flow of wind which can be addressed in upcoming future studies.

Answers to questions attempted by the research are as follows:

Can a semi-automatic approach be deployed to generate a 3-Dimensional database of an urban area?

A semi-automatic approach was utilized to generate 3-Dimensional Database. However, it was observed that to achieve planimetric accuracy of building footprints the Cartosat imagery needed to be orthorectified using GCP's. Also building heights were measured in a 3D environment which varied slightly from the field measured values. To make 3D measurements a strong stereo vision is required, as based on 3D perception, building heights are measured. Semi-automatic approach is a bit time consuming in comparison to fully automatic approach as it includes building footprint manual digitization and measuring building heights using 3D setup. On the other hand, when semi-automatic approach is compared to field based approach, it is far better when compared in terms of time and cost of execution. In this current study, limitations of cartosat-1 imagery played a huge role in using a semi-automatic approach to generate urban database.

How to automate the task of estimation of urban morphometric parameters?

The computation of urban morphometric parameters is complex and computation intensive. The complexity further increases as the area under consideration increases. Hence, automation is most required and hence a programming scripts were written to automate the estimation of parameters, during the course of automation an open source python and GIS based application was developed named UME. Python has a strong backing of variety of GIS processing, mathematical computations and geometry processing modules. The automation was not straightforward, but modification, manipulation of existing functions and creation of some new functionalities made it possible to compute various geometric parameters. The final application was tested on a sample dataset and the results achieved were legitimate and encouraging. Hence, it can be said that using python and GIS the calculation of urban morphometric parameters can be automated efficiently and fine accuracy can be accomplished for the computed parameters.

What are the set of morphometric parameters and the criteria's that can be utilized to perform microclimatic analysis?

The study identified four urban morphometric parameters sufficient to perform microclimatic analysis of the current study area. The identified parameters are:

- Roughness Length (z_0)
- Zero Plane Displacement Height (z_d)
- Frontal Area Index
- SVF

After scrutinising the various computed parameters, for the current study z_0 and z_d were the parameters that were used to identify the ventilation paths. Based on them a criteria set was defined:

- $z_0 < 0.5$
- $z_d < 3$

Based on this criteria set wind paths were identified and also validated using in-situ measurements.

To identify the effect of building distribution and its geometry in the urban ambient temperature, SVF was used. A strong negative correlation was found between temperature and SVF.

Thus, to study two microclimatic variables, three parameters z_0 , z_d (for wind flow) and SVF (for temperature) were identified suitable.

In the current study, UME was used to identify ventilation paths inside an urban area and during the course of this study UME has transformed into a robust application which can be used into a variety of applications. UME can be used for urban areas with varying geometries and urban areas covering larger geographic span. Currently UME computes fewer parameters as compared to its capability. However, work is in progress and computation capabilities for various others urban geometric parameters will be added in the coming future.

References

1. Ackerman, B., Hildebrand, 1978. Structure of the planetary boundary layer over a complex mesoregion. Final Report ATM76-15870, Illinois State Water Survey at University of Illinois, Urbana, Illinois 61801, USA
2. Angel, J. K., Hoecker, W. H., Dickson, C. R., Pack, D. H., 1974. Urban influence on a strong daytime air flow determined from tetroon flights. *Journal of Applied Meteorology*, 12,924-936.
3. Arakawa, H., Tsutsumi, K., 1967. Strong gusts in the lowest 250 m layer over the city of Tokyo *Journal of Applied Meteorology*. 6, 848-851.
4. Ariel, M. Z., Kliwchnikova, L.A., 1960. Wind over a City, *Trans Glav Geofiz Obs*, 94, 29-32.
5. Blumberg, D.G., Greeley, R., 1993. Field studies of aerodynamic roughness length. *J. Arid Environ.* 25, 39–48.
6. Bottema, M., 1995(a). Aerodynamic roughness parameters for homogeneous building groups—Part 1: Theory. Document SUBMESO 18, Ecole Centrale de Nantes, France, 40 pp.
7. Bottema, M., 1995(b). Aerodynamic roughness parameters for homogeneous building groups—Part 2. Results Document SUB-MESO 23, Ecole Centrale de Nantes, France, 80 pp.
8. Bottema, M., 1997. Urban roughness modelling in relation to pollutant dispersion. *Atmospheric Environment*, vol. 31, no. 18, pp. 3059–3075.
9. Brook, R. R., 1972. The measurement of turbulence in a city environment. *J. Appl. Meteorol.* 11, 443450
10. Brown, M.J., Grimmond, C.S.B. and Ratti, C., 2001. Comparison of methodologies for computing sky view factor in urban environment', Internal Report Los Alamos National Laboratory, Los Alamos, NM, LA-UR-01-4107.
11. Burian, S., Brown, M.J., Velugubantla, S.P., 2002. Roughness Length And Displacement Height Derived From Building Databases. 4th Symposium on the Urban Environment Norfolk, VA.
12. Burian, S.J., Stetson, S.W., Han, W.S., Ching, J., Byun, D., 2004. High-resolution dataset of urban canopy parameters for Houston, Texas. In: Proceedings of the 5th conference on urban environment. AMS meeting, Vancouver, CD 9.3.
13. Chapman, L. and Thornes, J.E., 2004. Real-time sky-view factor calculation and approximation. *Journal of Atmospheric and Oceanic Technology*, Vol. 21, pp.730–741.
14. Counihan, J., 1971. Wind tunnel determination of the roughness length as a function of the fetch and the roughness density of three-dimensional roughness elements. *Atmospheric Environment*. 5, 637–642.
15. Davenport, A. G., 1960. Rationale for determining design wind velocities. *J. Struct. Div. Amer. Soc. Civ. Eng.*, 86, 39–68.
16. Davenport, A.G. 1963. The relationship of Wind structures to Wind Loading. Proceedings of the symposium of wind effects on building and structures, Teddington, National Physical Laboratory. Vol. 1.
17. Dong, W.P., Sullivan, P.J., Stout, K.J., 1992. Comprehensive study of parameters for characterizing three dimensional surface topography-1: Some inherent properties of parameter variation. *Weur*, 159, 161–171.

18. Gál T., Sümeghy Z., 2007. Mapping the roughness parameters in a large urban area for urban climate applications. *Acta Climatol. Chorol.* vol. 40, no. 41, 27–36.
19. Gal, T., Unger, J., 2009. Detection of ventilation paths using high-resolution roughness parameter mapping in a large urban area” *Building and Environment*. 44, 198–206.
20. Grimmond C. S. B., T. R. Oke, 1999. Aerodynamic properties of urban areas derived from analysis of surface form. *Journal of Applied Meteorology*. 38, 1262-1292
21. Grimmond, C.S.B., Potter, S.K., Zutter, H.N., Souch, C, 2001. Rapid methods to estimate sky-view factors applied to urban areas| *International journal of climatology*, 21: 903–913.
22. Hanna, S. R., 1969. Urban Micrometeorology. *Proceedings American Nuclear Society Meeting*, San Francisco, CA, ATDL Contribution 35, 21.
23. Holmer, B., 1992. A simple operative method for determination of sky view factors in complex urban canyons from fisheye photographs’, *Meteorologische Zeitschrift*, N.F. Vol. 1, pp.236–239.
24. Holmer, B., Postgård, U. and Eriksson, M., 2001. Sky view factors in forest canopies calculated with IDRISI. *Theoretical and Applied Climatology*, Vol. 68, pp.33–40.
25. Jackson, P. S. 1978. Wind structure near a city center. *Boundary-Layer Meteorology*. 15, 323-340.
26. Jensen, I. M., 1958. The Model Law for Phenomena in the Natural Wind. Int. Edit., Danish Technical Press, Copenhagen. Volume 2, 4.
27. Jones, P. M., deLarzinaga, M. A. B., Wilson, C. B., 1971. The Urban Wind Velocity Profile. *Atmos. Environ.* 5, 89–102.
28. Lettau H., 1957. Compilation of Richardson Numbers, Classification of Profiles and Determination of Roughness Parameters. *Exploring the Atmosphere’s 1st Mile*. Vol. 1, pp. 328–336.
29. Lettau, H.H., 1969. Note on aerodynamic roughness parameter estimation on the basis of roughness element description. *J. Appl. Meteorol.* 8, 828–832.
30. Liang, C., Edward, N., Xipo, A., 2009. Air Path Detection in Urban Environment and its Implications on Morphological Analysis and Ventilation Assessment: A New Way to solve an old Problem. *Seventh International Conference on Urban Climate*, Yokohama, Japan.
31. Lindberg, F., 2004. Towards the use of local governmental 3-D data within urban climatology studies. *Mapping and Image Science*, Vol. 2, pp.4–9.
32. Lyles, L., Allison, B.E., 1979. Wind profile parameters and turbulence intensity over several roughness element geometries. *Transactions of the ASAE*.334-338.
33. Macdonald, R.W., Griffiths, R.F., Hall, D.J., 1998. An improved method for the estimation of surface roughness of obstacle arrays. *Atmos. Environ.* 32, 1857–1864.
34. Marshall, J.K., 1971. Drag measurements in roughness arrays of varying density and distribution. *Agric. Meteorol.* 8, 269–292.
35. Marullaz, D., 1975. Full-scale measurements of atmospheric turbulence in a suburban area. *Proceedings of the fourth international conference on wind effects on buildings and structures*, Heathrow, England. 23-31.
36. Matzarakis, A. and Mayer, H. 2008. Learning from the past: Urban climate studies in Munich. *Japanese-German Meeting on Urban Climatology*. 5, 271–276.
37. McCormick, R. A., Kurtis, K. R 1966. Vertical diffusion of aerosols over a city. *Q. J. R. Meteorol. SOC.* 92, 392-397

38. Nikaradse, J., 1933. Strömungsgesetze in rauhen Rohren," Beilaga zu Forschung auf dem Gebiete des Ingenieurwesens, VDI-Verlag, Berlin.
39. Oikawa, S., Meng, T., 1995. Turbulence Characteristics and Organized Motion in a Suburban Roughness Layer. *Boundary-Layer Meteorol.* 74, 289–312
40. Oke, T.R., 1981 —Canyon geometry and the nocturnal heat island:Comparison of scale model and field observations|| *Journal of Climatology*, 1: pp. 237-254.
41. Oke, T.R., 1987. *Boundary Layer Climates*, London and New York: Routledge.
42. Petersen, R.L., Parce, D.K., 1994. Development and Testing of Methods for Estimating Surface Roughness Length at Refineries. CPP Project 92-0890, Cermak Peterka Petersen, Inc., Fort Collins, Colorado.
43. Ramli, N.I., Ali, M.I., Saad, M.S.H., Majid, T.A., 2009. Estimation of the Roughness Length (z_0) in Malaysia using Satellite Image. 7th Asia-Pacific Conference on Wind Engineering, Taipei,Tiwan.
44. Ratti, C., Sabatino, S. Di., Britter, R., 2005. Urban texture analysis with image processing techniques: winds and dispersion. *Theor. Appl. Climatol.*
45. Raupach, M. R., 1994. Simplified expressions for vegetation roughness length and zero-plane displacement as functions of canopy height and area index. *Bound.-Layer Meteor.*, 71, 211–216.
46. Roth. M. 2000. Review of atmospheric turbulence over cities. *Q. J. R. Meteorol. SOC.* 126, 941-990.
47. Schaudt, Dickinson, 2000. An approach to deriving roughness length and zero-plane displacement height from satellite data, prototyped with BOREAS data. *Agricultural and Forest Meteorology*. 104, 143–155.
48. Shiotani, M., Yamamoto, G., 1950. Atmospheric turbulence over the large city-turbulence in the free atmosphere (2nd report), *Geophysics. Mag.* 21,134-147.
49. Soma, S., 1964. The properties of atmospheric turbulence in high winds. *J. Meteoml. SOC. Jpn.* 42, 372-396.
50. Souza, L.C.L., Rodrigues, D.S. and Mendes, J.F.G. (2003). The 3DSkyView extension: an urban geometry access tool in a geographical information system'. Proceedings of the Fifth International Conference on Urban Climate, Vol. 2, University of Lodz, Lodz, Poland, pp. 413–416.
51. Steyn, D.G. (1980) 'The calculation of view factors from fisheye-lens photographs', *Atmosphere-Ocean*, Vol. 18, pp.254–258.
52. Su, J.G., Brauer, M., Buzzelli, M., 2008. Estimating urban morphometry at the neighborhood scale for improvement in modeling long-term average air pollution concentrations. *Atmospheric Environment*. Volume 42, Issue 34, 7884–7893.
53. Taylor, G. I., 1918. Phenomena connected with turbulence in the lower atmosphere. *Proc. R. Soc. London. A949*, 137-155.
54. Tian, X., Li, Z.Y., Tol, C.V., Su, Z., Li, X. , He, Q.S., Bao, Y.F., Chen, E.X., Li, L.H., 2011. Estimating zero-plane displacement height and aerodynamic roughness length using synthesis of LiDAR and SPOT-5 data. *Remote Sensing of Environment*. 115, 2330–2341.
55. Unger, J., 2009. Connection between urban heat island and sky view factor approximated by a software tool on a 3D urban database. *Int. J. Environment and Pollution*, Vol. 36, pp. 59-80

56. Watson, I.D. and Johnson, G.T., 1987. Graphical estimation of sky view-factors in urban environments. *Journal of Climatology*, Vol. 7, pp.193–197.
57. Wever, N., 2012. Quantifying trends in surface roughness and the effect on surface wind speed observations. *Journal of Geophysical Research*, Vol. 117, D11104.
58. Wieringa, J., 1992. Updating the Davenport roughness classification. *Journal of Wind Engineering and Industrial Aerodynamics* Vol.41, 357-368.
59. Wong, M.S., Nichol, J. E., Ngb, E. Y. Y., Guilbert, E., Kwok, K. H., To, P.H., Wang J. Z., 2010. GIS Techniques for Mapping Urban Ventilation using Frontal Area Index and Least Cost Path Analysis. *The International Archives of the Photogrammetry, Remote Sensing and Spatial Information Sciences*, Vol. 38, Part II, 586-591.
60. Wong, M.S., Nichol, J.E., Edward, N., 2011. A study of the “wall effect” caused by proliferation of high-rise buildings using GIS techniques. *Landscape and Urban Planning*. 102, 245-253.
61. Wong, M.S., Nichol, J.E., To, P.H., Wang, J., 2010. A simple method for designation of urban ventilation corridors and its application to urban heat island analysis. *Building and Environment*. 45, 1880-1889.
62. Yuan, C., Ren, C., Edward, Ng., 2014. GIS-based surface roughness evaluation in the urban planning system to improve the wind environment – A study in Wuhan, China. *Urban Climate* (In press).
63. Zaki, S. A., Hagishima, A., Tanimoto, J., Mohammad, A.F., Razak, A.A., 2014. Estimation of Aerodynamic Parameters of Urban Building Arrays Using Wind Tunnel Measurements. *Journal of Engineering Science and Technology*. Vol. 9, No. 2, 176 – 190.